Innovations in Delivery of Theranostic Agents Across Biological Barriers for Applications in Alzheimer's Disease

By

Shawn Michael Barton

Dissertation

Submitted to the Faculty of the

Graduate School of Vanderbilt University

in partial fulfillment of the requirements

for the degree of

DOCTOR OF PHILOSOPHY

in

Neuroscience

January 31st, 2019

Nashville, TN

Approved:

Manus Donahue, Ph.D.

Wellington Pham, Ph.D.

John Gore, Ph.D.

Douglas McMahon, Ph.D.

DEDICATION

This work is wholeheartedly dedicated to my parents Mary & Leo Barton, who have been a source of unconditional love & support, without which none of this would be possible.

ACKNOWLEDGEMENTS

I would like to thank the faculty and staff of the Vanderbilt Institute of Imaging Science (VUIIS) and the Vanderbilt Brain Institute (VBI). In particular, I thank my committee for their support during my time in the Vanderbilt Neuroscience Graduate Program. Dr. Doug McMahon for allowing me to train in his lab and offering his expertise and insights to improve my dissertation work. Dr. John Gore for providing resources for my professional development and completion of this work and acknowledging my progress following presentations of the studies herein described. Dr. Manus Donahue for serving as my committee chair and undertaking the additional responsibilities required of this position as well as providing immensely useful assessments and guidance both during and outside committee meetings.

I would also like to thank current and former members of the Pham lab; Bo Li, Richard McClure, and Meiying Zhou for their training and assistance provided in and outside the lab. In particular, I thank my advisor Dr. Wellington Pham, who throughout my entire time working with him, was exceptionally supportive and available to discuss our work, my training, and whose encouragement was and will continue to be invaluable throughout my career pursuits as a physician scientist.

Additionally, I would like to thank the Vanderbilt Medical Scientist Training Program (MSTP) for their financial support which has allowed me to receive this training and given me the opportunity to present my work at both local and national meetings as well as the training they have provided. In particular, I would like to thank Dr. Terry Dermody, who represented the MSTP program so well during his tenure as director and who played a major role in my decision to come to Vanderbilt. Dr. Chris Williams, who later became director who has continued to be attentive and supportive of every MSTP trainee including

myself.

I want to thank my friends in both the MSTP program and Neuroscience Graduate Program. Having them to celebrate the successes and encourage me when times were hard made this journey not only tolerable but also one of the best times of my life. I look forward to having them as future colleagues and lifelong friends. Thank you to my family, who have fostered my interests ever since I can remember and always take an interest in my work even if they say they don't know what it means. Just having them there to listen means more to me than anything. To Drs. Michael and Holly Summers, who saw potential in me at a young age and were truly the impetus for me pursuing this career. Both have been mentors to me for more than a decade and I truly think of them as family. Finally, to Sadella Santos, whether it's keeping me company while I genotype mice or waiting for hours in the rain for hours at a race just to cheer me on for a moment, you've always given me the greatest encouragement and support that has allowed me to strive for my dreams. I hope that even as we live so far apart, I've been able to do the same for you. Thank you all.

TABLE OF CONTENTS

LIST OF TABLES

LIST OF FIGURES

Chapter I

Epidemiology & Clinical Features of Alzheimer's Disease

Prevalence and Risk Factors for Alzheimer's Disease

Alzheimer's disease (AD) is the leading cause of dementia and the sixth leading cause of death in the United States, just recently surpassing diabetes[1]. Currently 5.5 million Americans over the age of 65 are living with AD and as the aging population in America is increasing rapidly, the number of people with AD will also increase. By the year 2050, 13.8 million Americans are projected to develop AD unless an effective therapeutic or preventative treatment is discovered[2]. AD is also a leading cause of morbidity, with patients living for years beyond diagnosis as the disease progresses. Estimated healthcare costs for AD-related treatment in 2018 is $277 billion. In 2017, it is estimated that unpaid caregivers (including friends and family members) provided 18.4 billion hours of informal care, an estimated economic value of $232.1 billion[2].

The most apparent and unmodifiable risk factor for developing AD is aging[3]. Besides aging, both genetic and acquired risk factors contribute risk of future development. Early-onset AD (onset < 65 years old) is associated with an autosomal dominant inheritance pattern and is related to a mutation in genes with roles in amyloid precursor protein (APP) breakdown and cleavage including presenilin 1 (*PSEN1*) and presenilin 2 (*PSEN2*). Mutations in the *APP* gene itself can also confer greater risk of AD development[4]. Although early-onset AD is clinically identical to late-onset AD (onset ≥ 65 years old), early-onset usually has a more rapid rate of progression. Genetic contribution to late-onset is more complex as it does not follow typical mendelian inheritance. The most established genetic risk factor for late onset disease is associated with apolipoprotein E (*APOE*), which

is the principal cholesterol carrier protein in the brain[5]. The *APOE* gene has three common alleles: ε2, ε3, and ε4; but of the three, the ε4 allele was identified as a risk factor for late-onset AD[6]. Most studies have shown that having one copy of the ε4 allele confers a two- to three-fold increased risk of developing AD while having two copies confers an eight- to 12-fold increased risk[7]. In addition to *APOE*, more than 20 other candidate genes have been identified to significantly increase risk of AD[8–10]. A family history of dementia is also a risk factor for future development of AD. Those with a first degree relative with dementia have a 3.5% increased risk in developing AD and having two first degree relatives increases risk by 7.5%. Relative risk of AD also increases in a family history of Down's syndrome (2.7%) and Parkinson's disease (2.4%)[11].

In addition to genetic risk factors, acquired risk factors also can increase risk of developing AD. Many of these overlap with factors associated with increased risk of vascular disease and as such, effective management during midlife may reduce chances of later developing AD[12]. Such factors include hypertension[13–15], dyslipidemia[13,16,17], and cerebrovascular disease[18–21]. Interestingly, cerebrovascular disease may also contribute to increasing BBB permeability, providing a shared effect between vascular dementia and AD that may increase overall risk of developing either or mixed dementia where both clinical and pathologic features of both are present[18]. Type 2 diabetes and obesity are also associated with a 1.5-fold increased risk of AD[22,23]. Lifetime physical activity may actually reduce risk of developing AD and other types of dementia. Rates of AD were 45% lower in those who were physically active compared to those who were more sedentary[24]. There also may be sufficient evidence to conclude that healthy dieting and lifelong learning/cognitive

training may also reduce the risk of cognitive decline in advanced age[25].

Several environmental risk factors have been shown to also increase the risk of AD. For example, a study in China demonstrated that second hand smoke exposure increased relative risk by 2.28[26]. Other potential risk factors for AD include both air pollution[27–29] and pesticides[30,31]. However, more work needs to be completed to further evaluate these environmental exposures.

Clinical Features of Alzheimer's Disease

AD typically develops with advanced age as risk of dementia doubles every ten years after 60 years of age[32]. The average life expectancy after diagnosis of AD ranges from three to 11 years with a median of approximately five years, and greatly depends on the level of impairment at the time of diagnosis[33,34]. AD course is typically divided into four stages of disease progression: pre-dementia stage or mild cognitive impairment (MCI), mild AD, moderate AD, and severe AD[35].

Pre-dementia (mild cognitive impairment)

In the pre-dementia stage, signs of dementia are often subtle and undetected by the patient but are more apparent to family or close friends. Typical features of this stage are the patient will have impairment in acquiring new information or skills, impaired ability to plan tasks, dysfunctional access to semantic memory, deficits in concentration or a person could present with noncognitive alterations in behavior including social withdrawal and depressive dysphoria[35,36]. Deficits can be distinguished by neuropsychiatric testing. Typically, patients with MCI will progress to dementia within two to four years after being

diagnosed, but true duration is likely much longer as most patients won't be evaluated until symptoms become more severe. What separates MCI from mild dementia is that patients with MCI are still able to carry out activities of daily living (ADL)[35].

Mild Alzheimer's disease

The most prevalent feature of mild AD is a significant impairment in learning and memory. Old declarative memory and short term memory are relatively intact while there is usually a deficit in recent declarative memory[35]. This can manifest as an inability to recall major recent events such as a visit with a relative or close friend. A patient will have difficulty with planning and organizing, which interferes with ADLs such as paying bills or cooking. Often, a person with mild AD can live independently but will require assistance from a caregiver for some tasks. Verbal communication may also be impaired at this stage as vocabulary and fluency is diminished[35]. Patients are often aware of their cognitive deficits and will demonstrate a flattening affect and withdrawal as a means to hide their symptoms from others. The average duration of this stage is 1.5 years before progressing to moderate AD.

Moderate Alzheimer's disease

In moderate stages of disease, recent memory is drastically compromised and logical reasoning, planning, and organization are also significantly impaired[35]. Patients will require assistance to complete more basic ADLs such as dressing themselves and bathing. They may also become incontinent[36], often requiring a transition in care with either at home health care or transfer to an assisted living facility. There are also greater deficits in language including word finding difficulty and paraphasia as well as deficits in reading

comprehension. Patients will often have cortical visual agnosia including prosopagnosia, an inability to recognize faces of familiar people. Psychiatric symptoms are also common including delusional symptoms, loss of emotional control, restlessness, and aggression[35]. The moderate stage of AD lasts for 2.5 years on average[36].

Severe Alzheimer's disease

In severe AD, even early memories are compromised and can impair a patient's ability to recognize or recall their closest friends and family. Language is dramatically reduced, and patients are unable to articulate basic sentences. Aggression, restlessness, apathy and exhaustion are more apparent and worsen progressively[35]. Motor deficits also occur including dysphagia, immobility, rigidity, and contractures in extremities. Other motor signs can be discerned on examination such as myoclonus and emergence of primitive reflexes like the Babinski plantar extensor reflex. The most frequent cause of death is pneumonia resulting from aspiration due to dysphagia or from being bedridden. Patients also commonly develop infected decubital ulcers which can lead to fatal septicemia[35,36].

Clinical Diagnostic Criteria

A definitive diagnosis of AD requires histopathologic examination[33,34]. However, this is rarely done in life and therefore diagnosis is dependent on following clinical criteria. The first classification scheme of AD, established in 1984, was the National Institute of Neurological and Communicative Disorders and Stroke and the Alzheimer's Disease and Related Disorders Association (NINCDS–ADRDA) criteria. These criteria would classify a case as probable, possible and definite AD[37]. Updated criteria for a probable diagnosis of AD were established by the National Institute on Aging and the Alzheimer's Association

(NIA-AA) and recently updated in 2011[38]. This classification system provides criteria for the diagnosis of probable AD (Table.1-1), possible AD (Table.1-2) and MCI due to AD. The Diagnostic and Statistical Manual of Mental Disorders (DSM-V) criteria for AD were updated in 2013 and are also commonly used for clinical diagnoses[39]. In general, these criteria are very similar in that they focus on cognitive decline and its effect on a patient's ability to function. However, these guidelines require that delirium and other medical causes of cognitive dysfunction are considered before diagnosing a patient with possible/probable AD or other dementia.

NIA-AA Core Clinical Criteria for Probable AD

Neuropsychiatric symptoms that:

1) Interfere with ability to function at work or at usual activities
2) Are not explained by delirium or major psychiatric disorder
3) Cognitive impairment established by history-taking from the patient AND a knowledgeable informant in addition to objective bedside mental status examination
4) Cognitive impairment involving a minimum of two domains:
    a. Impaired ability to acquire and remember new information
    b. Impaired reasoning and handling of complex tasks, poor judgement
    c. Impaired visuospatial abilities
    d. Changes in personality, behavior, or comportment
5) Insidious onset
6) Clear-cut history of worsening symptoms
7) Initial and most prominent deficits are in one of the following:
    a. Amnestic presentation: recent memory impairment
    b. Non-amnestic presentation:
        i. Language impairment with word-finding deficits
        ii. Visuospatial impairment with visual cognitive deficits
        iii. Dysexecutive presentation with prominent impairment of reasoning, judgement, or problem solving
8) No Evidence of substantial:
    a. Concomitant cerebrovascular disease
    b. Core features of Dementia with Lewy bodies
    c. Features of behavioral variant of frontotemporal dementia
    d. Features of semantic or nonfluent/agrammatic variants of primary progressive aphasia
    e. Other concurrent, active, neurological or non-neurological disease process or modification

Table 1-1. NIA-AA Core Clinical Criteria for Probable AD[38].

NIA-AA Core Clinical Criteria for Possible AD
Atypical course – meets the core clinical criteria in terms of the nature of cognitive deficits for AD dementia, but either has a sudden onset of cognitive impairment or demonstrates insufficient historical detail or objective cognitive documentation of cognitive decline OR Etiologically mixed presentation – meets all core clinical criteria for AD dementia but has evidence of (a) concomitant cerebrovascular disease, defined by a history of stroke temporally related to the onset or worsening of cognitive impairment; or the presence of multiple or extensive infarcts or severe white matter hyperintensity burden; or (b) features of Dementia with Lewy bodies other than the dementia itself; or (c) evidence for another neurological disease or non-neurological medical comorbidity or medication use that could have a substantial effect on cognition

Table 1-2. NIA-AA Core Clinical Criteria for Possible AD[38].

Differential Diagnosis

Delirium

When evaluating a patient with cognitive impairment, it is important to first differentiate between delirium or dementia. Dementia is a chronic and global deterioration in cognition while delirium is acute and transient with fluctuating changes in attention, cognition, and consciousness. Unlike most causes of dementia, delirium is often reversible and rapid identification of the underlying etiology is critical for effective management[40,41]. Delirium is further characterized by inattention, changes in consciousness, disorganized speech and thinking, hallucinations, delusions, and paranoia. Onset of delirium is usually abrupt, with symptoms fluctuating over minutes to hours while symptoms of dementia are typically more consistent throughout the day and cognitive decline is progressive. The most common causes of delirium are drugs (particularly anticholinergics, opioids, and psychoactive drugs), dehydration, and infection but many other conditions are also possible causes and differentiation is dependent on history, physical examination and lab testing[40].

Vascular Dementia

When diagnosing a patient with a specific type of dementia, AD accounts for over half of all dementias[42] and thus is the most likely cause, especially in an elderly patient. However, other etiologies must also be considered and will be reviewed here. Vascular dementia accounts for approximately 20% of all cases of dementia[42]. It compromises any cerebrovascular etiology and is divided into two general classifications: multi-infarct dementia and diffuse white matter disease. Having several strokes may result in chronic cognitive deficits and is thus called multi-infarct dementia. Unlike the gradual deterioration

seen in AD, patients report episodes of sudden worsening of symptoms in a stepwise progression, coinciding with another stroke that may otherwise be asymptomatic. On neuroimaging, multiple infarcts can be seen. However, mixed dementia, a combination of two or more types of dementia are very common and are most often from both AD and vascular dementia[43]. In fact, AD was shown to be comorbid with vascular pathology in over 80% of cases based on neuropathological exam[44]. Therefore, multiple infarcts on imaging does not preclude the possibility of AD also contributing to clinical symptomatology. Neuroimaging evidence of bilateral abnormalities of subcortical white matter is known as diffuse white matter disease and is often associated with lacunar infarctions, though other rarer causes are also possible. Symptoms of dementia may progress more slowly but can also occur stepwise similar to multi-infarct dementia. However, pyramidal and cerebellar signs may also be present in diffuse white matter disease[43]. Treatment focuses on preventing future cerebrovascular events by addressing underlying causes such as hypertension or diabetes[43].

Frontotemporal Dementia

Frontotemporal dementia (FTD) is the third most common form of dementia behind AD and dementia with Lewy bodies (DLB)[45]. Similar to AD, prevalence of FTD increases with aging and often is diagnosed in patients 50 to 70 years of age[43]. Early symptoms of FTD are categorized into behavioral, language, and motor abnormalities and manifestation is dependent on the site of neurodegeneration. Unlike AD, behavioral symptoms usually occur early while memory is spared until later in disease progression and these key differentiating features are important in distinguishing the two types of dementia. Typical behavioral features in FTD include apathy, disinhibition, weight gain, food fetishes,

compulsive behaviors, and loss of empathy[43]. Pathologically, FTD is characterized by abnormal protein aggregation in brain regions which undergo neurodegenerative changes including the frontal lobes, anterior temporal lobes, anterior cingulate cortex, and insular cortex. Structural and functional neuroimaging techniques are able to visualize atrophy, hypoperfusion, and hypometabolism of affected brain regions in later stages of disease[46,47]. The most commonly found aggregated proteins on postmortem examination are the microtubule-associated protein tau (MAPT), the TAR DNA-binding protein (TDP-43), or fused-in-sarcoma protein (FUS)[45]. Though the clinical features and underlying pathology between FTD and AD are different, the prognosis is the same as there are no disease-modifying therapeutics available. Patients with FTD have an average life expectancy of eight years after symptom onset[45].

Parkinson's Disease Dementia and Dementia with Lewy Bodies

Parkinson's disease (PD) is classically described by characteristic motor symptoms including bradykinesia, muscular rigidity, resting tremor, and postural and gate abnormalities[48]. Prevalence of PD increases with age and has an average age of onset close to 60 years, though there are cases that can develop earlier in life even as early as 30 years of age[49]. The key pathologic feature of PD is loss of dopaminergic neurons in the substantia nigra pars compacta (SNpc), resulting in basal ganglia dysfunction and the characteristic motor symptoms. Another pathological finding in PD are intraneuronal α-synuclein protein aggregates known as Lewy bodies[50]. However, neuronal loss is not restricted to the SNpc as other brain regions are also affected[50]. Total neurodegenerative changes likely account for non-motor symptoms also seen in PD. Of these, cognitive dysfunction and dementia frequently develop in PD patients. In fact, there is a six-fold

increase in risk of developing dementia when compared to age-matched controls without PD[51]. This is collectively known as Parkinson's disease dementia (PDD). Dementia can also precede motor symptoms, and this is known as dementia with Lewy bodies (DLB). Thus, in the absence of motor symptoms in the early stages of DLB, differentiating from AD can be more challenging. However, both DLB and PDD differ from AD in that attention, executive, and visuo-spatial dysfunction is more prevalent in DLB and PDD while language and memory deficits are less characteristic[52]. Additional clinical features including fluctuating cognition, visual hallucinations, and rapid eye movement (REM) behavioral sleep disorder. These features make it possible to clinically distinguish from AD on getting an accurate history and careful cognitive testing[53]. Though the motor symptoms of DLB and PDD dementia can be managed with levodopa or deep-brain stimulation, pharmacologic management of cognitive symptoms and hallucinations is difficult as many medications can improve one symptom while making others worse[53].

Creutzfeldt-Jakob Disease

Creutzfeldt-Jakob Disease (CJD) is a spongiform encephalopathy, also known as a prion disease. The normal prion protein (PrP^{C}), encoded by the prion gene (*PRNP*), is found in all mammals but it's function is unknown[54]. In prion disease, the protein-only hypothesis states that abnormally misfolded protein (PrP^{Sc}), replicates by converting normally folded protein into PrP^{Sc}, thereby serving as the infectious agent. This hypothesis is supported by many observed characteristics of disease such as injection of PrP^{Sc} into animals induces prion disease, PrP knockout mice are resistant to prion infection, and PrP^{Sc} self-propagates in vitro through induction of misfolding in PrP^{C}. However, the mechanism by which this processes causes neurodegeneration remains unknown[55], though buildup of PrP^{Sc}

aggregates may have a role. CJD is heterogenous disorder and can occur sporadically, be transmitted, or acquired by inheritance. Of these, sporadic disease is the most common, accounting for 85% of cases[55]. Regardless of the mode of acquisition, characteristic brain lesions consisting of diffuse or clustered vacuolation that can range from mild to severe and be found in varying brain regions. The location and severity of changes is used to classify the disease[55,56].

As the location and extent of neurodegeneration is highly variable, there can also be significant variability in the clinical features, especially early in disease pathogenesis. Classically, CJD presents with rapid cognitive decline, ataxia, and myoclonus[54]. A rapid decline with death typically occurring within the first year of symptom onset is what typically differentiates CJD from AD and DLB, which have slower rates of progression[57,58]. However, the initial signs and symptoms can have significant overlap, making it difficult to differentiate in early stages especially in cases where CJD presents with only dementia and none of the motor deficits associated with disease[58]. Even when motor deficits and focal abnormalities are present, it may be difficult to differentiate CJD from DLB clinically as they share more features than what is typically seen in early AD. MRI is useful in differentiating CJD from other types of neurodegeneration with characteristic findings including cortical and/or basal ganglia hyperintensities seen in 96% of sporadic cases of CJD. Elevated CSF levels of specific protein biomarkers including 14-3-3, S100b, and tau are also diagnostically useful[54]. Though neuroimaging and CSF measures can be useful in differentiating CJD, there are currently no therapeutics available and disease is always fatal.

Reversible Causes of Dementia

Though there are limited treatments available, differentiating what neurodegenerative disease a patient has is important for symptomatic management as well as preparing for future complications. However, it is critical to first rule out reversible causes, as these may account for as many as 23% of patients first presenting with dementia[59]. Though there are many potential causes, the most likely include alcohol and drug related dementia, depression induced cognitive impairment, CNS infections, metabolic disorders (hypothyroidism, hypoparathyroidism, vitamin B12 deficiency), normal pressure hydrocephalus, tumors, and chronic subdural hematomas[59]. In a routine evaluation of dementia, the American Academy of Neurology recommends structural neuroimaging, screening for depression, and serum testing including complete blood count, blood glucose, thyroid function tests, serum electrolytes, BUN/creatinine ratio, serum B12, and liver function tests to rule out most common causes of reversible dementia[60]. However, a detailed history and thorough clinical exam can be helpful in what additional testing should be done for other reversible causes of dementia[59].

Clinical Evaluation

A possible/probable diagnosis of AD is dependent on clinical assessment when using the NIA-AA or DSM-V classification schemes. Although sensitivity and specificity may be limited[38], misdiagnoses are most commonly a non-reversible cause of dementia with either vascular or mixed dementia being most likely, as together they account for 25-40% of dementia cases while AD makes up 50-60%. An algorithm for initial evaluation of a patient with dementia is provided in figure 1-1. Clinical evaluations are highly dependent on establishing a history of onset and progressive cognitive decline. In this circumstance,

accounts from those close to the patient are paramount to establish a diagnosis. Beyond the history, interviewing the patient directly can also provide insight into cognitive function. Evidence of word finding difficulties, aphasia, and unusual behavior can provide evidence to the type of dementia. Also, if a patient appears unalert or unresponsive, it is important to consider drug use or delirium before further workup is done[42]. When interviewing a patient or caregiver, consider the following: symptoms at onset, progression of symptoms, impact on work and family, safety issues (driving, etc.), risk factors for dementia (as described above), and past medical history[42]. It is also important to account for a patient's age as AD is more likely in elderly patients. In a young patient, AD should still be considered but also genetic and metabolic disorders are more common than in older patients and should also be included in the differential diagnosis[42].

Following history, a cognitive and neurological exam must also be completed to rule out other possible causes. The Mini-Mental Status Examination (MMSE) can easily be administered in five to ten minutes and is the most commonly used mental status examination used clinically. It tests various cognitive domains including memory, orientation to place and time, naming, reading, visuospatial orientation, writing, and the ability to follow commands. A patient is scored from zero to 30 and less than 24 is considered positive for cognitive impairment[61]. However, MMSE scores can vary with age and education level[62]. Thus, the MMSE is not a diagnostic test but instead a way to identify current cognitive deficits and can be used to show cognitive decline on repeated testing. The functional activity questionnaire (FAQ) does not measure mental status but instead reviews ADLs that may be more difficult with dementia. As a patient with dementia may be unaware of their functional capacity, the FAQ is answered by a family member or friend

who is around the patient regularly[61]. At first evaluation, blood tests should also be done to identify or rule out reversible causes of dementia. A typical panel would include complete blood cell count, electrolytes, glucose, renal and liver function tests, thyroid stimulating hormone, serological tests for syphilis, and vitamin B_{12} as an abnormal result in these may indicate a treatable cause.

Structural neuroimaging may be done if other causes of dementia are suspected including vascular disease, normal pressure hydrocephalus, tumors, abscess, or subdural hematoma[61]. The yield for identifying a potentially reversible cause of dementia is low. However, the American Academy of Neurology recommends either an MRI or non-contrast CT on initial workup of dementia. Other neuroimaging techniques including linear or volumetric MRI or CT, and PET imaging are not recommended[63]. Following the initial evaluation, more formal neuropsychological testing may be done. Testing is done by either a trained psychologist or psychometrician to identify specific deficits in higher cognitive function including memory, attention, processing speed, reasoning, judgement, and problem-solving, spatial, and language functions[64]. Results provide a more objective measure of function, may identify deficits in patients with higher cognitive function and distinguish between MCI and dementia[61]. Neuropsychological testing may aid in determining the type of dementia in addition to establishing a baseline of function to track progression and may also provide guidance into a patient's ability to carry out ADL such as driving or managing their own finances as well as determining the level of assistance they may require at that time[65]. Further evaluation can be done in suspected cases of AD using biomarker measurements. However, these techniques are also not recommended for routine diagnosing of AD and are mainly reserved for research purposes[38]. Both established and

experimental biomarkers of AD as well as neuroimaging will be discussed in more detail in chapter three. Genetic testing is also not done in routine evaluation except in cases of early-onset AD or with a strong family history where mutations in *APP*, *PSEN1*, or *PSEN2* may result in an autosomal dominant pattern of inheritance[65].

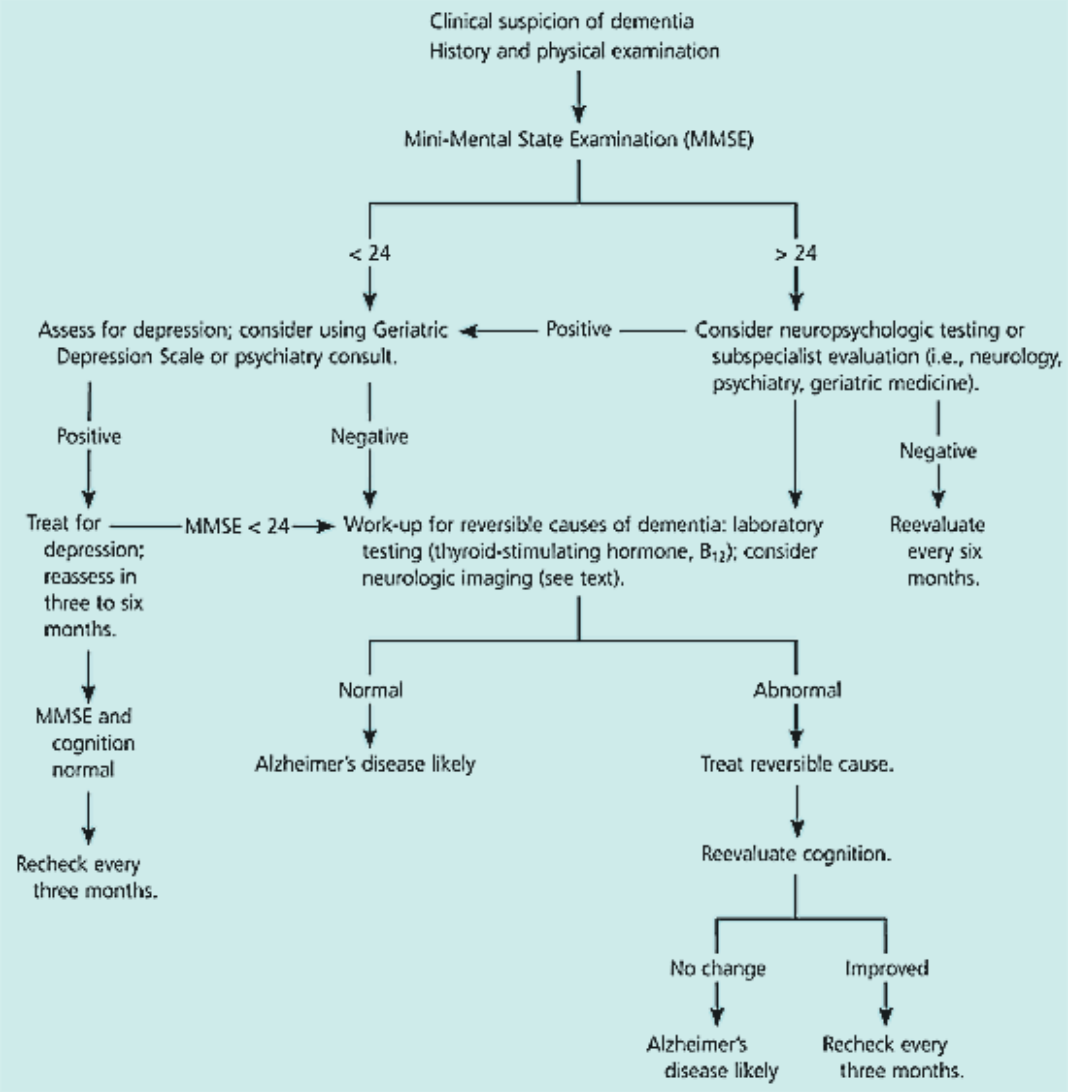

Figure 1-1. Algorithm for initial evaluation of a patient with dementia. Reprinted with permission from American Academy of Family Physicians[61].

Chapter II

Alzheimer's Disease Pathology, Progression, and Pharmacological Intervention

Amyloid Pathology and the Amyloid Cascade Hypothesis

Abnormal accumulation of Aβ is a key pathologic feature of AD and the central principle of the amyloid cascade hypothesis. According to this hypothesis, under normal physiologic conditions, the amyloid precursor protein (APP) is sequentially cleaved by α-secretase and γ-secretase to produce three soluble fragments which are readily cleared from the brain. This is known as the non-amyloidogenic pathway[66]. Alternatively, in the amyloidogenic pathway, sequential cleavage of APP by β- and γ-secretase to produce Aβ peptide[67,68] (Fig.2-1). Aβ then aggregates in β-sheet conformations to form insoluble Aβ plaques, which cause microglial activation, cytokine release, reactive astrocytosis, inflammatory activation, and induce tau hyperphosphorylation leading to formation of neurofibrillary tangles (NFTs)[69–72] (Fig.2-2). Aβ deposition also results in synaptic loss and neuronal death, though the primary mechanism of toxicity is still under investigation[73]. Aβ-induced pathological changes in particular brain regions, including the hippocampus, are thought to cause the cognitive deficits associated with AD[74]. The amyloid cascade hypothesis was further supported by studying familial cases of AD. Mutated genes identified in studying inherited forms of AD have been shown to increase Aβ production or accumulation[75]. Also, early onset AD occurring before the age of 65 is highly prevalent in people with Down syndrome (DS) (trisomy 21), with most individuals developing AD in their 50s[76]. The APP gene is located on chromosome 21 and triplication of this chromosome in DS results in an increased gene dosage effect to accelerate Aβ plaque deposition[77].

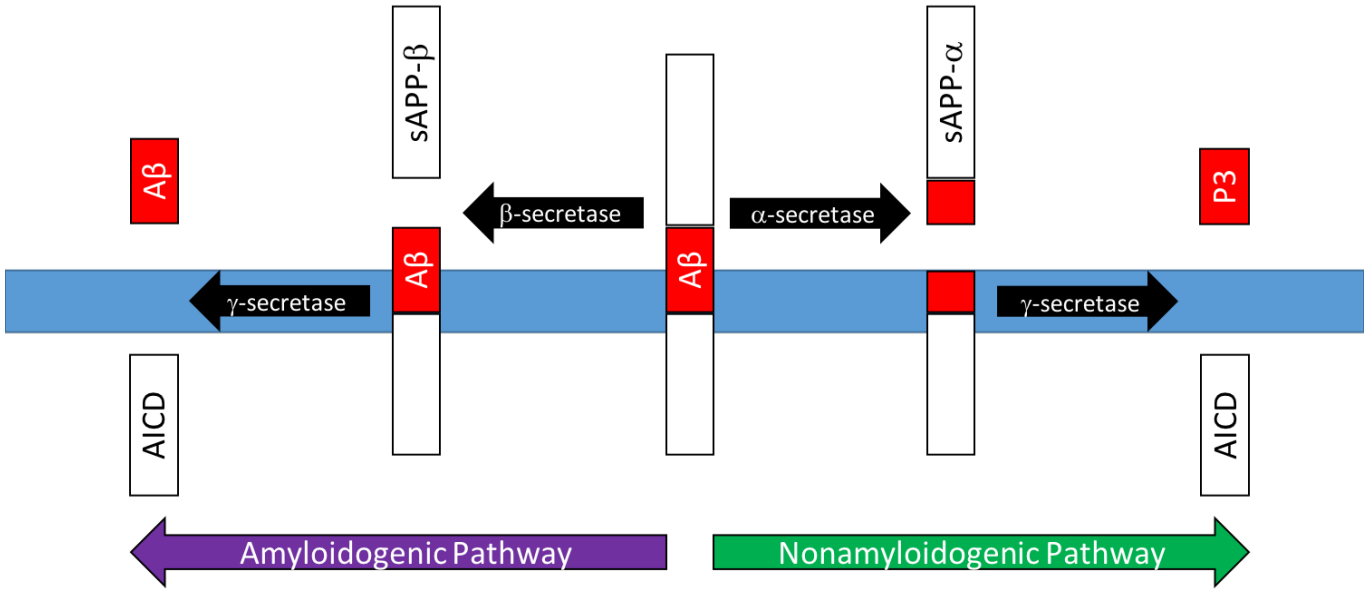

Figure 2-1. APP can be processed by the amyloidogenic or nonamyloidogenic pathway. In the nonamyloidogenic pathway, APP cleaved by α-secretase at the Aβ fragment and the soluble APP-α (sAPP-α) fragment is released. The remaining domain is then cleaved by γ-secretase to release the APP intracellular domain (AICD) and the P3 fragment. In the amyloidogenic pathway, APP is instead cleaved by β-secretase to first release the soluble APP-β (sAPP-β) fragment then further cleaved by γ-secretase to form AICD and Aβ.

Although Aβ plaque deposition is a key feature in most models of AD pathogenesis, total accumulation does not correlate well with clinical severity of disease[78] or brain volume loss[79]. In fact, significant Aβ plaque deposition can be found in cognitively normal elderly individuals[80]. The reason for poor correlation between Aβ plaque deposition and neuropathological changes as well as with clinical severity may be explained by the existence of soluble Aβ oligomers, which have been shown to be neurotoxic and impair synaptic activity[81,82]. Soluble Aβ also correlates more closely with indices of disease severity[78]. These findings suggest that Aβ exists in equilibrium between soluble and insoluble states and it is the soluble form that exerts some of the neurotoxic effects that have been previously associated with Aβ plaques. However, as large insoluble protein aggregates are likely to be surrounded by smaller and more diffuse Aβ oligomers, it becomes difficult to determine which is actually causing neuronal injury *in vivo* as most research into the cellular and molecular mechanisms of toxicity have been conducted *in vitro*[83]. For the purposes of therapeutic development, determining the contribution of soluble and aggregated Aβ-mediated toxicity is essential as an effective therapeutic may preferentially target one or both. However, findings demonstrating Aβ-mediated toxicity support the utility of targeting either soluble or insoluble Aβ as a biomarker for AD.

Other Pathological Features of Alzheimer's Disease

Neurofibrillary tangles

Another pathologic feature of AD is NFT formation. NFTs are composed of hyperphosphorylated tau aggregates. Under normal conditions, tau proteins associate with microtubules and function in both microtubule assembly and stabilization, which are

critical in intracellular and axonal transport. The ability of tau to associate with microtubules can be modulated via phosphorylation, where hyperphosphorylation reduces binding affinity[84]. In AD, pathologic hyperphosphorylation of tau results in intracellular aggregation to form NFTs. This is thought to disrupt axonal transport activity and lead to eventual neuronal death. Although Aβ has been shown to induce tau hyperphosphorylation[72], the way by which these two pathologic features of AD are associated remains unclear. One proposed hypothesis is that elevated activity of glycogen synthase kinase 3β (GSK3β), a regulatory kinase that mediates phosphorylation at serine/threonine[85], may play a key role in AD pathogenesis. Several studies have shown that GSK3β activation results in increased levels of Aβ as well as phosphorylating tau, leading to NFT formation (Fig.2-2). The role of GSK3β in AD pathogenesis was supported by showing that inhibition of GSK3β led to a reduction in AD pathology and ameliorated cognitive decline in transgenic mouse models[86–90]. It is also possible that Aβ formation may elevate GSK3β activity[91]. GSK3β is also implicated in voltage-dependent anion channel 1 (VDAC1) phosphorylation, causing detachment of hexokinase from VDAC1 at the outer mitochondrial membrane[92]. Hexokinase is a glycolytic enzyme functioning in transfer of a phosphate group to hexose for the purposes of adenine triphosphate (ATP) synthesis. Hexokinase also inhibits apoptosis when bound to VDAC1 by preventing the release of cytochrome c, an electron transport chain protein which induces apoptosis when released from mitochondria into the cell cytoplasm[91,93–95] Inhibited interaction between VDAC1 and hexokinase mediated by GSK3β may lead to low ATP availability in mitochondria via reduced glucose metabolism as well as promote neuronal apoptosis in AD[91]. However, recent evidence suggests that tau pathology may originate in the lower

brainstem rather than in the transentorhinal region as previously described and thus may precede initial cortical plaque formation[96]. These findings imply that both Aβ oligomer and NFT formation must occur independently for development of AD. In addition to the unclear relationship between Aβ oligomers and NFTs, tau aggregation is a pathologic feature of other neurodegenerative diseases (collectively known as tauopathies) including frontotemporal dementia, the most common form of dementia after AD[97]. The presence of tau aggregation in other diseases limit its use as a biomarker, particularly in presymptomatic stages of disease, to differentiate various types of dementia. However, because it is a shared pathologic feature, therapeutic targeting thus has the potential for application not only in AD, but for all tauopathies.

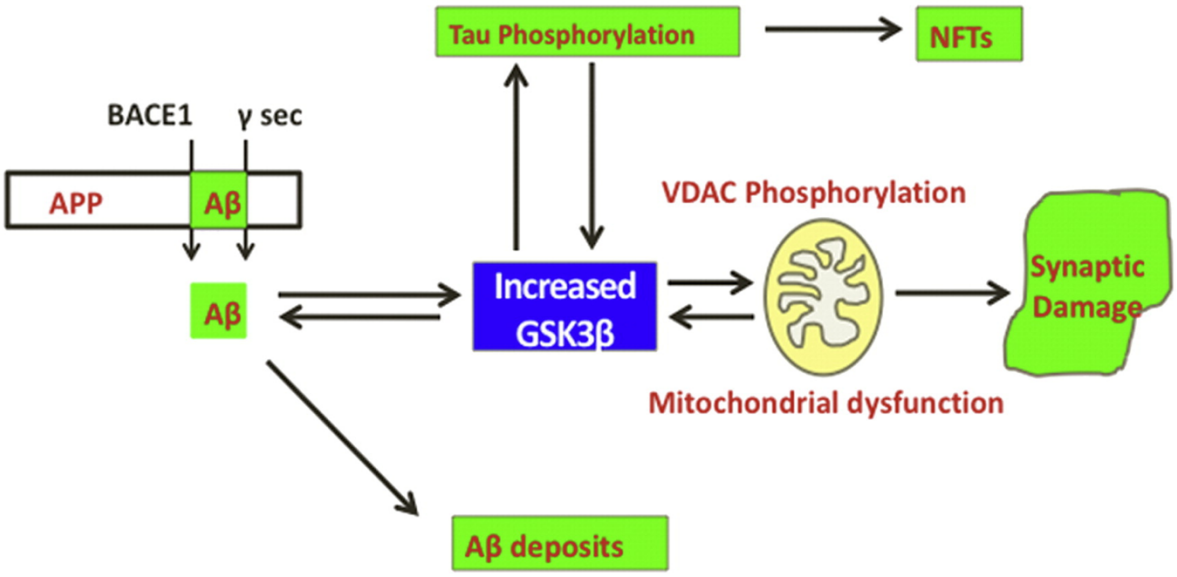

Figure 2-2. Glycogen synthase kinase 3β and AD pathology. Aβ-induced elevated GSK3β activity is a key event in abnormal APP processing, increased Aβ production, and phosphorylation of tau and synaptic pathology in AD. GSK3β is proposed to activate VDAC1 phosphorylation that leads to mitochondrial dysfunction and synaptic damage in AD. Reprinted from BBA Molecular Basis of Disease[91] with permission from Elsevier.

Vascular pathologies

Recent evidence suggests there is significant overlap in patients having both cerebrovascular disease (CVD) and AD with further evidence suggesting an additive or synergistic effect on cognitive decline and development of clinically observable dementia[98]. Risk factors of cardiovascular disease prior to AD diagnosis including high cholesterol, elevated low-density lipoprotein (LDL), and a history of diabetes are all associated with a faster cognitive decline in AD patients[99]. AD also presents with findings of CVD including small vascular disease (SVD), microvascular injury, and cerebrovascular lesions (CVLs)[98]. Cerebral amyloid angiopathy (CAA) shares similar pathology to AD and occurs when Aβ peptide aggregates in small cerebral vessels, particularly arterioles of the cortex, which can lead to serious complications in advanced stages including vascular rupture and spontaneous hemorrhage[100]. Sporadic CAA is present in 82% to 98% of AD cases, more often in patients with ApoE2 and ApoE4 alleles[101] and has been suggested to contribute to neurodegenerative changes seen in AD[102]. However, other evidence supports that AD and CVD, including CAA, exert an additive rather than interactive effect on cognitive decline[103]. Further studies are needed to determine the relationship between AD and CVD as well as the role each plays in progression from normal cognitive function to dementia.

Current Therapies in Alzheimer's Disease

Currently there are only five Food and Drug Administration (FDA)-approved treatments available for AD, none of which are disease-modifying therapies. Instead these drugs provide symptomatic relief for the cognitive symptoms of AD with the goal of maintaining or improving quality of life and prolonging patient independence before more intensive

care is required in later stages of disease. Three of the approved treatments are from the same class, known as cholinesterase inhibitors (ChIs), which act to increase the levels of synaptic acetylcholine (ACh). The fourth drug, memantine, is an N-methyl-D-aspartate (NMDA) receptor antagonist and acts to reduce glutamate toxicity[104]. The fifth medication (Namzaric), is a combination of a single acetylcholinesterase inhibitor and memantine[105]. In addition to currently available treatments, there are experimental AD therapies in various stages of development, including clinical trials, targeted at reducing Aβ plaque and NFT formation. Both FDA-approved and experimental treatments will be reviewed below.

FDA Approved Therapies

Acetylcholinesterase inhibitors

The cholinergic hypothesis of AD states that ACh deficiency contributes to the neuropsychiatric symptoms seen in AD. This hypothesis is supported by the observations that there is a cholinergic deficiency in AD, resulting from atrophy of the nucleus basalis of Mynert, which produces ACh and has efferent projections throughout cortical regions[106]. AD patients develop an array of neuropsychiatric disorders including agitation, psychosis, mood changes, anxiety, personality changes, purposeless motor activity, and alterations of sleep, appetite and sexual behavior[106–108]. The cholinergic hypothesis is further supported by observations that AD patients become more hostile when given anticholinergic agents[109], while drugs that increase ACh activity reduce agitated behaviors[110,111].

Therefore, increasing ACh neurotransmission should provide symptomatic relief of neuropsychiatric symptoms in AD. One strategy for increasing ACh in the cortex is using ChIs, which function by inhibiting cholinesterase, an enzyme found within synapses whose

function is to degrade ACh[112]. Tacrine (Cognex, First Horizon Pharmaceuticals) was the first ChI approved for AD in 1993[104]. However, it was discontinued due hepatotoxicity[113]. Currently there are three ChIs available for treating AD including donepezil (Aricept, Pfizer), rivastigmine (Razadyne, Novartis) and galantamine (Exelon, Janssen)[114]. Rivastigmine and galantamine are approved for treatment of mild-to-moderate AD while donepezil is approved to treat all stages of disease[105,115]. ChIs are commonly used as the first line of treatment for AD disease as they delay a decline in cognitive function for six to 12 months following initiation of treatment[116]. Early initiation of treatment shortly after diagnosis is preferred as early intervention conserves a patient's ability to carry out activities of daily living (ADL) and maintain independence. However, beyond six to 12 months, ChIs do not show additional therapeutic benefit.

NMDA receptor antagonists

Another FDA-approved drug, memantine (Namenda, Lundbeck) protects neurons from excitotoxicity damage by acting as an uncompetitive NMDA receptor antagonist to prevent glutamate-mediated activation[104]. Clinical trials using memantine demonstrated improvements in cognition while reducing behavioral and psychological symptoms when used in AD patients with moderate-to-severe stages of disease[117,118]. Further work demonstrated when memantine is used in combination with donepezil, patients with moderate-to-severe AD showed improvement in cognition, ADL, and behavior than compared to memantine alone[119–121].

Experimental Therapies

Targeting Aβ plaques

Given that Aβ plaques are a key pathologic feature and demonstrated to mediate characteristic neurodegenerative changes associated with AD, significant efforts are underway to develop drugs that prevent or reduce aggregate formation. One approach for this was to develop drugs that inhibit amyloid aggregation. Tramiposate (Alzhemed, Neurochem Inc.) is a glycosaminoglycan (GAG) mimetic that competes for the GAG-binding to prevent fibril formation[122]. The drug was well tolerated in phase I and phase II trials, while CSF Aβ levels were reduced from baseline by up to 70% after three months. However, there was no difference in clinical symptoms between treatment and placebo groups[123,124]. Other compounds designed to prevent Aβ plaques aggregation, including colostrum (O-CLN, ReGen Therapeutics) and *scyllo*-inositol (ELND005, Transition Therapeutics/Elan), similarly demonstrated unsustained or no therapeutic benefit[104,125].

Another approach for reducing total plaque burden is in developing selective $A\beta_{42}$-lowering agents. $A\beta_{42}$ is formed by sequential cleavage of APP by β-secretase and γ-secretase. This is known as the amyloidogenic pathway of APP processing. γ-secretase can cleave at either amino acid position 40 or 42 of Aβ and both of these cleavage products are implemented in formation of senile plaques in AD. In particular, $A\beta_{42}$ has the greatest tendency to aggregate into fibrils and form plaques. Conversely, if APP is cleaved by α- then γ-secretase, known as the non-amyloidogenic pathway, this is not associated with AD plaque formation[104]. Therefore, by increasing α-secretase activity or inhibiting either β- or γ-secretase cleavage, Aβ plaque formation will be reduced[126]. One promising approach was targeted inhibition of β-site APP cleaving enzyme (BACE). However, inhibition of BACE presents a challenge for two key reasons. First, BACE functions in cleavage of many

different proteins and inhibition may be detrimental to other essential physiologic processes. Second, BACE has a large active site requiring large compounds for inhibition, many of which are unable to penetrate the BBB[104]. Despite these limitations, several BACE inhibitors have made it to clinical trials[127]. The most recent phase II/III clinical trials were carried out by Merck studying the BACE inhibitor verubecestat on patients with mild-to-moderate AD. Unfortunately, as in other trials of BACE inhibitors, verubecestat had no effect on the cognitive or functional decline of patients despite reducing CSF concentrations of $A\beta_{40}$ and $A\beta_{42}$ by over 70%. Additionally, adverse events were more common with verubecestat than in the placebo group[128]. The trial was stopped early due to the lack of clinical benefit and increased risk posed to patients. Similar to BACE, γ-secretase has many substrates and inhibiting cleavage could produce toxic side effects[123]. Despite this, several γ-secretase inhibitors have undergone clinical trials and yielded no therapeutic benefit[129–132]. A trial involving semagacestat (LY-450139) even caused a decline in cognitive function likely due to accumulation of neurotoxic peptides[129]. Finally, efforts have been made to develop an α-secretase activator, with the goal of increasing APP processing via the non-amyloidogenic pathway to reduce Aβ formation[133]. Several α-secretase activators have been studied in clinical trials but further studies were either not pursued or findings of these trials have not yet been published[134].

Targeting tau aggregation

Multiple experimental therapeutics have been identified to act as tau aggregate inhibitors[104]. One such therapeutic, methylene blue, has been previously used clinically to treat a variety of conditions including resistant plaque psoriasis[135] and

methemoglobinemia[136]. It is also used as a stain in various procedures such as sentinel lymph node identification and biopsy in breast cancer[137]. Surprisingly, methylene blue also blocks tau-tau binding to prevent aggregation[138]. Phase II clinical trials demonstrated improvement in AD patients after treatment with methylene blue. However, the compound also turns urine blue, making true blinding in clinical trials impossible and this must be considered when interpreting results.

A different approach would be to develop tau kinase inhibitors, that would reduce tau phosphorylation as hyperphosphorylated tau is what forms intracellular aggregates characteristic of AD. Glycogen synthase kinase 3 (GSK3), a serine/threonine protein kinase, is a potential therapeutic target to reduce NFT formation[139]. Lithium, a GSK3 inhibitor has been shown to improve cognitive function in MCI and therefore may be used as a therapeutic in AD[140].

Active Immunotherapy

Immunotherapy is one of the most sought after treatments for AD with both active (vaccination) and passive immunization (monoclonal antibodies) currently being pursued[104]. In 1999, vaccination with Aβ as an antigen was first demonstrated to attenuate plaque formation in AD transgenic mice overexpressing APP. Immunizing was shown to be effective both in young and aged mice at varying stages of pathologic progression[141]. One of the first trials done in humans was carried out in 2001 using human $A\beta_{42}$ administered with an adjuvant. Unfortunately, the trial had to be terminated after completion of only two to three injections due to complications including

meningoencephalitis in 6% of enrolled patients. Of the 300 enrolled patients, only 19.7% developed the predetermined antibody response[142]. Follow-up on patients enrolled in this trial including an autopsy study suggested that the immunization did in fact slow AD pathologic progression and cognitive function declined less rapidly in patients receiving the immunization[143]. These findings suggested that if the clinical safety of vaccination was improved then active immunization could be a viable approach. However, these conclusions were later refuted with a separate long-term follow-up study demonstrating that plaque reduction was highly variable in treated patients. There was no improved survival in immunized patients and plaque clearance did not prevent neurodegeneration[144]. Despite the inconclusive results and clinical risks associated with this approach, investigation into active immunization is ongoing[145].

Passive Immunotherapy

An alternative approach to vaccination that is under investigation is passive immunotherapy through administration of monoclonal antibodies directed against various Aβ epitopes. Vaccination approaches for tau pathology have also been considered but development is complicated by the fact that tau aggregates form intracellularly[123]. Bapineuzumab is one of the earliest and most well studied anti-Aβ human monoclonal antibodies. Phase II clinical trials of this antibody, which binds to the N-terminal of Aβ, was shown to improve cognition and reduce brain atrophy in patients lacking the ApoE4 allele. However, some patients in the treatment group developed vasogenic edema, a potentially lethal complication[146]. Later, phase III clinical trials testing intravenous bapineuzumab in both ApoE4 carriers and noncarriers yielded no benefit in biomarker or

cognitive measures[147]. Three phase III clinical trials were conducted using solanezumab, a more recently developed humanized monoclonal antibody that binds the mid-domain of Aβ. The results of the most recent of these clinical trials was published in January 2018. In all trials, solanezumab did not significantly slow cognitive decline in patients with mild AD[148]. Failures in clinical trials using both active and passive immunization along with the high cost of administering repeated dosing of antibodies and conducting massive clinical trials have deterred many pharmaceutical companies from further investigating immunotherapy for AD.

Chapter III

Diagnostic Biomarkers of Alzheimer's Disease

The development of effective biomarkers for AD have the potential to aid in earlier diagnosis of patients in presymptomatic stages of disease and offer the possibility of initiating treatment prior to significant neurodegenerative changes. Intervening early on could therefore improve clinical outcomes. An effective biomarker can also allow for measurements of disease progression such as in the presence or absence of an experimental therapeutic and thus measure treatment efficacy in a quantitative manner. Efforts have been made using a variety of measurements and modalities to identify a reliable predictive biomarker of AD. These have included measurements of cerebrospinal fluid (CSF) proteins, plasma tests and various neuroimaging techniques. The following sections will review current biomarker detection methods in AD and how they are currently used.

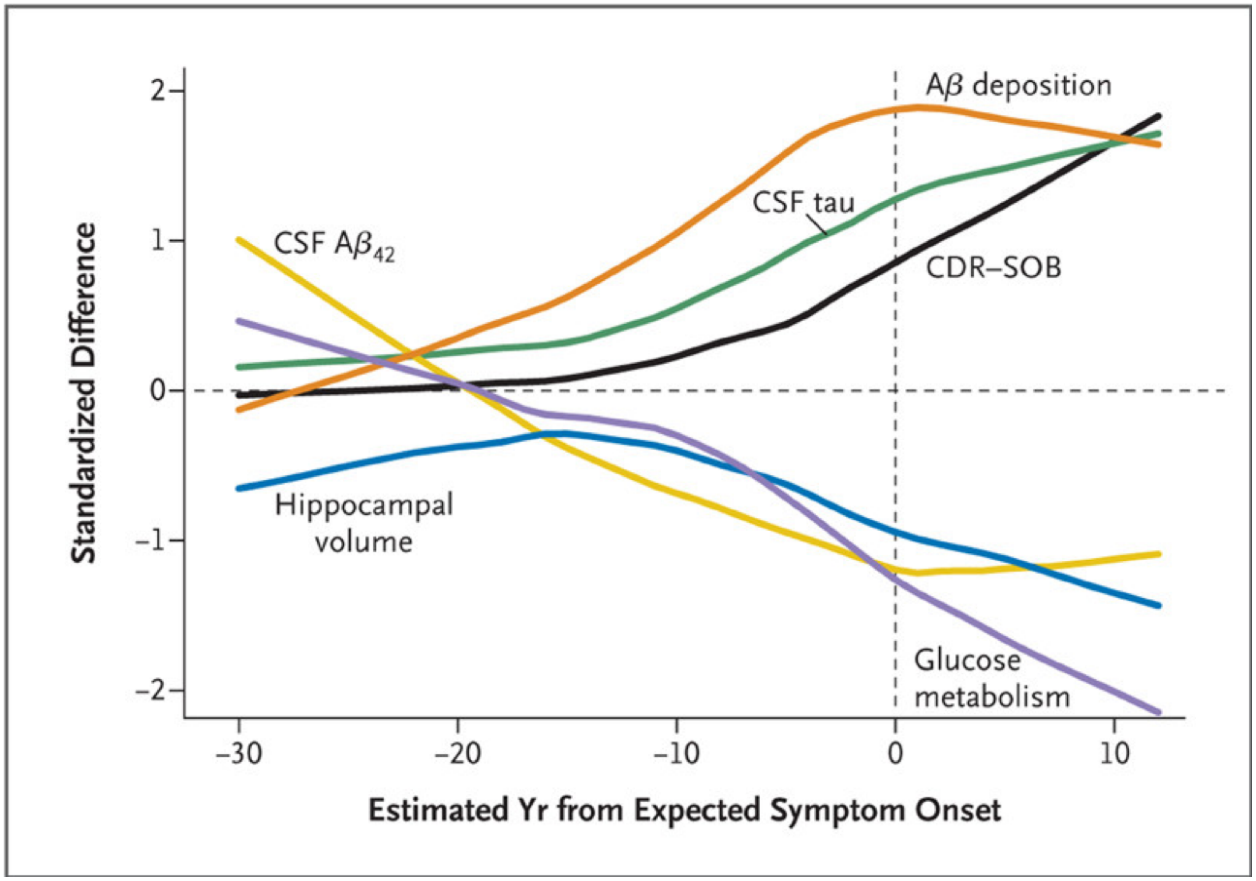

Figure 3-1. Comparison of clinical, cognitive, structural, metabolic, and biochemical changes as a function of estimated years from expected symptom onset. The normalized differences between mutation carriers and noncarriers are shown versus estimated years from expected symptom onset and plotted with a fitted curve. The order of differences suggests decreasing Aβ42 in the CSF (CSF Aβ42), followed by fibrillar Aβ deposition, then increased tau in the CSF (CSF tau), followed by hippocampal atrophy and hypometabolism, with cognitive and clinical changes (as measured by the Clinical Dementia Rating–Sum of Boxes [CDR-SOB]) occurring later. Mild dementia (CDR 1) occurred an average of 3.3 years before expected symptom onset. Reproduced with permission from The New England Journal of Medicine[149], Copyright Massachusetts Medical Society.

Cerebrospinal Fluid Biomarkers

Biomarkers of the CSF represent one of the most direct methods of studying pathology in AD short of a brain biopsy. Although a lumbar puncture is an invasive procedure, CSF physically contacts the brain and therefore, protein composition of CSF is more likely to reflect that in the brain as opposed to plasma measurements, which are separated from the brain by the BBB[150]. Measures of APP metabolism (APP, $A\beta_{40/42}$, truncated Aβ) and neurodegeneration (tau) in the CSF are some of the most intensely studied biomarkers for AD[151,152]. APP levels in the CSF were thought to correlate with expression in the brain, which could be a potential biomarker in AD. However, studies of APP CSF have been inconsistent, with results showing increased[153,154], decreased[155,156], or unchanged levels[157] when compared between cognitively normal individuals and patients with AD[158]. Since $A\beta_{42}$, a cleavage product of APP, is a major component of plaques seen in AD, many studies have examined CSF measures of $A\beta_{42}$ and other APP cleavage products as biomarkers of disease[150]. Most studies have shown that CSF $A\beta_{42}$ levels decrease in AD patients[159–161]. This effect is thought to result from sequestration of $A\beta_{42}$ in the brain due to plaque formation[162]. However, other studies have also shown CSF $A\beta_{42}$ remaining the same[163] or increasing in AD patients[164]. Despite these inconsistencies, a reduction in CSF $A\beta_{42}$ has been correlated to increased plaque burden in the brain as demonstrated through positron emission tomography (PET) imaging[165] and supports CSF $A\beta_{42}$ as a biomarker for AD. Interestingly, $A\beta_{40}$, which is a less amyloidogenic cleavage product of APP, remains unchanged in AD patients[166]. A reduction in CSF $A\beta_{42}/A\beta_{40}$ ratio was significantly decreased in patients with MCI who later progressed to AD, suggesting this measure could serve as a more accurate predictive biomarker for AD[167]. Studies comparing CSF $A\beta_{42}$ to

other APP cleavage products have demonstrated potential predictive capabilities as well[168–170].

Tau is an intracellular protein and CSF measures are low in cognitively normal individuals but increases indicate neuronal damage and is seen following a stroke or traumatic brain injury[171,172]. Several studies have demonstrated that CSF total tau (t-tau) is increased in AD compared to healthy controls[152,173]. However, similar findings are seen in other types of dementia as well as other causes of neuronal damage, and thus this finding has limited utility as a diagnostic for AD in early or presymptomatic stages of disease[152]. In AD, tau becomes hyperphosphorylated, causing formation of NFTs and thus, this led to the hypothesis that measuring phosphorylated tau (p-tau) may be more specific to AD[150]. CSF measurements revealed that p-tau concentration is increased in AD and may be more specific to AD than t-tau[152,174,175].

Plasma Biomarkers

Lumbar punctures for CSF measurements are expensive and time-consuming procedures. These limitations as well as tolerability in a demented patient population limit clinical utility and application of CSF biomarkers. In comparison, a plasma biomarker would be more practical and could be more readily implemented in an asymptomatic population for early detection of AD. However, biomarkers in the blood will be found in much lower concentrations than compared to CSF. Additionally, biomarkers of AD need to be quantified accurately from the plasma, which contains a vast array of other proteins that bind AD-related peptides and make detection more difficult[176]. Most studies of plasma biomarkers have focused on quantification of Aβ using enzyme-linked immunosorbent

assays (ELISAs). However results have been variable, with some showing a slight increase in $A\beta_{40}$ or $A\beta_{42}$ in while most show no difference in AD patients compared to healthy controls[177]. Recently developed ultrasensitive measurement techniques including Immuno-Magnetic Reduction (IMR) and Single-molecule array (Simoa) methods, are capable of accurately quantifying proteins in the subfemtomolar range and their emergence have revived work in studying plasma biomarkers for CNS disorders[178]. A recent study published in 2018 measured blood-based amyloid biomarkers by immunoprecipitation coupled with mass spectrometry[179]. $APP/A\beta_{42}$ and $A\beta_{42}/A\beta_{40}$ ratios were measured in two separate patient populations (Australia and Japan), with both sets including cognitively normal individuals, patients with MCI, and patients with AD. All tested serum biomarkers demonstrated high performance for predicting plaque burden in the brain as measured using PET imaging and correlated well with CSF measurements. These findings suggest plasma Aβ can accurately predict total amyloid plaque burden using a method that is minimally invasive and cost effective[179]. However, this is an early finding and further validation is needed.

Neuroimaging and Alzheimer's Disease

Various imaging modalities have been applied to AD using structural techniques to identify gross changes in anatomy, functional techniques to visualize changes in neuroactivity, and molecular techniques for noninvasive visualization of AD-related pathology. These methods are under development of the purposes of identifying early biomarkers of AD, monitor progression to better understand AD pathophysiology, and to also evaluate efficacy of experimental treatments[180]. The need for clinical neuroimaging strategies in AD

led to the formation of the Alzheimer's Disease Neuroimaging Initiative (ADNI), a multi-institutional initiative established in 2004 for the validation of AD imaging biomarkers for use in clinical trials. After more than a decade, ADNI has led to many advances in AD neuroimaging including development of standardized biomarkers for clinical trials, standardized protocols across multiple centers, provided a model for data sharing, and generated considerable data to better understand the relationship between biomarkers and AD progression[181].

MRI: structural & functional

Structural imaging is chiefly carried out using computed tomography (CT) and magnetic resonance imaging (MRI). Compared to MRI, CT is more readily available, less expensive, and imaging is much faster, which is beneficial in studying a patient population with dementia. However, CT is not used for diagnosing AD but rather for ruling out potentially reversible causes of dementia such as a subdural hemorrhage or a tumor[182]. In AD, CT may visualize findings of cerebral atrophy including enlarged ventricles and sulci. Unfortunately, these will only be present in late stages of disease and are not specific to AD. Thus, CT cannot not be used as an early diagnostic test.

MRI is preferential in many clinical applications as it offers spatial resolution of tens of microns, does not expose patients to ionizing radiation, and can provide insight into anatomical and functional changes seen in AD[180]. Longitudinal studies conducted on AD patient cohorts have identified gross anatomical changes detectable with MRI. Structural MRI studies have consistently shown atrophy in the entorhinal cortex and hippocampus (Fig.3-2); observed both in patients with MCI and AD[183,184]. In fact, atrophy in either

region strongly predicts future cognitive decline and progression from MCI to AD[185–188]. These observations led to the development of a visual rating system, which measures atrophy in medial temporal lobe (MTL) structures (hippocampus, entorhinal cortex, perirhinal cortex). Measures of MTL atrophy are capable of identifying patients with probable AD and MCI as well as predict progression from either cognitively normal to MCI or MCI to AD[189,190]. Standardized evaluation of gross anatomical changes using MRI can thus be applied to evaluation of experimental therapeutics through reduction in the rate of atrophy compared to untreated controls and imaging biomarkers can then be compared to clinical measures of dementia[191]. Further work has also demonstrated that hippocampal volume loss correlates with amyloid plaque burden as measured using PET imaging[192,193], which will be discussed later in detail. The relationship between hippocampal volume and Aβ accumulation, both soluble and insoluble, was observed in ApoE4 transgenic mouse models of AD as measured using MRI and Aβ assessed using immunohistochemistry (ICH). The same study, also demonstrated that cognitive decline in these mice as measured using behavioral studies also correlated with hippocampal atrophy and inversely correlated with plaque burden[194]. Interestingly, several studies have also shown that hippocampal atrophy precedes cognitive impairment and that atrophy in select hippocampal subfields occurs with Aβ plaque accumulation[192]. In fact, detectable anatomical changes in the MTL lobe measured using MRI can precede clinical signs of AD by at least five years[195].

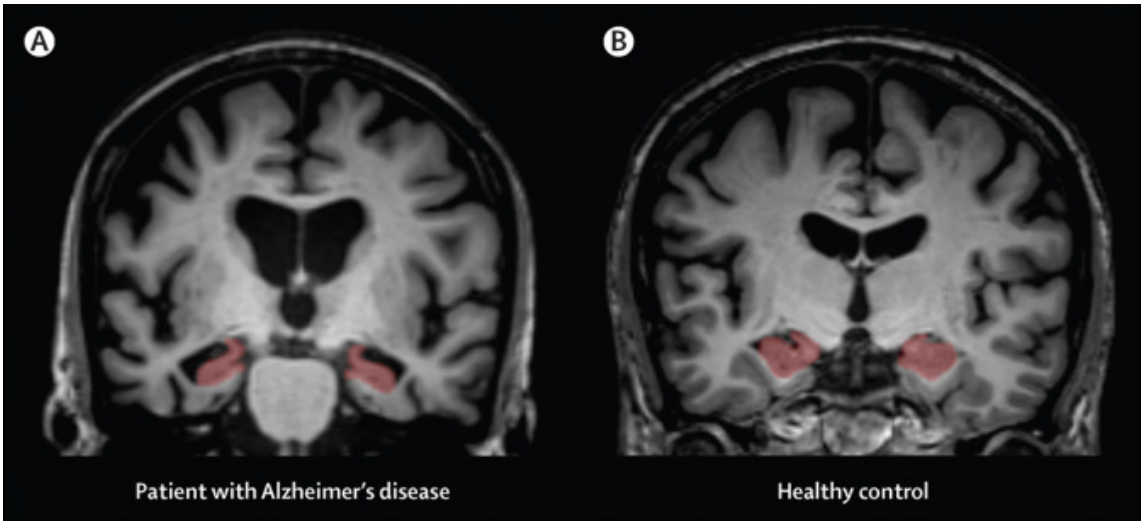

Figure 3-2. Hippocampus atrophy as shown by high-resolution structural MRI scans. Coronal sections shown from high-resolution structural MRI scans depicting the head of the hippocampus (labelled in red) in a patient with Alzheimer's disease (A) and a healthy age-matched control (B). Severe atrophy of the hippocampus in the patient with Alzheimer's disease is evident by visual comparison with the healthy control. Reprinted from the Lancet with permission from Elsevier [196].

In addition to measuring atrophy using volumetric techniques, other MRI structural methods have been studied including diffusion tensor imaging (DTI), which measures water diffusion in the brain for the purposes of measuring white matter integrity[182]. DTI measures of white matter connectivity perturbation in AD have been observed by several independent studies[197–199]. Additional work has shown that alterations in white matter tracks of AD patients precede gross changes[200] and that DTI may help differentiate AD from other types of dementia including DLB[201]. These findings support the utility of structural MRI techniques as predictive biomarker for later development of AD and for monitoring disease progression. However, currently their use is limited to research settings and are not regularly used clinically[202], likely due to availability and cost.

Functional MRI (fMRI) as the name suggests, is a method of measuring functional activity in the brain. Most fMRI studies measure changes in blood oxygen level dependent (BOLD) signal to show task-induced or spontaneous changes in neural activity[203]. BOLD signal is measured at baseline and then subtracted from activity measured when the subject is completing a specific cognitive task. Changes in signal between the two states indicate a change in neural activity at a select brain regions[204]. Thus far, fMRI studies have demonstrated that AD patients have altered functional activity in hippocampus, inferior parietal lobes and cingulate cortex than compared to control subjets[205]. Functional connectivity within the parahippocampal gyrus may be associated with clinical severity of AD[206] and other fMRI measures may in fact predict clinical stage of AD and effectively track disease progression[207]. Based on these studies, fMRI has the potential to detect functional variation in AD patients at early stages of disease. Unfortunately, like structural MRI, its use has been limited to research purposes. For now, MRI remains difficult in

cognitively impaired patients because of an inability to carry out complex cognitive tasks and difficulty keeping patients still during long scan times, which is essential for interpretable data as MRI is highly sensitive to motion artifacts[202].

PET imaging

PET imaging has been used as a means to evaluate brain metabolic activity and to visualize pathology of AD. ^{18}F-2fluoro-2-deoxy-D-glucose (FDG)-PET is used to measure tissue metabolic activity and demonstrates synaptic activity in the brain[202]. When comparing AD patients to cognitively normal controls using FDG-PET, AD patients have a dramatic reduction in cortical metabolic activity[208]. This effect was particularly evident in the parietal-temporal cortex, posterior cingulate cortex, and the lateral frontal cortex[209]. Although FDG-PET demonstrates changes in neural activity that account for symptomatology seen in AD, the technique is less able to detect changes in early stages of disease and thus has little utility as a diagnostic test[182].

Several PET tracers have been developed that bind and visualize Aβ, but the most widely used agent is Pittsburgh Compound-B (PiB)[210] (Fig.3-3). PiB is a thioflavin derivative labeled with the ^{11}C positron-emitting nucleus and is highly sensitive for detecting Aβ, with most studies showing 96% of AD patients were Aβ-positive[180,202]. The assumption in this study was that Aβ-negative patients received the wrong clinical diagnosis and had some other form of dementia or that PiB was not sensitive enough to detect pathology and it would become visible later in disease progression[202]. One caveat to these findings is that amyloid deposition can be observed in cognitively normal individuals using PiB (Fig.3-

3B). This could be interpreted as PiB identifying patients in preclinical stages of AD or Aβ pathology alone is not sufficient to cause AD. Longitudinal studies of Aβ-positive and cognitively normal individuals are needed to determine the implications of this observation[80]. A limitation of using ^{11}C-labeled PET tracers including PiB, is that ^{11}C has a half-life of ~ 20 minutes and must therefore be used shortly after radiosynthesis[180]. ^{18}F has a longer half-life (~110 minutes), making it easier for use in human imaging. Several ^{18}F tracers have been developed for measuring amyloid burden, including florbetapir, which has demonstrated high sensitivity and specificity to amyloid plaques as confirmed on autopsy in patients who died within two years of PET imaging with florbetapir[211]. A recent meta-analysis of florbetapir and other ^{18}F tracers (florbetaben, flutemetamol) found each had sensitivity and specificity of ~90%, which is comparable to PiB. However, the number of subjects and each study was low and thus require further validation[212].

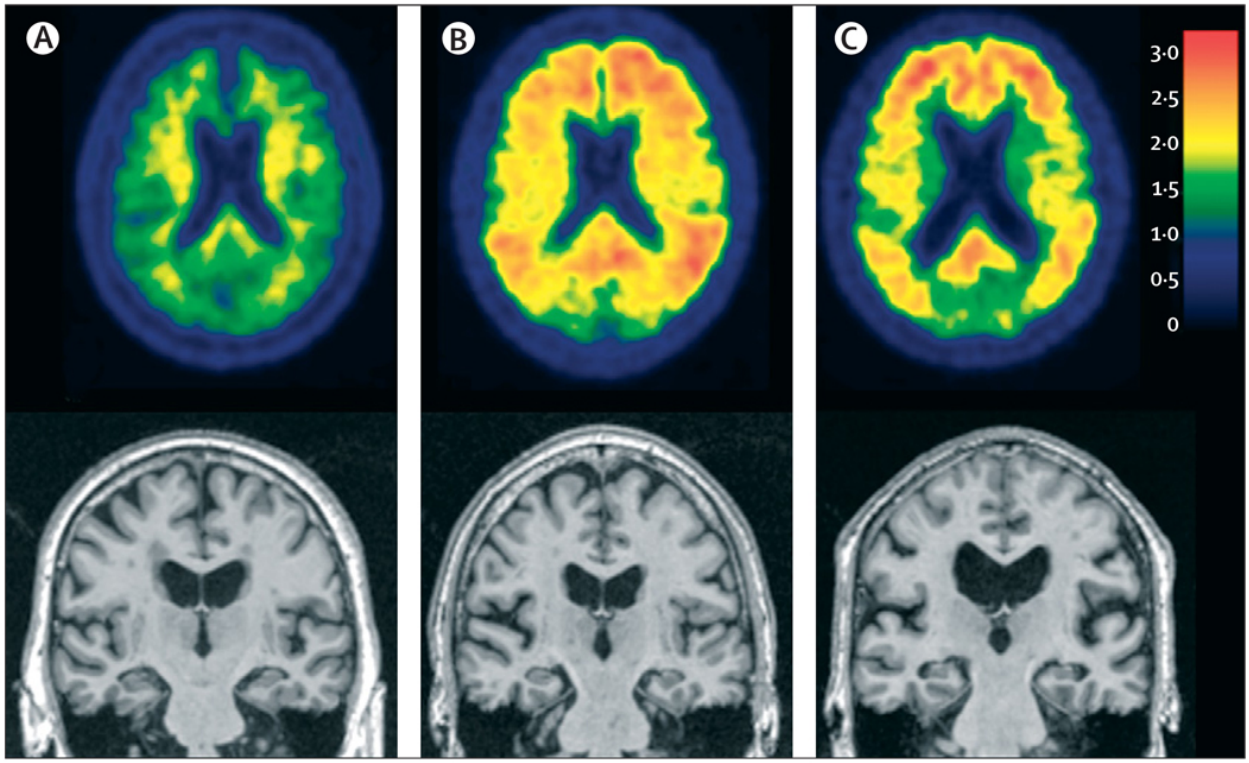

Figure 3-3. Elderly individuals are placed in order from left to right by use of proposed biomarker staging scheme. (A) A cognitively normal individual with no evidence of Aβ on PET amyloid imaging with PiB and no evidence of atrophy on MRI. (B) A cognitively normal individual who has no evidence of neurodegenerative atrophy on MRI but has significant Aβ deposition on PET amyloid imaging. (C) An individual who has dementia and a clinical diagnosis of Alzheimer's disease, a positive PET amyloid imaging study, and neurodegenerative atrophy on MRI. Aβ=β-amyloid. PiB=Pittsburgh compound B. Reprinted from the Lancet with permission from Elsevier[213].

Tau-specific PET tracers were also developed including ^{18}F-labeled tau aggregate ligands T-807 and T-808, which have both been studied in clinical trials[214,215]. However, further work must be done to understand the utility of tau-PET tracers for diagnostic applications in AD as well as understanding tau's role in AD and other tauopathies[216]. Although PET is capable of identifying whether or not a patient has AD pathology with good certainty, PET has poor spatial resolution on the order of 5-10 mm, which limits the ability to detect fine neuroanatomy features and effectively localize pathology. Additionally, unlike MRI, PET exposes patients to radiation and thus limits its use in longitudinal studies where multiple scans on a patient would be required. Finally, the use of PET imaging clinically is restricted due to its high cost and limited availability. Because PET agents have short half-lives, distribution remains challenging[180]. As many as 11 states in the US and much of the rest of the world are not able to order from PETNET, the distributer of PET agents from Siemens Healthineers[217]. Efforts have been made to reduce cost and increase accessibility but, until that is achieved, PET use in AD will be largely restricted to research-based applications.

Chapter IV

Blood Brain Barrier: Structure, Function and Challenges in Neuropharmacology

Structure and Function

The BBB is composed of the vasculature found within the CNS, which prevents diffusion of most compounds into the brain parenchyma and spinal cord. There are three main classes of capillaries and these include continuous nonfenestrated, continuous fenestrated, and discontinuous, all of which differ in their ability to regulate transfer of solutes between the blood and tissue parenchyma[218]. CNS capillaries are continuous nonfenestrated, preventing paracellular transport of most molecules, but they also have additional properties that allow for tighter regulation of transport between the blood and CNS[219].

The three cellular elements which compose the BBB are endothelial cells, astrocyte end-foot processes, and pericytes[220]. Brain endothelial cells are connected at a junctional complex by tight junctions and adherens junctions[221]. These junctions prevent free diffusion of compounds between the blood and CNS with the exception of small lipid-soluble molecules <400 Da, which can cross the BBB via lipid-mediated diffusion[222]. Endothelial cells also express the multidrug resistant transporter P-glycoprotein (P-gp), an ATP-dependent efflux pump which actively effluxes lipophilic metabolites from the brain, including many potential neurotherapeutics[223,224].

Astrocytes, a type of glial cell, extend processes that almost completely ensheath the vascular tube[218]. They provide a cellular link between neural circuitry and blood vessels to allow for the regulation of blood flow in response to neuronal activity[218,225,226]. Though

astrocytes do not structurally contribute to the BBB[227], they potentially promote CNS endothelial formation, as demonstrated by the ability of purified astrocytes to induce development of BBB properties in non-CNS blood vessels in culture[228]. Astrocytes may have a role in regulating CNS vasculature permeability, but their exact function in controlling BBB differentiation and permeability requires further study as there have been conflicting findings[219]. Pericytes, contractile cells that wrap around endothelial cells, provide structural support and vasodynamic capacity[220]. In the CNS, pericytes also provide mechanical stability[229] and further support through matrix deposition as well as promoting endothelial differentiation and quiescence via molecular signaling[230]. However, the molecular mechanism by which pericytes mediate endothelial stabilization is not well understood[219].

Implications in Neurodiagnostic and Therapeutic Development

Highly regulated transport of substances across the BBB is essential in maintaining homeostasis within the CNS and preventing entry of harmful toxins or pathogens. However, the existence of the BBB presents an obvious problem of delivering potential diagnostic or therapeutic agents to the brain. In fact, the BBB excludes delivery of nearly 100% of large-molecule neurotherapeutics and over 98% of all small-molecule drugs[231]. For a small-molecule drug to cross the BBB via passive paracellular diffusion across the CNS endothelium, the compound must have a molecular mass under 400- to 500- Da and be highly lipid soluble[232]. This severely limits treatment options for CNS disorders as many will not respond to molecules that have those characteristics. Exceptions include affective disorder, chronic pain, epilepsy, and migraine headaches[231].

By designing a molecule that is small enough and sufficiently lipid soluble to cross the BBB, this also increases its penetration to other tissues systemically. Because of this, larger dosing is required to sufficiently deliver enough of the compound to the brain and mediate a therapeutic effect. This is especially important to consider if the experimental compound exhibits toxicity at higher doses or has off-target effects that could result in side-effects beyond what is tolerable or safe.

Although more lipid-soluble molecules should traverse the BBB, many actually have worse penetrance than predicted due to the presence of ATP-binding cassette (ABC) transporters including P-gp[233]. Many lipid-soluble drugs are substrates of transporters that actively efflux from endothelial cells, preventing delivery into the CNS. Targeted efflux provides a further challenge in design of neurotherapeutics as well as in comparing animal models to patients since ABC transporter expression varies across species[223]. Although P-gp's role in drug efflux is well characterized, there are many other transporters expressed within the BBB whose roles in drug resistance are less understood. These include breast cancer resistant protein (BCRP), members of the of the organic anion transporting polypeptide (OATP) family and organic anion transporter (OAT) family[223]. Additionally, genetic variants including polymorphisms in transporters may result in inconstant targeting of drugs for efflux and account for some of the variability seen between patients in their response to the same treatment[223].

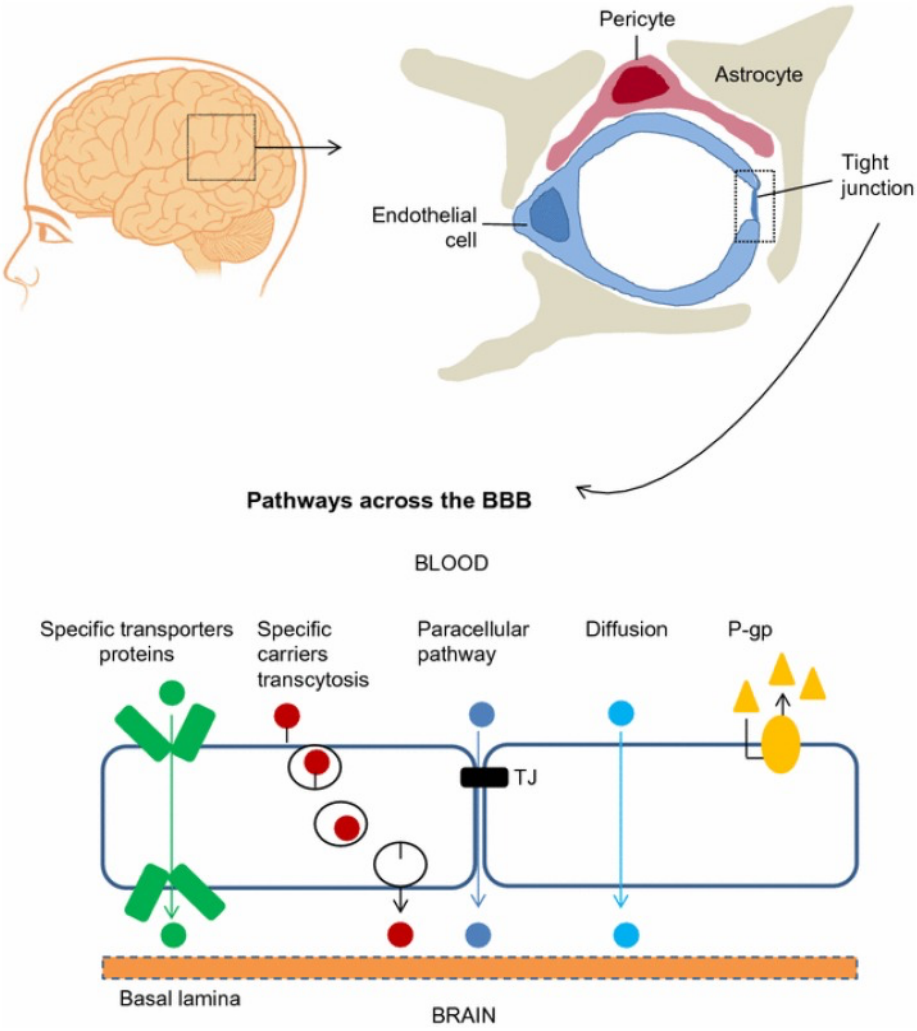

Figure 4-1. The blood-brain barrier (BBB) is composed of brain microvascular endothelial cells, pericytes, astrocytes, tight junctions, neurons, and basal membrane. Ions and solutes utilize concentration gradients to pass the BBB by passive diffusion through the paracellular pathway between adjacent cells. The transcellular pathway includes different mechanisms such as passive diffusion, transporters and transcytosis. Efflux transporters, e.g., P-glycoprotein (P-gp), also influence BBB permeability. Abbreviations: BBB: blood-brain barrier; P-gp: P-glycoprotein. Reprinted from Theranostics with permission from Ivyspring International Publisher[234].

Current Methods of Neuropharmacological Drug Delivery

Transcranial drug delivery

Restrictions in drug delivery imposed by the BBB require development of alternative approaches to expand the pool of potential therapeutics beyond those that can passively diffuse across the brain endothelium. One method is transcranial delivery using neurosurgical approaches such as intracerebral implantation, intracerebroventricular (ICV) infusion, and convection enhanced delivery (CED). A limitation of intracerebral or ICV injections is the poor diffusion of compounds beyond the site of administration[231]. A study in rats showed that the concentration of a small molecule decreases by 90% when 0.5 mm from the injection site[235]. Limited diffusion within the CNS may be preferential in certain applications such as in administering chemotherapeutics for brain tumors, but hinders application in more global neurological disorders including AD. Drug penetration into the brain can be improved using CED, where fluid is forced through the brain following drug administration[231]. Although direct administration can be effective, these approaches have limited clinical application because they are invasive, expensive, and require surgical expertise and hospitalization.

BBB disruption

Another approach to improve drug delivery is to transiently increase BBB permeability pharmacologically. For example, intracarotid infusion of osmotic agents such as mannitol disrupt the BBB by shrinking endothelial cells[236]. However, this approach results in chronic neuropathological changes in rodents[237] and can cause seizures in both rodent models and humans[238,239]. Other compounds used for BBB disruption include those for solvent/adjuvant-mediated disruption such as ethanol or dimethyl sulfoxide (DMSO)[231,240–

[242]. When drugs are prepared in either of these solvents, delivery to the brain significantly increases than when using a physiological buffer through destabilization of the BBB. Immune adjuvants are used regularly in vaccines to enhance immune response to a presented disease-specific peptide. An adjuvant mediates improved response by recruiting immune cells to the injection site. Additionally, adjuvants induce an inflammatory response that can increase BBB permeability[231]. In fact, adjuvants can disrupt the BBB enough such that IgG antibodies can enter the brain for weeks after an injection[243]. This property of BBB disruption is especially relevant in efforts to develop a vaccine for AD where antibodies must enter the brain for immune-mediated clearance of Aβ. Additional studies have demonstrated that other pro-inflammatory substances can also change BBB permeability including tumor necrosis factor-α (TNF-α)[244], nitric oxide (NO)[245], prostaglandins[246], and pathogen-associated molecular patterns (PAMPs) such as the bacterial endotoxin lipopolysaccharide (LPS)[245,247,248], which I will discuss in more detail in chapter seven. Pretreatment or co-administration of any of these with a drug may therefore improve delivery to the brain but the effect of BBB disruption must be weighed against the potential risk of permanently damaging the brain endothelium and inducing systemic inflammation that could lead to aseptic shock.

In addition to chemical and inflammatory mediated BBB disruption, efforts have been made using focused ultrasound (FUS) to enhance delivery of neurotherapeutics. In this approach, low frequency ultrasound waves are delivered using a noninvasive trans-cranial technique[249,250]. Using a low frequency is advantageous in that it reduces the risk of permanent tissue damage[249]. FUS can also be targeted to select brain regions when

employed in conjunction with MRI where BBB disruption can be observed by contrast extravatisation[251]. These features offer a unique advantage than when compared to chemically-induced BBB disruption, which affects all tissues even beyond the CNS and comes with an inherent risk of toxicity or permanent damage especially in the context of chronic administration[231]. Many preclinical studies investigating application of FUS for delivery of antibodies[251] and chemotherapeutics[252,253] to the brain are underway as regional specificity could be used to target treatment to the site of a brain tumor. Furthermore, FUS has been used to deliver anti-Aβ antibodies to the brain of AD transgenic mouse models and treatment resulted in rapidly reduced plaque burden[254,255]. Interestingly, MRI-guided FUS administered to AD mouse models in the absence of anti-Aβ antibodies also resulted plaque reduction, likely through increased delivery of endogenous immunoglobulins to the brain and enhanced activation of glial cells, which correlated with increased internalization of Aβ in microglia and astrocytes[256].

Targeting endogenous BBB transporters

Another promising approach for delivering pharmacologic agents to the brain is by targeting endogenous transport systems within the CNS endothelium whose primary role is to shuttle nutrients, metabolites and proteins between the brain and blood[257]. Carrier-mediated transport (CMT) provides a means of transporting small hydrophilic molecules such as glucose and amino acids[258]. By linking small molecule drugs to a natural CMT ligand, delivery to the brain can be improved[259]. However, targeting CMT for larger compounds has been unsuccessful[257]. Receptor-mediated transport (RMT) occurs when an endogenous ligand binds a receptor on the apical endothelial surface and then undergoes

endocytosis to form an intracellular vesicle, which migrates to the basolateral plasma membrane to be released into the brain parenchyma[260]. RMT is responsible for transport of many endogenous proteins including uniform proteins such as transferrin and more heterogenous macromolecules such as lipoproteins[257,261–264]. Targeting RMT for drug delivery involves coupling therapeutics to a receptor targeting moiety such as the endogenous RMT ligand, a peptide ligand mimic, or an anti-receptor antibody[257]. This approach has been successfully implemented targeting several RMT systems including the transferrin receptor (TfR)[265], insulin receptor[266,267], and low density lipoprotein receptors[268–270].

A recently designed bispecific antibody developed at Genentech targets the transferrin receptor for delivery of a potential AD antibody therapeutic. Transferrin (Tf) is an iron-binding protein that transports iron to different tissues. TfRs found on endothelial cells facilitate transcytosis of iron-bound transferrin into the brain[271]. The antibody is bivalent in that one arm has a TfR domain while the other arm has a therapeutic domain, which binds and inhibits BACE1 to prevent Aβ peptide production. By having a domain to bind transferrin, this antibody utilizes RMT transport to reach the brain and the other domain then inhibits BACE1 activity to reduce Aβ production. Intravenous dosing of macaques with anti-TfR/BACE1 antibodies demonstrated significantly increased delivery to the brain than anti-BACE antibodies that lacked a TfR binding domain. The bivalent antibody also reduced Aβ both in cerebral spinal fluid and in brain tissue, and the degree of reduction correlated with the brain concentration of anti-TfR/BACE1 antibody. These results demonstrate that the TfR bispecific antibody platform can robustly and safely deliver therapeutic antibody across the BBB in the primate brain[272]. Although RMT transport has

had some therapeutic benefit in preclinical animal models, this approach is hindered in that reliance on a specific transport mechanism will require significant optimization for every tested compound and may not work for all potential neurotherapeutics.

Intranasal administration

Intranasal administration of drugs is a promising approach as a non-invasive method for direct delivery of both small and large molecule neurotherapeutics to the brain[273–278]. The exact mechanism of delivery by intranasally administered compounds to the CNS is not well understood. However, there are several routes of transport that are thought to contribute. Molecules are able to cross the olfactory epithelium via transcellular or paracellular pathways. In transcellular transport, a compound can be taken up either by the olfactory or trigeminal cranial nerve, both of which innervate the nasal cavity, and are transported to the CNS by receptor, carrier-mediated or vesicular transport[273,279]. As transcellular transport is dependent on cellular processes for uptake and delivery of compounds, delivery is saturable and can take hours to days for delivery to the brain[280]. Conversely, paracellular transport involves rapid transport of molecules between olfactory epithelial cells. Olfactory receptor neurons (ORNs) are chiefly responsible for mediating smell by conveying sensory information to the CNS. However, because ORNs are directly exposed to potential neurotoxins in the environment, they will regenerate every three to four weeks[281]. This constant cellular turnover is thought to make the olfactory epithelium "leaky" and allow for transport directly to the CNS[277,282]. Specialized Schwann cells called olfactory ensheathing cells (OECs) are responsible for ensheathing ORN axons. Interestingly, OEC channels remain intact while ORNs are undergoing regeneration, creating passageways that may facilitate rapid transport from the nasal cavity to the

brain[283]. In fact, paracellular transport of intranasally administered molecules to the brain can occur in 30 minutes or less[282]. Improved delivery to the brain through intranasal administration has been demonstrated for both currently available and experimental AD therapeutics including benzodiazepines[284,285], vaccine antigens[278,286], Aβ immunogens[287–290], insulin[291–298] and cholinesterase inhibitors[299–307]. Targeting olfactory uptake of diagnostic and therapeutic agents could allow for noninvasive and safe delivery of compounds that previously had limited clinical application due to poor BBB permeability. Direct uptake also avoids systemic extraction or alteration and improved delivery to the brain would permit the use of lower doses to reduce peripheral toxicity. This delivery mechanism could also theoretically target specific brain regions through selective transport along the olfactory nerve via direct uptake and delivery or bulk flow mechanisms such as perivascular transport[277]. The entorhinal cortex receives afferent input from the olfactory nerve but is also immediately adjacent to and sends projections to the hippocampus. Both brain regions demonstrate high pathologic burden in AD and thus selectively targeting these regions through intranasal administration could improve therapeutic efficacy[276,308].

Blood Brain Barrier Changes in Alzheimer's Disease

Extensive studies have demonstrated that the BBB is in fact disrupted in various conditions including physical trauma[309], ischemia[310] and CNS infections such as bacterial meningitis and human immunodeficiency virus (HIV)[311–313]. Similarly, the BBB is also disrupted in other neurological diseases including multiple sclerosis, CNS tumors, Parkinson's disease and AD[313,314]. Enhanced BBB permeability in pathologic states is thought to result from either opening of endothelial tight junctions to permit paracellular transport or increased pinocytosis activity and formation of transendothelial channels, both of which allow

transcellular transport[315]. BBB dysfunction leads to increased transport of blood-borne molecules to the brain as well as cellular infiltration from trans-endothelial migration[314]. Early postmortem studies in patients with known cases of AD demonstrated various changes within the brain endothelium including decreased number of mitochondria, increased pinocytosis vesicles, collagen accumulation in the basal lamina and necrosis[316]. Clinical studies on AD patients confirmed BBB dysfunction by gadolinium-enhanced MRI and measuring CSF/blood albumin ratio[317]. Influx of Aβ peptide into the brain is facilitated by the receptor for advanced glycosylation products (RAGE) while efflux of Aβ is the result of lipoprotein receptor protein (LRP)-1. Under normal conditions, these transport mechanisms work in tandem to regulate Aβ levels in the brain to prevent excess accumulation and aggregation. However, age-dependent impairment of LRP-1 activity and increased RAGE expression leads to Aβ accumulation and formation of neurotoxic senile plaques[314]. Early studies identified IgG and complement protein aggregates in close proximity to Aβ plaques within the brain parenchyma, suggesting plaque formation causes focal changes in BBB permeability[318]. In fact, neuroinflammation is a characteristic feature of AD and thought to be essential in AD progression, possibly through BBB disruption[313]. Some research has shown that treatment of AD transgenic mouse models with nonsteroidal anti-inflammatory drugs (NSAIDs) including COX-2 inhibitors may be neuroprotective[319]. However, another study demonstrated COX-2 inhibition actually led to hippocampal cell death[320], suggesting further work must be done investigating therapeutic applications of ant-inflammatory drugs in AD.

Though BBB compromise in AD may allow proinflammatory molecules and toxins to get into the brain, increased permeability offers a unique opportunity for improved bioavailability of potential therapeutics. Active immunization with Aβ immunogens or passive immunization with anti-Aβ antibodies may have reduced plaque burden effectively in animal models[321] at least partially due to improved antibody transport into the brain resulting from disease-mediated BBB disruption of endothelial tight junctions in addition to RMT mechanisms[313,322]. Interestingly, if the BBB is selectively disrupted in areas with AD-related pathologic change, more targeted delivery of therapeutics to affected brain regions can be achieved[313] and reduce the risk of off-target neurological effects.

Chapter V

Alzheimer's Disease and the Eye

Although vision is difficult to study in a patient population with dementia, a range of visual deficits have been reported in patients with AD. In particular, higher order visual processing such as object and face recognition appear to be affected while there is dispute as to whether lower order visual processing, including color vision and visual acuity are also impaired as a result of AD-related pathology[323,324]. Similarly, pathologic changes in the optic nerve fiber, hypothalamus, and visual cortex are well studied while evidence of pathology in the eye itself, including the retina and lens, are controversial[323]. However, as evidence of ocular changes in AD grows, efforts to evaluate these changes as potential biomarkers of disease are underway.

Cholinergic Deficits and Pupillary Response in Alzheimer's Disease Patients

Acetylcholine deficiency is a known feature of AD, resulting from loss of presynaptic cholinergic pyramidal neurons[325]. This observation is supported by the clinical efficacy of acetylcholinesterase inhibitors, which improve cognition and global function in AD patients[326]. An interesting early observation demonstrated that patients already diagnosed with AD exhibited marked hypersensitivity to tropicamide, a cholinergic antagonist used for pupillary dilation. Using tropicamide, variations in pupillary dilation were capable of accurately differentiating patients with AD or suspected AD from cognitively normal controls[327]. Pupillary constriction is regulated by the Edinger-Westphal nucleus, which provides preganglionic parasympathetic innervation to the eye. Treatment with tropicamide inhibits terminal signaling in this pathway and causes pupillary dilation. Exaggerated pupil dilation with cholinergic antagonist treatment in AD patients results from selective

targeting of the Edinger-Westphal nucleus by AD pathology and reduced parasympathetic cholinergic signaling to the pupil[328]. Neuronal loss and AD pathology were also observed in the Edinger-Westphal nucleus of some samples from cognitively normal patients on postmortem examination. This observation may explain why some elderly subjects with normal cognition also exhibit pupillary hypersensitivity to tropicamide[329]. However, testing with tropicamide can elicit a similar hypersensitivity response in patients with vascular dementia and Parkinson's disease[330,331]. Additionally, other studies evaluating the use of tropicamide as a diagnostic test for AD showed no significant difference in pupillary response between AD patients and healthy controls[330]. As a result of these inconsistent findings, tropicamide testing cannot be used as a diagnostic test for AD.

Evidence of Aβ in the Lens

In an effort to find a noninvasive method for detecting plaques, studies have focused on identification of Aβ in the lenses of affected individuals. However, results from these studies have produced conflicting results. Goldstein et al. were the first to identify Aβ deposition in lens specimens from individuals diagnosed with AD[332]. They identified Aβ40 and Aβ42 in lenses of both people with and without AD. Concentrations of both species were comparable to those seen in the cerebral cortex. On slit-lamp surveys in the same study, supranuclear cataracts were seen in all AD samples but not in the controls. Supranuclear cataracts are an uncommon presentation[333] and are potentially unique to AD[334]. Histological analysis of these lenses demonstrated colocalization of supranuclear cataracts with Aβ immunoreactivity, suggesting regionally-specific Aβ aggregation in AD patients[332]. Comparable findings were seen in a study evaluating lenses from people with

DS[335]. The APP gene is located on chromosome 21 and triplication of this chromosome in DS results in overexpression. Aβ accumulation occurs rapidly in those with DS[336] and results in early-onset AD in this population[337]. Those with DS also characteristically develop cerulean "blue dot" cataracts of unknown composition[338]. Moncaster et al. reported supranuclear cerulean cataracts in the lenses of DS patients that developed in an age-dependent manner[335]. Anti-Aβ immunoreactivity was observed and further localized to the cytoplasm of supranuclear fiber cells in the lens. These results suggest a common molecular origin between the increased prevalence of specific cataract phenotypes and increased prevalence of early-onset AD in people with DS and sporadic AD[332,335]. Cataract formation is also observed in transgenic mouse models of both DS and AD[339,340]. Interestingly, Melov et al. demonstrated that treating a transgenic mouse model of AD with the antioxidant EUK-189 resulted in significantly fewer severe cataracts compared to the untreated group[339]. This finding suggests that cataracts seen in AD form through an oxidative mechanism, which is also implicated in Aβ-related pathogenesis seen in the brain. Taken together, these results support common pathology existing in both the brain and lens in AD, particularly localized to supranuclear cataracts. Concentrations of Aβ in the lens were comparable to those seen in the brain[341] and Aβ-containing cataracts developed in an age-dependent manner in those with DS[335]. Based on these findings, plaque deposition in the lens reflects that seen in the brain and measuring Aβ concentrations in the lens could therefore serve as a biomarker for AD.

Other groups have failed to replicate the findings originally reported by Goldstein et al. in 2003. In a similarly designed study, Michael et al. examined lenses from patients

diagnosed with AD, several of which had pronounced cortical lens opacities[342]. Lenses from AD donors and age-matched controls with some also containing lens opacities were stained using Congo red, thioflavin, and immunohistochemical staining but Aβ was not detected in any lenses. This led to the conclusion that Aβ is not present in either AD or control cataracts[342]. The same group later published further negative results when examining the lenses of AD patients using confocal Raman microspectroscopy[343]. Using this technique, they are able to measure β-sheet content in different tissues. Comparing measurements between lenses from those with AD to age-matched controls, they were unable to detect any difference in β-sheet levels within the lens even in the presence of opacities. As a control, Michael et al. measured β-sheets present in hippocampus samples from AD donors and were able to detect an increase in β-sheet levels, supporting the use of confocal Raman microspectroscopy in examining the lenses. Their findings were further supported by negative results in repeat staining analysis using Congo red, thioflavin, and immunostaining for both Aβ and tau[343]. Ho et al. were also unable to identify Aβ in the lens when stained with Congo red or immunostaining[344].

It is possible that the discrepancies between these studies were caused by differences in sample preparation. The lens is a particularly challenging structure to work with as it is more difficult to preserve than brain tissue, which was used as a positive control in the described studies. Since there was a longer postmortem interval in Michaels et al.[342], this may have reduced their ability to detect Aβ plaques. Additionally, Michaels et al. had to rely on a clinical diagnosis of AD for their lens samples as postmortem brain studies were not always possible[342,343]. There were also differences in the sample preparation and

staining protocols used, which may account for some variation. However, since there is no definitive positive control for Aβ plaque detection in the lens, it is nearly impossible to show which differences in sample preparation could account for discrepancies in the presented studies. In addition, because confocal Raman microspectroscopy was used to measure the β-sheet content of a tissue, it could be argued that Aβ in the lens has not formed β-sheet fibrils and may instead be present as soluble oligomers. This would also explain the lack of findings when staining with Congo red and thioflavin. However, absence of fibrils in the lens would not explain why Aβ is not detected with specific immunostaining[343]. In summation, with such discrepancy in Aβ detection within the lens, it is controversial whether it can be considered a reliable biomarker for AD at this time.

Lens Pathology as an Ocular Biomarker of Disease

Although there are discrepancies in findings for whether or not Aβ is truly present in the lens of AD patients, efforts are underway to study Aβ in the lens as a biomarker for AD. One such effort, led by Lee Goldstein, is to utilize a custom-built quasi-elastic light scattering (QLS) instrument for noninvasive in vivo detection of Aβ plaques. It was previously shown that synthetic Aβ incubated with human lens protein extract potentiated aggregation and increased backscatter light intensity on QLS analysis[335]. These findings suggest that QLS analysis may be used to quantitatively assess lenses *in vivo* for AD pathology. Since then, QLS has been applied to noninvasively detect AD lens pathology in subjects with DS[345]. Kebege et al. have applied the SAPPHIRE system, a fluorescent ligand in combination with a laser scanning device, to detect Aβ in the human lens *in vivo*[346]. In this study, an ointment is prepared containing a fluorescent naphthalene-based

ligand, which has been shown to bind aggregated Aβ peptide (Fig.5-1)[347]. The ointment was applied to a subject's eye and the lens was analyzed using a laser scanning device. Five subjects were included in the AD cohort and the cognitively normal control group. Fluorescent signal intensity from the Aβ-targeting ligand was higher in the supranuclear regions among AD patients when compared to controls[346]. These results complement the initial findings observed by Goldstein et al. that supranuclear opacifications in lenses from AD patients contained Aβ plaques[332]. Of note, one control subject determined normal by cognitive testing exhibited fluorescent measurements higher than other control subjects and may be interpreted as a false positive. This patient, though cognitively normal, had the ApoE4variant. Having the ApoE4 gene variant increases risk of developing late-onset AD[6] and therefore, the identified control subject has an increased risk of developing AD in the future. The clinical study had no serious adverse effects and results were promising that the SAPPHIRE System could in fact differentiate between those with AD and control subjects[346]. Future studies using this technique must include larger sample sizes and include longitudinal studies of subjects who are cognitively normal or with mild cognitive impairment to see if the SAPPHIRE System can be used as a screening method to predict who will later develop AD.

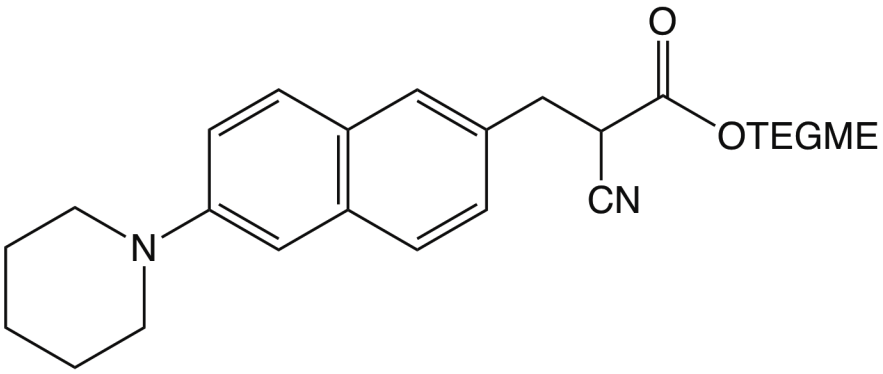

Figure 5-1. Naphthalene-based probe capable of binding pre-aggregated and aggregated Aβ. Binding results in a 76 nm red shift and is accompanied by a 9.3-fold fluorescence intensity increase[347]. The probe was applied as a gel to the eyes of AD patients and cognitively normal individuals to noninvasively detect and evaluate Aβ in the lens as a biomarker for AD[346].

Evidence of Aβ in the Retina

Other research has focused on determining whether Aβ plaques form in the retina of AD patients and if detection of these could be utilized as an early diagnostic tool. The retina is a part of the central nervous system with a high density of neurons and thus may exhibit comparable Aβ accumulation as that seen in the brain. Retinal abnormalities have previously been described in AD patients including ganglion cell loss[348,349]. Ganglion cell death was also reported in a transgenic mouse model of AD[350]. However, ganglion cell death is not a feature specific to AD[351] and thus detection may not serve as an effective biomarker for early diagnosis of AD if seen in other types of dementia. Aβ deposition has been observed in the retinas of postmortem eyes from AD patients as well as in suspected early cases using immunostaining but were not seen in age-matched controls[351]. Aβ and APP immunoreactivity has also been observed in the retinas of several different transgenic mouse models of familial AD[352–355]. This deposition was shown to occur within multiple layers of the retina and in an age-dependent manner[352]. Retinal Aβ deposition in transgenic mice was shown to closely correlate with total plaque burden in the brain[351] and cause retinal degeneration as well as retinal functional impairment[352,355]. Importantly, Aβ was detected in the retinas of transgenic mice prior to cognitive decline as demonstrated with behavioral testing and was also detected in postmortem retinal samples from people suspected to be in early stages of AD[351]. These findings suggest that an ophthalmic test designed to detect retinal Aβ could identify plaques early in AD progression and be used as an early diagnostic tool. Liu et al. also demonstrated that administration of Aβ vaccinations resulted in reduction of both brain and retinal plaque deposition in transgenic mouse models of AD[354], suggesting that noninvasive monitoring of retinal plaques could serve as

a surrogate measure for changes in total plaque burden during therapeutic trials. However, vaccination also led to an increase in Aβ in retinal vasculature[354]. Taken together, the presented studies in both human postmortem retinas and transgenic mouse models of AD provide evidence that detection of retinal Aβ could be used as an early diagnostic for AD and potentially to monitor therapeutic efficacy over the course of a clinical trial. The lack of published studies refuting Aβ in the retina as was seen within the lens suggest that detection in the retina may be a more reliable measure and pursuit of a noninvasive detection method is warranted. However, the postmortem study which identified retinal Aβ plaques in AD patients was done only for eight cases[351]. Therefore, Aβ plaques in retinas from AD patients should be demonstrated using a larger sample size to provide more justification for pursuit of a noninvasive retinal detection test. It is also important to consider that Aβ has recently been reported in the retinas of those with age-related macular degeneration (AMD) and Aβ levels correlated with AMD progression[355]. Thus, since Aβ is present in the retina for both AMD and AD, retinal detection of Aβ in patients could potentially lead to either diagnoses and must be paired with clinical features to effectively differentiate between them, especially in early stages of disease. Despite these caveats, it is imperative that an *in vivo* method of detection be developed to evaluate retinal Aβ plaque deposition and its utility as a biomarker for AD.

In vivo Retinal Imaging in Alzheimer's Disease

Previous efforts have attempted to identify retinal abnormalities that may be used as a diagnostic indicator of AD. In one such study, a scanning laser ophthalmoscope (SLO), used to evaluate patients with glaucoma, was used to study the optic nerve head in those

with AD. It was demonstrated that patients with AD had a significant reduction in optic nerve fibers compared to control subjects[356]. Another technique used to noninvasively evaluate retinal changes in AD is optical coherence tomography (OCT), which allows for cross-sectional imaging of the retina[357]. *In vivo* studies using OCT has shown that peripapillary retinal nerve fiber layer thickness was significantly decreased in patients with AD[356,358–363] and mild cognitive impairment[359] than that seen in cognitively normal controls. This suggests that retinal nerve fiber layer thinning may occur early in AD progression and may serve as a potential diagnostic measure. However, retinal ganglion cell death as identified using OCT has also been observed in other disorders including glaucoma[364,365] making it less specific for early detection of AD. Measurements of retinal nerve fiber layer thickness using OCT in patients with AD did not correlate with either Alzheimer's specific CSF measurements or mini-mental status exam scores, suggesting retinal nerve fiber layer thickness may not correlate with disease progression or severity[366]. The same study by Jentsch et al. also investigated a newly developed technique of fluorescence lifetime imaging ophthalmoscopy (FLIO), which measures global changes of retinal autofluorescence. Fluorophore composition within the retina will change as a result of disease-specific accumulations and FLIO attempts to identify these changes to be used for early diagnoses and monitoring of disease progression. Jentsch et al. demonstrated that changes in FLIO parameters in AD patients compared to controls do in fact correlate with measures of AD severity[366]. However, the identified FLIO parameters may not be specific to AD. Other diseases affecting the retina must also be studied to see if measured parameters vary. Future studies using FLIO should also include patients with mild cognitive impairment who later develop AD to evaluate whether FLIO can identify changes in the retina early in disease progression. A separate study sought to identify

retinal vascular biomarkers of AD by comparing retinal photographs between AD patients and healthy controls. Several retinal vascular parameters were altered in AD patients or healthy controls who demonstrated high Aβ cortical plaque burden as identified using PET imaging. These results suggest that analysis of retinal vasculature could potentially be used for detection of AD or for monitoring AD progression[367]. However, none of the described techniques targeting the retina are directly measuring pathology specific to AD.

Efforts are underway to develop a method of imaging retinal Aβ plaques noninvasively *in vivo*[351]. One such approach is through use of curcumin, a component of turmeric that is capable of crossing the BBB and binding cortical Aβ plaques upon intravenous injection or oral administration[368]. Additionally, curcumin's natural fluorescence allows it to be readily identified when associated with Aβ plaques. Following intravenous administration, dissected retinas from AD transgenic mouse models were found to have plaques labeled with curcumin as determined by fluorescence and colocalization with Aβ-specific immunostaining. Plaques were not detected in wild-type mice receiving the same curcumin injection. These findings indicate that curcumin is capable of crossing the blood-retinal barrier and associating with retinal Aβ plaques. Preliminary *in vivo* imaging of AD transgenic mice injected with curcumin using a rodent retinal imaging microscope showed that plaques can be identified by detecting curcumin fluorescence. *Ex vivo* results confirmed curcumin specificity seen using *in vivo* retinal imaging. Additionally, immunotherapy treatment known to reduce cortical plaque burden was also shown to reduce curcumin-visualized retinal plaques compared to non-immunized transgenic mice. Results from this study demonstrate that intravenously-administered curcumin can label

Aβ plaques and be detected noninvasively[351]. This technique could potentially be used to detect Aβ plaques in patients for diagnosing AD or to monitor therapeutic efficacy in clinical trials as curcumin is known to have low toxicity even at high concentrations or with frequent dosing[369]. However, curcumin's amphiphilic properties require high levels of detergents for it to dissolve, causing the formulation to be too viscous for peripheral intravenous injection in humans[370] and thus would need to be administered via other means in clinical trials. Frost et al. reported preliminary results from a clinical trial testing the efficacy of curcumin to detect retinal Aβ plaques in AD patients. Curcumin was given orally to subjects with AD and cognitively normal controls. Retinal imaging was done to quantify curcumin fluorescence and compared to PET amyloid imaging as a measure of cortical plaque burden. Results found that curcumin retinal testing could differentiate AD patients from controls with 100% sensitivity and 80.6% specificity. The full study was expected to be completed in 2014[371] but results have not yet been published. It is important to consider that curcumin has poor bioavailability due to poor absorption, rapid metabolism, and rapid systemic elimination[372,373]. This may reduce its efficacy in retinal Aβ detection when administered orally to humans. Recent studies have reported methods for improving curcumin's bioavailability[373] and could potentially be applied to improving noninvasive retinal plaque detection in humans.

Chapter VI

Introduction to Specific Aims

As outlined in the previous chapters, there currently lies a major deficit in the field of AD in development of effective disease modifying therapeutics. Two major contributing factors are (1) the BBB severely restricts the breadth of experimental treatments that can be tested as it prevents passage of most compounds from peripheral circulation to the brain and (2) it is likely that significant neurodegenerative changes have already occurred at the time of diagnosis and thus, treatment is initiated too late in disease progression to inhibit further cognitive decline. To address both challenges, we sought to identify ways to improve delivery of compounds to the brain parenchyma that could be used clinically for either novel diagnostic testing or therapeutic applications. We are also developing a noninvasive method of detecting AD pathology that could potentially be readily implemented clinically to identify patients presymptomatic stages of AD such that therapy can be initiated earlier and potentially improve clinical outcomes.

This work has three primary specific aims:

Specific aim 1: To evaluate lipopolysaccharide-mediated opening of the blood brain barrier for improved theranostic delivery in Alzheimer's Disease. We hypothesize that controlled induction of a systemic inflammatory response can increase permeability of the BBB and improve delivery of both small molecules and larger agents, including nanoparticles, that previously had limited clinical applications due to poor BBB permeability. As this approach is not dependent on specific trans-endothelial transport mechanisms, it could be used to improve delivery of a variety of agents for both diagnostic and therapeutic purposes.

Specific aim 2: To demonstrate that aerosolized thioflavin S can bypass the blood brain barrier and bind Aβ plaques *in vivo*. In addition to increasing BBB permeability, we are also investigating aerosol administration to target olfactory-mediated transport to the brain and thus completely bypassing the BBB. Similar to specific aim 1, this approach also generalizable to a variety of compounds and has the added advantage of not directly altering the BBB, which is accompanied by inherent risks of exposing the brain to a host of circulating pathogens or toxins. For this study, we are using thioflavin S, a fluorescent Aβ-binding agent with poor BBB permeability.

Specific aim 3: To demonstrate that aerosolized fluorescent probes can bind retinal Aβ plaques and be detected noninvasively. Using aerosol administration, we hypothesize that thioflavin S and curcumin can bind retinal Aβ plaques and be detected using noninvasive retinal imaging. If successful, this approach could be used to evaluate retinal plaque burden as a biomarker and early diagnostic for future development of AD.

Chapter VII

Immune-Mediated Blood Brain Barrier Opening for Improved Reagent Delivery in Alzheimer's Disease

Introduction

The exact mechanism of neuronal degeneration in AD remains unknown; however, the cytopathological hallmarks of the disease appear to be the formation of extracellular Aβ plaques, which leads ultimately to profound neuron toxicity and atrophy characteristic of disease[374]. Since the formation of Aβ plaques is one of the underlying mechanisms implicated in AD, detection and eventual disruption of their formation, particularly at the onset of the disease and prior to significant neurodegeneration, would be an ultimate goal in treating AD.

Toward that end, experimental therapeutics, including small molecules[375,376] and antibodies[377] that target Aβ were developed. Although these approaches demonstrated significant promise and widespread appeal, as discussed in chapter two, many demonstrated little or no therapeutic benefit during clinical trials. Several limitations exist in the development of drugs intended for the brain. For instance, a variety of criteria must be considered in all related initiatives, such as the drug's ability to cross the BBB and bind Aβ. In fact, AD clinical trials using antibodies may have largely been unsuccessful because they are unable to traverse the brain endothelium under normal physiologic conditions and thus not be effectively delivered to mediate a therapeutic benefit. As basic neurological research continues to reveal novel targets for AD therapy, the necessity to

deliver therapeutic agents across the BBB becomes of paramount importance. The improved bioavailability of drugs or imaging probes in the brain for the detection/treatment of AD produces a prolonged therapeutic effect and, as a consequence, reduces toxicity, cost, and importantly is expected to eradicate the disease[210,378–380].

Unfortunately, drug delivery across the BBB is still a significant challenge and lags behind other areas in molecular neuroscience, because of the difficulties posed by this barrier[381]. The brain contains blood capillaries that are different from the blood capillaries in other tissues. Peripheral capillaries have open interendothelial junction spaces and active pinocytosis, which forms a paracellular route and a transcellular route, respectively, for the free diffusion of molecules from the blood to the organ interstitium. However, brain capillaries are lined with a unique layer of endothelial cells that lack fenestrations and are sealed with intercellular tight junctions that effectively prevent diffusion through paracellular pathways. Furthermore, these cells have minimal pinocytosis that eliminates the nonspecific transcellular route of molecular transport from blood to brain[382]. This is exacerbated by the fact that brain capillaries are also reinforced to eliminate nonspecific molecular transport into the brain with a matrix of astrocyte foot processes and P-gp active drug efflux transporter proteins in the luminal membrane of the cerebral capillary endothelium[383,384]. Due to these unique properties of vertebrate brain capillaries, the distribution of molecules from blood to the brain interstitial space is facilitated mainly via two mechanisms, namely, lipid-mediated free diffusion of small molecules and catalyzed transport of small or large molecules[381]. Certain large molecules such as peptides can be transported across the BBB via RMT systems[257]. To facilitate the delivery of drugs, which do not belong to the aforementioned categories or in special circumstances, a number of

active techniques have been developed, such as intracranial injection[385], electroporation or incorporation of a drug into cationic liposomes[386,387], dendrimers[388] or bacterial toxins[389,390], focused ultrasound[252,391], pulsed electric field[392] and intracerebroventricular injection methods using convection-enhanced delivery[393] and intraventricular catheters to bypass the BBB[394]. It has been known that the BBB also can be compromised during disease conditions, such as meningitis, encephalitis, sepsis and local and systemic infections[395]. Even in AD itself, increased inflammatory activity may be responsible for inducing BBB dysfunction[313,316,396,397]. Inflammation has also long been known for disrupting the BBB[398–400]. For example, lipopolysaccharide (LPS), a bacterial endotoxin has been shown to affect the permeability of the BBB in animal models[247]. LPS is a molecular motif structurally similar amongst gram-negative bacteria that is recognized by the innate immune system and results in pro-inflammatory cytokine release mediated by the transmembrane protein, toll-like receptor 4 (TLR-4)[401]. Vascular changes occur as a result of this inflammatory state, including increased expression of leukocyte adhesion molecules, cytokine release and increased permeability, which are all seen in brain endothelium as well[402–404]. Previous studies have shown that LPS can alter BBB permeability[405,406], increase absorptive endocytosis and immune cell adhesion/trafficking[403,407,408], and direct application of LPS to brain endothelial cells increases intracellular leakage[409]. However, innate immune response to LPS mediated by leukocyte recruitment and activation[410–416] can become maladaptive in severe localized and systemic infections, leading to septic shock due to rapid cytokine release[417].

Given the complexity of the biological and immunological events that emerge after treating animals with LPS, questions arise over the relative benefits and pernicious effects of LPS.

In this work, we want to examine the toxicity threshold, kinetics of BBB opening and the benefit of LPS-induced opening of the BBB on a transgenic mouse model of AD. The data suggest that the BBB in 5XFAD mice remains intact even when the animals are old, however, it is prone to be compromised by LPS compared to the wild type counterpart. We conclude that LPS has gravitas as a BBB opener, albeit careful dosing is necessary to avoid potential toxicity.

Materials and Methods

Materials

Thioflavin S and LPS were obtained from Sigma Aldrich (St Louis, MO) and superparamagnetic iron oxide nanoparticles (SPIO) were developed in-house as previously described[418]. All reagents and solvents were of analytical grade and used as received from the commercial source without further purifications.

Animals

5XFAD and control C57BL/6J mice were maintained at Vanderbilt University under standard conditions, in a 12 hr light/dark cycle and with free access to food and water. The 5XFAD mice over express both mutant human amyloid precursor protein (APP) and presenilin 1 (PS1), correlating with high burden and accelerated accumulation of the Aβ. A colony of 5XFAD transgenic mice obtained from Jackson Laboratories was maintained by crossing 5XFAD mice with a wild-type (wt) C57BL/6J strain. The mice were genotyped by a standard polymerase chain reaction using DNA isolated from tail tips with the following primers: PSEN1 forward, 5'–TCATGACTATCCTCCTGGTGG-3' and reverse, 5'-CGTTATAGGTTTTAAACACTTCCCC-3'. For APP, forward, 5' -AGGACTGACCACTCGACCAG-3' and reverse, 5'-CGGGGGTCTAGTTCTGCAT-3'. We also genotyped mice for the presence of retinal degeneration Pde6brd1 mutation using forward, 5'-AAGCTAGCTGCAGTAACGCCATTT-3' and reverse, 5'-ACCTGCATGTGAACCCAGTATTCTATC-3'. After polymerase chain reaction amplification, the DNA product of each reaction was analyzed by size fractionation through a 1% agarose gel; with Pde6b mutant=560 bp, APP transgene= 377 bp and PSEN1

transgene=608 bp. The 5XFAD mice were maintained as heterozygous. Animal experiments were conducted per the guidelines established by Vanderbilt University's Institutional Animal Care and Use Committee. At the end of the study, animals were euthanized by cervical dislocation after sedation with 2.5% isoflurane. Clinical signs were used to verify euthanasia, including heartbeats and reflection to toe-pinching. Further, if animals showed signs of illness (weight loss, food withdrawal, or infection) they were sacrificed before the endpoints. All experimental procedures in this study were approved by the Vanderbilt University IACUC panel.

LPS Dose Thresholds

In a series of pilot studies, the maximal dose with which LPS, derived from Escherichia coli O111:B4 (Sigma Aldrich, St Louis, MO), could be administered was determined to be 3mg/kg. Additional pilot studies supported previously published results[402] that LPS-mediated BBB permeation can be observed 24 hr after administration. To illustrate the dosage-dependent effect of LPS on BBB opening, LPS was administered via tail vein injection at varying doses (0.01mg/kg, 0.1mg/kg, 1mg/kg, 3mg/kg) on sedated mice, which received 2.5% isoflurane mixed with 2 liter/minute of oxygen. Approximately 24 hr later, LPS-treated mice (3-5-month-old or 13-15-month-old) were treated with either i.v. thioflavin S (5XFAD n=3) or SPIO nanoparticles [5XFAD n=6 (3 young, 3 old mice), wt n=10 (3 young, 7 old mice) age-matched]. Brain specimens were harvested 8 hr following this final injection using the cardiac perfusion protocol (described below).

Thioflavin S/SPIO formulation and administration

Thioflavin S was prepared in sterile saline and filtered using 45μm Luer-Lok syringe

filters. During preparation, samples were wrapped in foil to prevent photodegradation. A 2 mg/kg dose of thioflavin S was administered to each animal. 10 mg/kg SPIO nanoparticles were given to respective mouse cohorts. SPIO was stored in 1x PBS but diluted in sterile saline prior to administration. Intravenous injection of both thioflavin S and SPIO solutions were accomplished through the caudal tail vein in mice anesthetized with 2.5% isoflurane. While anesthetized, hot water in a standard latex glove was applied to the tail to induce dilation of the caudal tail vein. A catheter prepared from an insulin syringe and capillary tubing was filled with saline and inserted into the tail vein. To ensure intravenous delivery, catheter position was confirmed by observing blood back-filling the catheter. The experimental compound was then injected, and the catheter was flushed with saline. Following administration, mice were observed until they regained consciousness and returned to the mouse facility for recovery.

Cardiac perfusion procedure

Following exposure or treatment, mice were anesthetized with isoflurane and laid on a bed of ice after which the thoracic cavity was accessed via a sharp transverse incision into the abdomen. This was followed by a series of longitudinal cuts with surgical scissors to open the thoracic cavity by cutting the sternum to the right of the xyphoid process, which then was stabilized with a thoracic retractor to expose the heart. Perfusion was performed with a 25-gauge syringe containing ice-cold PBS (30 mL, pH 7.4) inserted into the apex of the heart through the left ventricle and injected slowly into the ascending aorta. Upon initiation of perfusion, the right atrium was snipped using micro scissors to facilitate drainage of the systemic venous return. Immediately following PBS perfusion, 30 mL of 4% paraformaldehyde (PFA) (pH 7.4) was perfused. With perfusion completed, the animals

were decapitated, and their brains quickly harvested. Brains were removed by making incisions from the cervical spine to the auditory canal. A shallow incision was made at the interparietal and parietal bone junction. Surgical scissors were inserted into the incision in the skull and a cut was made along the sagittal suture, being careful not to damage the brain. The skull was then removed in pieces using forceps. Cranial nerves and the olfactory bulbs were cut to free the brain from the skull. After removal, brains were fixed in 4% PFA overnight at 4°C. Brains to be immuno-stained were cryoprotected for two days in 10% sucrose at 4°C. Cryoprotected brains were then embedded in Tissue-Tek optimum cutting temperature (OCT) compound for cryosectioning and stored at -80°C until sectioned. All other fixed tissue was embedded in paraffin by the histology core for sectioning.

Immunohistochemistry

Brains embedded in OCT were cut into sagittal sections (10 μm) using a Tissue-Tek cryostat and mounted onto Fisher Premium plain, charged glass slides (Fisher Scientific). Prior to staining, slides were washed with PBS for 5 min before being subjected to a citrate buffer antigen retrieval protocol. Slide mounted sections were incubated for 30 min in a 100°C bath of sodium citrate buffer (10 mM sodium citrate, 0.05% Tween 20, pH 6.0) and allowed to cool for 20 min before being washed in PBS for another 5 min. Sections were blocked in 3% bovine serum albumin (BSA) in PBS with 0.05% Tween-20 (PBST) for 1 hr at room temperature. Treated sections were then incubated overnight at 4°C with primary antibodies: beta amyloid 17-24 (4G8) mouse monoclonal antibody (1:200 dilution, Biolegend, San Diego, CA, USA) diluted in blocking solution. Following two 5 min washes with PBST, the sections were subsequently incubated with secondary antibodies goat anti-mouse Alexa 647-conjugated IgG (1:200, ThermoFisher Scientific, Pittsburgh,

PA, USA) for 1 hr at room temperature. The sections were then washed with PBS and coverslipped with a fluorescent-specific antifade mounting medium (Vector Laboratories, Burlingame, CA) and allowed to dry in the dark at room temperature overnight.

Perls' staining for SPIO nanoparticle detection

Brains were manually cut into 2 mm coronal sections using a mouse brain matrix and all sections were embedded into a single paraffin block. Splenic tissue taken exclusively from untreated wt mice were also embedded in each paraffin block and sectioned. Because spleens naturally contain a high level of iron, it serves as an internal positive control for Perls' Prussian Blue staining on each slide. 5 μm coronal sections were cut on a microtome and mounted onto charged glass slides. Paraffin sections were deparaffinized in xylene and rehydrated in a series of ethanol baths. Following rehydration, slides were incubated in freshly prepared Perls' Prussian Blue solution (1:1 potassium ferrocyanide and hydrochloric acid) for detection of ferric iron, including SPIO nanoparticles found in tissue parenchyma. After washing in water, slides were counterstained in nuclear fast red solution for 5 min. Finally, sections were washed, dehydrated in a series of ethanol baths, cleared in xylene, and mounted using Organo/Limonene mount (Sigma Aldrich, St Louis, MO). After mounting, slides were allowed to dry at room temperature overnight.

Assessment of the distribution of the probes via stereological analysis

High-resolution digital images of whole slides in brightfield at 20x magnification to a resolution of 0.5 μm/pixel were produced using the Leica SCN400 Slide Scanner (Fig.7-1). Images were then analyzed in a web-based digital slide-viewing environment called the

Digital Imaging Hub (Leica Biosystems) using Tissue Image Analysis (TIA) tools. A color definition file was made to identify positive Perls' Prussian Blue stain in mouse spleen tissue, which naturally contains a high level of iron and serves as a positive control tissue (Fig.7-1B). Regions of interests (ROIs) manually drawn for individual brain sections were then analyzed for total tissue area and positive stained area as determined by the color definition profile. These values were used to calculate percent positive tissue area, which represented SPIO nanoparticle delivery to the brain.

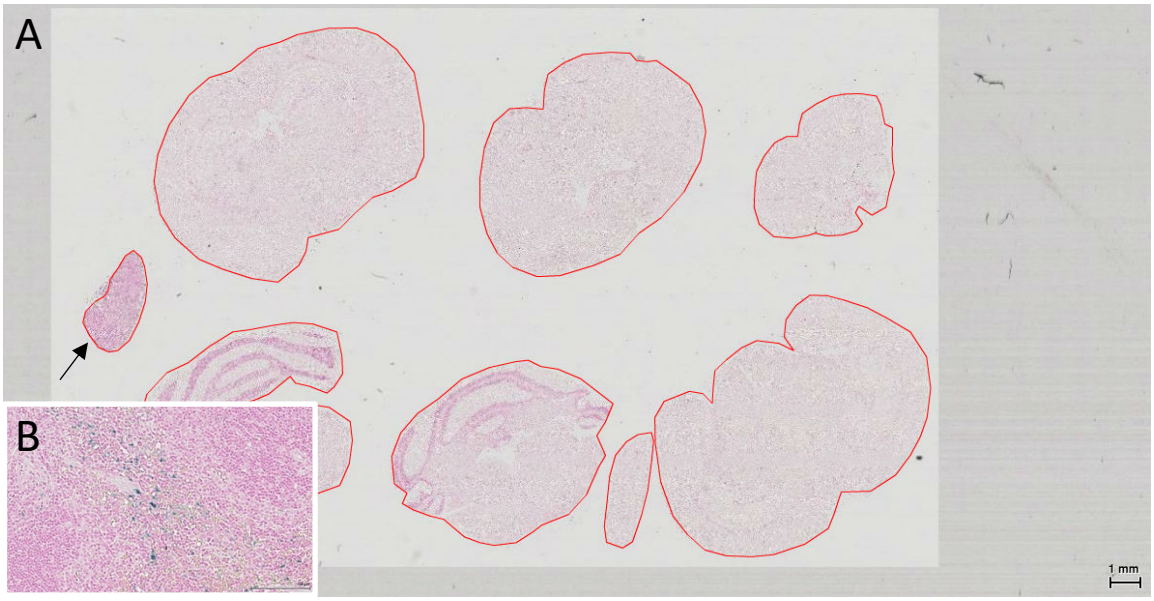

Figure 7-1. Digital image of mouse brain and spleen. (A) ROIs were drawn around each brain section and spleen (shown with arrow). (B) High magnification of spleen with positive Perls' staining (blue).

Confocal microscopy

Whole section fluorescence imaging was performed on mounted slides from LPS-treated and untreated mouse cohorts with i.v. injection of thioflavin S to assess the BBB permeability for small molecules. Imaging was performed on spinning disk confocal system equipped with a Nikon Eclipse Ti microscope, a Yokogawa CSU-X1 spinning disk head, and Andor DU-897 EMCCD camera. The sections were visualized by montage scan with 10x Plan Apo (air) 0.45 NA WD 4.0 mm objective, with or without 1.5x intermediate magnification, with 488 nm and 647 nm laser lines to excite thioflavin S and Alexa Fluor 647 respectively, and appropriate emission filters 525 nm (+/- 18 nm), and 641nm (+/- 75 nm) were used. All slides were imaged with identical settings utilizing NIS-Elements imaging software for acquisition and analysis.

Statistical analysis

All statistical analysis was performed using Graphpad Prism 7.0 (Graphpad Software, Inc.). Error bars represent the standard error of the mean (SEM). To assess differences in survival at 24 hr post LPS treatment between 5XFAD and wt mice receiving the same treatment, a chi-square test was used. Comparison of means of more than two groups was done using one-way analysis of variance (ANOVA) followed by the Newman-Keuls post-test.

Results

Maximal tolerable dose of LPS in wt mice

To assess the extent to which LPS could induce effective BBB opening without causing severe side effects or lethality, animals were treated with a series of concentrations of LPS via i.v. injection. Previous studies reported that i.p. injection of 3 mg/kg LPS is safe and significantly increased BBB permeability 24 hr post injection in a mouse model[248,402]. In this work, we want to compare the same dose using wt mice albeit with i.v. injection. In the first approach to assess the dose-toxicity relationship, mice (n=2) were treated with 3 doses of 3 mg/kg LPS, with each injection 5 hr apart. Immediately after injection, all animals were recovered from anesthesia and appeared healthy, nevertheless, the slow but probably strong inflammation[419] caused by repeated doses resulted in 100% fatality (Table 7-1). When the injection frequency was reduced to two doses (n=3) of 3 mg/kg LPS, 5 hr apart, treatment was still highly lethal at 24 hr post LPS injection. Similar to the previous report for i.p. injections, we found that i.v. injection of a single dose of 3 mg/kg of LPS was well tolerated with approximately 90% survival in wt mice (n=18), albeit 5XFAD mouse (n=21) survival using the same dose is much lower, at 57% ($p<0.05$, chi-squared test). There is a small chance of death in mice if combined with large injection volume. However, if the injection volume was reduced from 120 μL to less than 100 μL, the animals were able to tolerate the treatment. At low LPS doses ranging from 0.01-1 mg/kg, there was 100% survival in wt mice (n=4, each).

LPS Dose (mg/kg)	# Animals Treated	# Died	% Lethality
0.01	4	0	0
0.1	4	0	0
1.0	4	0	0
3.0	18 (21)	2 (9)	11 (43)
3.0 (x2)	3	2	67
3.0 (x3)	2	2	100

Table 7-1. Effect of LPS dose on lethality of wt and 5XFAD mice. From 0.01-3 mg/kg of LPS was injected i.v. via the tail vein of mice in a volume <100 μL. Double (x2) or triple doses (x3) were injected 5 hr apart. Data for 5XFAD mice is shown only for 3 mg/kg dose, in parentheses. Reprinted from Journal of Alzheimer's Disease with permission from IOS Press[420].

LPS-induced blood brain barrier opening in 5XFAD mice for thioflavin S

Next, we assessed BBB permeability on 5XFAD mice using the highest tolerable dose of 3 mg/kg LPS as described in the toxicity study above. To facilitate the detection and visualize the distribution of the delivered molecules upon BBB compromise, we used thioflavin S, since not only does it have high affinity for Aβ but it cannot cross the BBB under normal physiological conditions[421]. Further, thioflavin S is a fluorophore that can readily be detected in tissue sections. As shown in Fig.7-2A, *ex vivo* treatment of a 5XFAD mouse brain section with thioflavin S resulted in robust staining of Aβ in the hippocampus, cortex and subiculum. This finding is expected as thioflavin S is currently used for amyloid staining. However, due to its inability to penetrate the BBB, i.v. injection of 2 mg/kg thioflavin S to 5XFAD mice does not show signal in the brain (Fig.7-2B).

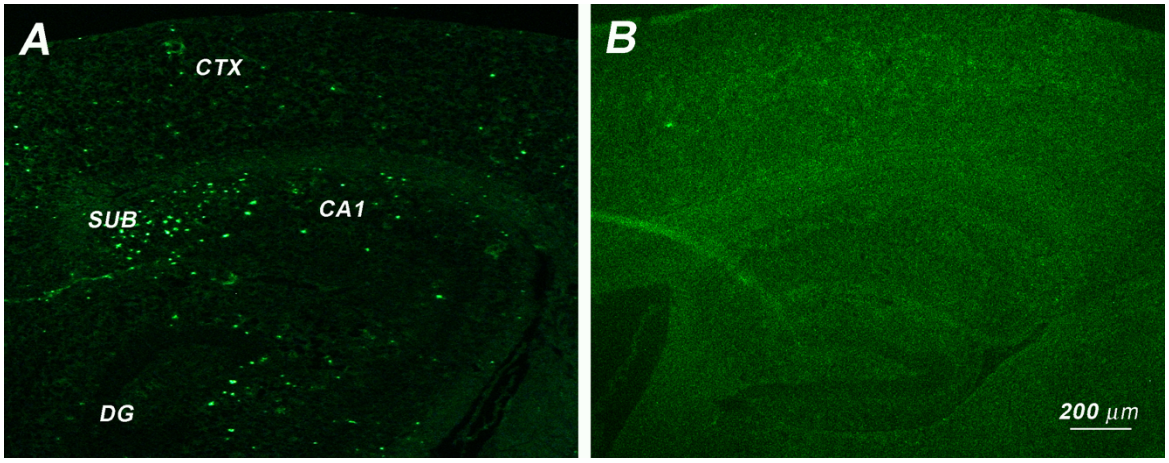

Figure 7-2. Assessment of BBB penetration capability and Aβ specificity of thioflavin S on 5XFAD mice. (A) *ex vivo* thioflavin S staining of the brain slide depicting the hippocampal region; (B) i.v. injection of 2 mg/kg thioflavin S resulted in no fluorescence signal in the hippocampus or cortex (CTX = cortex, SUB = subiculum, DG = dentate gyrus). Reprinted from Journal of Alzheimer's Disease with permission from IOS Press[420].

In the next experiment, as depicted in the timeline of Fig.7-3, aged 5XFAD mice (13-15 month-old) were injected i.v. with 3 mg/kg LPS, then 24 hr later the same LPS-treated animals were injected with i.v. thioflavin S (2 mg/kg). This optimized BBB opening timeframe was previously reported[402]. 8 hrs later, animals were cardiac perfused, sacrificed and brain sections were prepared for imaging. As shown in Fig.7-4A, if 5XFAD mice were treated with thioflavin S alone, this resulted in no fluorescence signal in the brain, albeit remarkable Aβ amyloid expression was detected via immunohistochemistry (Fig.7-4B&C). In contrast, when 5XFAD mice were i.v. injected with the same thioflavin S dose after BBB compromise by LPS, the compound now can reach the brain and bind to Aβ plaques at regions of high plaque burden, such as the cortex (Fig.7-4D) and the data correlate with Aβ immunostaining on consecutive slides (Fig.7-4E&F). Thioflavin S distribution to the other areas in the brain, including subiculum, CA1, CA2 regions is shown in Fig.7-5.

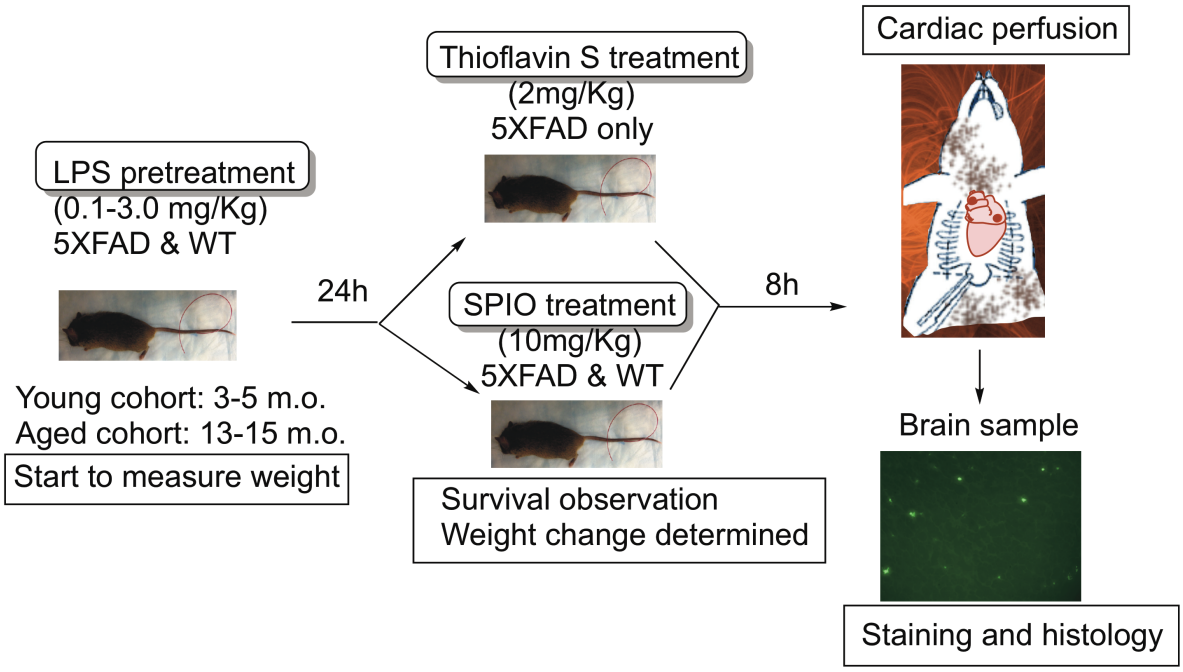

Figure 7-3. Timeline and procedures to test LPS-mediated opening the BBB in transgenic and wt mice using small and large materials. Reprinted from Journal of Alzheimer's Disease with permission from IOS Press[420].

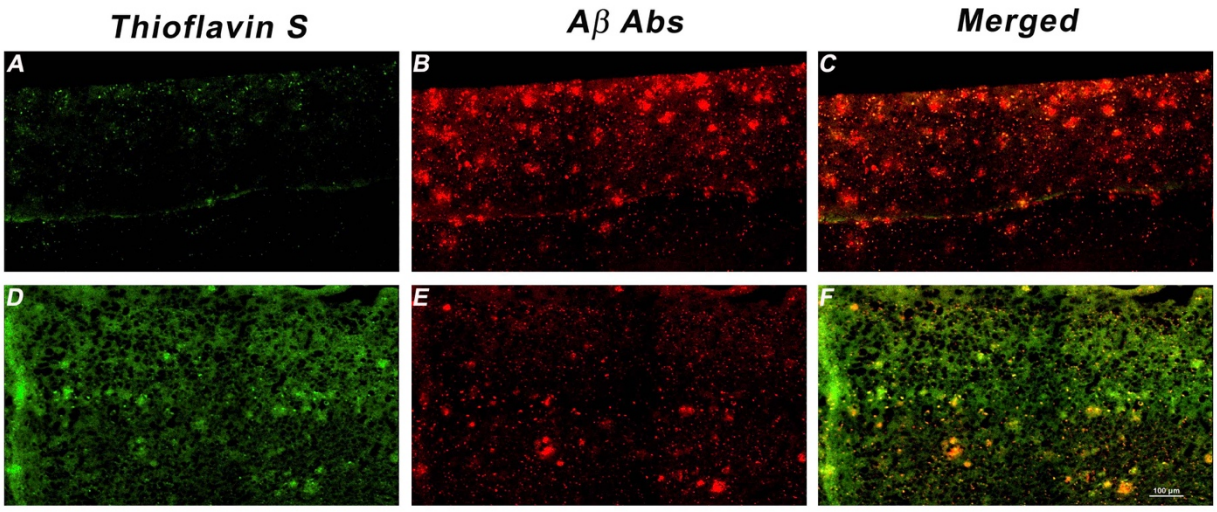

Figure 7-4. Effect of LPS on BBB opening in cortex. 5XFAD mice were injected i.v. with 2 mg/kg thioflavin S alone, (A) thioflavin S channel (green), (B) anti-Aβ antibody channel (red), and (C) merged data on the same section or pretreated with LPS 24 hr before thioflavin S injection (D) thioflavin S channel (green), (E) anti-Aβ antibody channel (red) and (F) merged data on the same section. Reprinted from Journal of Alzheimer's Disease with permission from IOS Press[420].

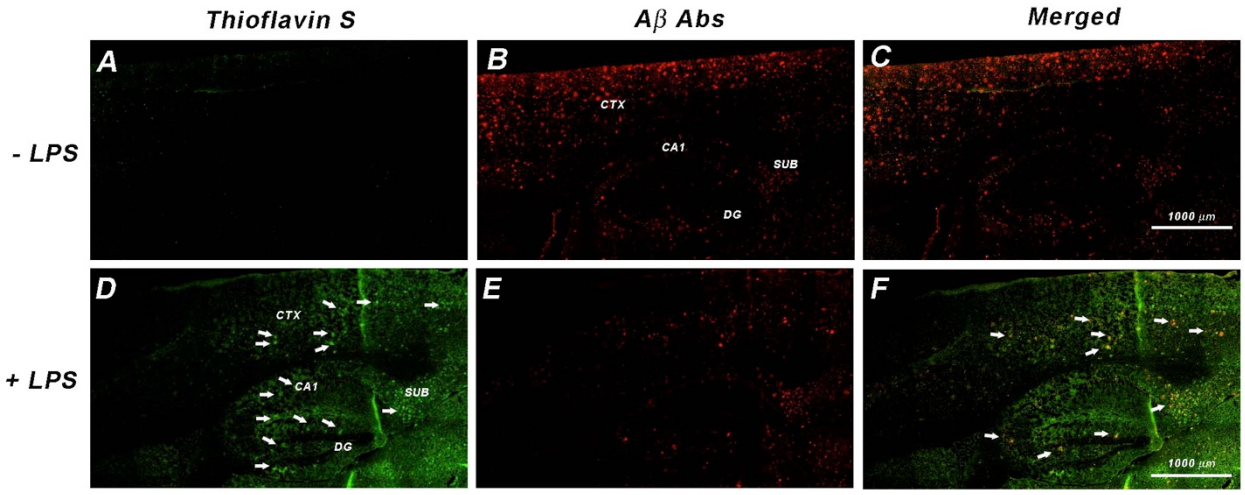

Figure 7-5. Effect of LPS on BBB opening in cortex and hippocampus. 5XFAD mice were injected i.v. with 2 mg/kg thioflavin S alone (A) thioflavin S channel (green), (B) anti-Aβ channel (red), and (C) merged data on the same section or pretreated with LPS 24 hr before thioflavin S injection (D) thioflavin S channel (green), (E) anti-Aβ antibody channel (red) and (F) merged data on the same section. Reprinted from Journal of Alzheimer's Disease with permission from IOS Press[420].

LPS-induced blood brain barrier opening for large materials

Next, we determined whether LPS pretreatment makes the BBB permeable to large materials for future delivery applications of not only small molecules but also large vehicles, such as antibodies or nanoparticles. In this work, 30 nm SPIO nanoparticles (10 mg/kg) were injected i.v. into wt and 5XFAD mice 24 hr post LPS treatment (3 mg/kg) also via i.v. injection (Fig.7-3). Brains were collected 8 hr later following transcardial perfusion, and prepared sections were stained for iron using our previously described protocols[418,422]. When young (3-5 month-old) wt and 5XFAD mice were pretreated with LPS, they showed similar results of minimal positive Perls' stain in the brain, at the detection threshold, suggesting limited nanoparticle delivery to the brain (Fig.7-6G). However, when these procedures were repeated on aged 5XFAD mice (13-15 month-old) with LPS before SPIO injection, significant SPIO positive stain was detected in the brain parenchyma (Fig.7-6CDEF). Aged 5XFAD mice injected with SPIO but not LPS showed little stain, suggesting that with advanced age and disease progression, the BBB is intact enough to limit SPIO delivery to the brain in the absence of LPS pretreatment (Fig. 7-6B). Overall, the data suggest that even at advanced stages of disease in our model of AD, the BBB is still partially intact but more susceptible to increased BBB permeability mediated by LPS to allow delivery of nanoparticles as large as 30 nm to the brain.

Finally, we sought to determine whether LPS-mediated BBB opening is due to AD pathology or through normal aging processes. Aged wt animals (13-15-month-old, n=7) were treated with LPS and SPIO in identical dose and process as mentioned with other cohorts. As shown in Fig.7-6G, there is no significant difference in the SPIO permeability in the aged wt mice versus the young, 3-month-old counterparts. Taken together, the data

suggest that LPS-induced opening of the BBB is due to AD pathology and not aging alone.

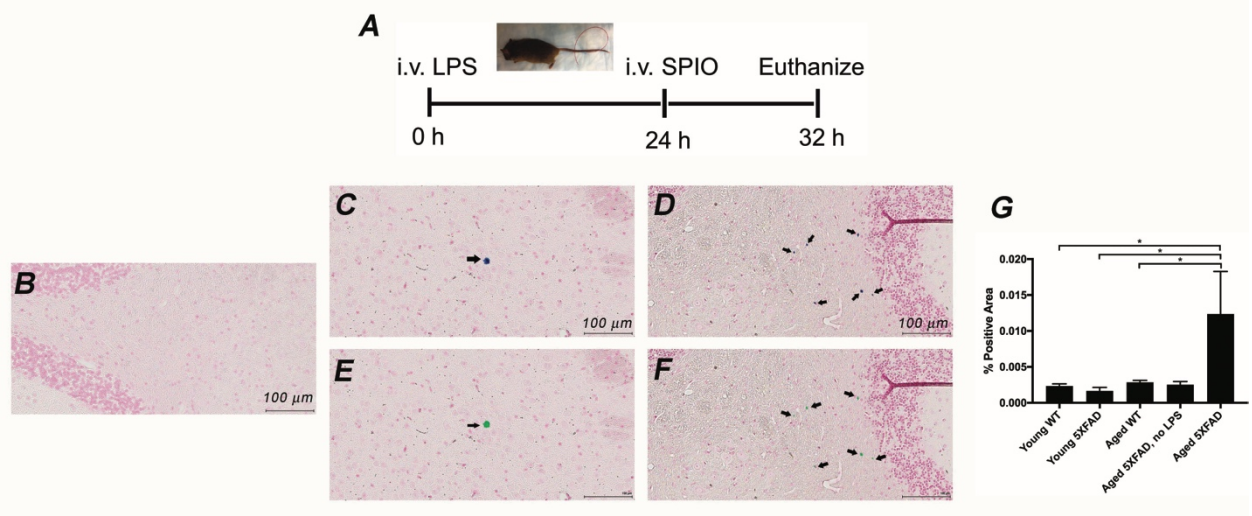

Figure 7-6. LPS-induced BBB opening allows delivery of large molecules. (A) Timeline of the study with a figure showing caudal tail vein injection; (B) Mouse brain section receiving SPIO injection but no LPS pretreatment; (C & D) Detection of SPIO nanoparticles (arrows) in the brain parenchyma of 5XFAD mice after i.v. injection; (E & F) are default color of (C & D) for analysis; (G) quantitative analysis of SPIO distribution in the brain of 5XFAD vs wt mice of different ages after the animals were pretreated with or without LPS, aged mice were 13-15 month-old while young mice were 3-5 month-old; *$p<0.05$. Reprinted from Journal of Alzheimer's Disease with permission from IOS Press[420].

Discussion

The natural paradox of the BBB is that it serves as a formidable barrier to protect the brain from being harmed by exogenous and foreign materials. On the other hand, it also excludes many drugs intended for therapy[231]. The endothelial cells of the BBB provide an important interface between the brain and other tissue environments and possess tight junctions of severely limited permeability[423]. Actively induced opening of the BBB faces the reality of the impact of the material on the body as a whole, as the effect may not be targeted to only brain endothelium. Although it has been demonstrated that bacterial products such as LPS could be used to induce BBB opening via robust inflammation[424], the toxicity caused by the agent is conspicuous because of LPS production of different inflammatory mediators including IL-1β, IL-6, TNF-α, nitric oxide, MMP-2 and prostaglandins[425–427]. Specifically, IL-1β is implicated in failure of the BBB[428,429]. Our data suggest that the maximal tolerable i.v. dose of LPS for wt mice is 3 mg/kg without co-administration of anti-inflammatory drugs. When this threshold dose is combined with large injection volume or with repeated doses, even at an extended interval between injections, the combination can cause fatality. However, the same dosing in 5XFAD mice was approximately 30% more lethal ($p<0.05$, chi-squared test), suggesting that the disease model is more susceptible to LPS-mediated toxicity.

To test the BBB of aged 5XFAD mice, a transgenic model of AD, one of the candidate compounds we studied is thioflavin S. It is a small molecule, but its possession of a charge moiety prevents it from penetrating the BBB[421]. Another advantage for this particular study is that thioflavin S is a fluorescent dye, suitable for characterization of BBB compromise

via direct visualization using microscopic imaging and histology. Further, thioflavin S is an Aβ-binding molecule and we demonstrated that if the BBB is compromised by LPS, thioflavin S not only will cross the barrier but it will report the expression of Aβ in the areas of interest, such as the subiculum, CA1, CA3, dentate gyrus (Fig.7-5) and cortex (Fig.7-4D&F), all known to have high plaque burden in 5XFAD mice. The data also showed that the BBB in aged 5XFAD mice (13-15 month-old) is somewhat intact as thioflavin S fluorescence is not detected in the brain without LPS treatment (Fig.7-4A&C), suggesting that even at advanced ages, AD-related pathology has not disrupted the BBB significantly enough to allow thioflavin S to enter the brain parenchyma and target Aβ plaques. Further, the results suggested that aside from small molecules, the LPS-compromised BBB in aged 5XFAD mice is also permeable to large structures such as SPIO nanoparticles. These data provide useful information for future applications of antibodies and nanoparticles as therapeutics for AD. The SPIO nanoparticles used in this work are 30 nm in size, much larger than any tested anti-Aβ antibodies in clinical trials and could cross the BBB to enter the brain parenchyma in aged 5XFAD mice with LPS pretreatment. Interestingly, the degree of SPIO detected in 5XFAD mice was 4-fold higher than that found in wt mice (both 3-5 and 13-15-month-old cohorts) receiving the same LPS pretreatment (Fig.7-6G), alluding that AD pathology and not aging-related changes play a role in susceptibility to BBB compromise after LPS treatment. A caveat worth mentioning is that regardless of the route of distribution, our i.v. injection data corroborates earlier studies using i.p. injections[402] that all tested doses of LPS, even a very small amount, causes significant body weight loss (Fig.7-7). Animals treated with LPS experienced significant weight loss within 24 hr following i.v. injection of any LPS dose described

above. All doses of LPS produced a significant decrease in body weight compared to untreated controls, even at a very low dose, such as 0.01 mg/kg LPS, where 8% weight loss occurred. If comparing the effect across the tested doses, there is an increase in weight loss of animals receiving a dose of 3 mg/kg LPS compared to those that received 0.01 mg/kg. In conclusion, we have demonstrated that the BBB of aging 5XFAD mice is intact, albeit more vulnerable than wt counterparts 24 hr after i.v. injection of LPS. Theoretically, LPS-induced opening of the BBB can potentially be used to deliver antibodies or large materials for therapy or diagnostic application, but for future clinical translation, the use of LPS should be administered with great circumspection. As demonstrated in this work, LPS dose will likely need to be reduced to prevent toxicity. Another caveat worth mentioning is that even at low doses of LPS, weight loss of treated subject is inevitable. Therefore, clinical implementation of LPS-induced BBB opening, particularly for AD patients would require ways to overcome the weight loss and increased lethality seen in our preclinical study either through the use of a different pro-inflammatory compound, different dosing, or even pairing with an anti-inflammatory agent that reduced unintended effects while not inhibiting BBB opening.

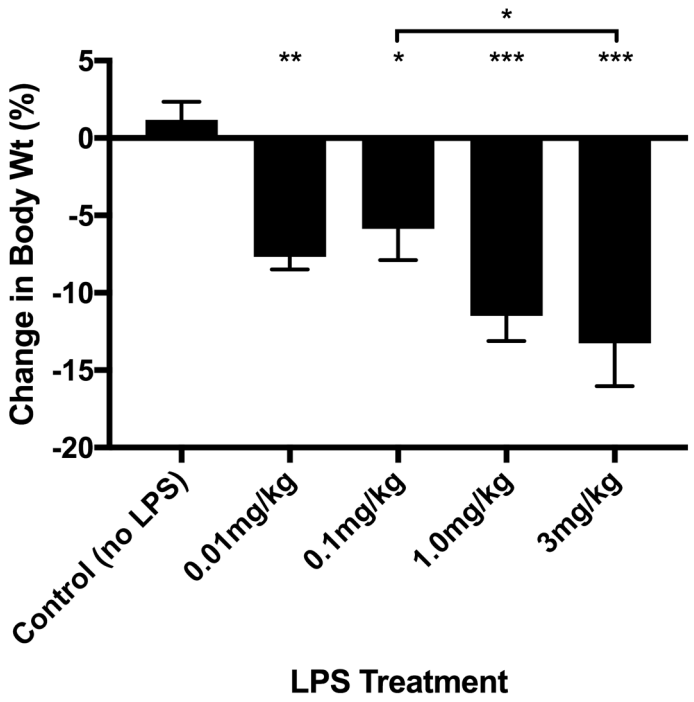

Figure 7-7. Effect of LPS on weight loss 24h after wt mice were injected i.v. with different doses of LPS ranging from 0.01-3mg/kg; * $p \leq 0.05$, ** $p \leq 0.01$, *** $p \leq 0.001$. Reprinted from Journal of Alzheimer's Disease with permission from IOS Press[420].

LPS-mediated opening of the BBB offers exciting new avenues of research in the development of diagnostic and therapeutic agents for AD and other neurodegenerative disorders. In future studies, as improved nanoparticle delivery is achieved, SPIO nanoparticles can be targeted to bind Aβ plaques by coating with amyloid binding motifs. Nanoparticles can then be detected noninvasively by MRI imaging techniques[430,431]. This can be achieved by conjugating nanoparticles with monoclonal antibodies or any other receptor with high plaque affinity. Further, Aβ-binding agents with poor BBB permeability can now be studied for therapeutic efficacy upon pretreatment or co-administration with low dose LPS. As an example, thioflavin S has never been studied as therapeutic for AD due to its inability to traverse the brain endothelium[421]. However, our results clearly show using that we can now effectively deliver thioflavin S to the brain and target Aβ. Investigation into the longitudinal effects of LPS/thioflavin S on AD pathology could demonstrate therapeutic efficacy not otherwise seen with thioflavin S. A similar study could also be done using anti-Aβ antibodies to show that LPS pretreatment not only increases antibody delivery to the brain but also improves therapeutic efficacy as demonstrated through plaque reduction.

As previously mentioned, there are several caveats for use of LPS clinically, especially in an AD patient population. Our results show that our AD transgenic mouse model was not only more susceptible to LPS-mediated BBB opening but also more susceptible to the negative effects of inducing systemic inflammatory activation, as demonstrated by increased lethality when compared to wt mice receiving the same dose. Additionally, even low dose LPS treatment resulted in significant weight loss, which would hinder its use in

AD patients, who already exhibit clinically substantial weight loss[432]. In future studies, we plan to characterize specific immune response to LPS in 5XFAD mice by measuring changes in cytokine expression, studying immune cell mobilization and activation, and how each factor affects BBB permeability through selective upregulation or direct administration of endogenous immune mediators. By isolating a specific immune-mediated mechanism of BBB opening, targeted activation could be accomplished by co-administering LPS with an anti-inflammatory such that immunologic factors affecting BBB opening are preferentially upregulated. Additionally, other immunogenic compounds besides LPS could be used. If we are able to selectively target mechanisms affecting BBB permeability, we could potentially reduce the negative systemic effects of LPS treatment including increased lethality and weight loss, making immune-mediated opening of the BBB a viable approach for improved therapeutic delivery in AD and other neurodegenerative disorders.

Chapter VIII

Aerosolized Thioflavin S Bypasses the Blood Brain Barrier and Binds Aβ Plaques in 5XFAD Mice

Introduction

Aβ peptide can aggregate to form insoluble Aβ plaques extracellularly and these have been shown to be neurotoxic, though the exact mechanism of toxicity is still under investigation[73]. Although how Aβ mediates neurodegenerative changes is uncertain, development of therapeutics to prevent Aβ formation or promote clearance are being studied. Many compounds are available that can bind Aβ but have limited clinical efficacy either as a diagnostic or therapeutic agent due to limited BBB penetrance. In fact, the BBB excludes 98% of small molecule drugs and, with few exceptions, ~100% of large molecule drugs[231]. Attempts to target specific transport mechanisms including RMT[265–270], although can be effective, is not a generalizable approach and requires extensive optimization for each compound. Other methods of drug delivery, including transient pharmacologic opening of the BBB and direct intracerebroventricular or intraparenchymal injections, are unsafe and could lead to permanent neurological damage.

Recent work from our lab demonstrated that FMeC1, a curcumin analogue that binds Aβ, displayed improved delivery to the hippocampus when delivered as an aerosol than compared to intravenous injection[370], and we hypothesize that delivery is enhanced through improved bioavailability through uptake in the lungs as well as olfactory-mediated transport. Improved delivery through intranasal administration to the brain has been

demonstrated for a variety of experimental AD therapeutics including benzodiazepines[284,285], vaccine antigens[278,286], Aβ immunogens[287–289,433], insulin[291–298] and cholinesterase inhibitors[299–307]. One study demonstrated enhanced and more rapid delivery of intranasally administered curcumin to the hippocampus as compared to intraperitoneal injection[276], which corroborated our findings with FMeC1[370]. Multiple pathways mediate transport from the nasal cavity including vascular and lymphatic uptake, which contribute to peripheral distribution of compounds. Surprisingly, some molecules have been shown pass through the olfactory epithelium either through intracellular or extracellular transport and travel along the olfactory and trigeminal nerves, which connect the nasal passage to the brain[273] (Fig.8-1). It is this mechanism that is thought to allow fast and improved transport to the brain by bypassing the BBB. Targeting olfactory uptake with diagnostic and therapeutic agents could allow for noninvasive and safe delivery of compounds that previously had limited clinical application due to poor BBB permeability. Direct uptake also avoids systemic extraction or alteration and improved delivery to the brain would permit the use of lower doses to reduce peripheral toxicity. This delivery mechanism could also allow for targeting of specific brain regions through selective transport along the olfactory nerve through direct uptake and delivery or bulk flow mechanisms such as perivascular transport[277]. The entorhinal cortex receives afferent input from the olfactory nerve but is also immediately adjacent to and sends projections to the hippocampus. Both brain regions demonstrate high pathologic burden in AD and thus selectively targeting olfactory uptake could improve therapeutic efficacy.

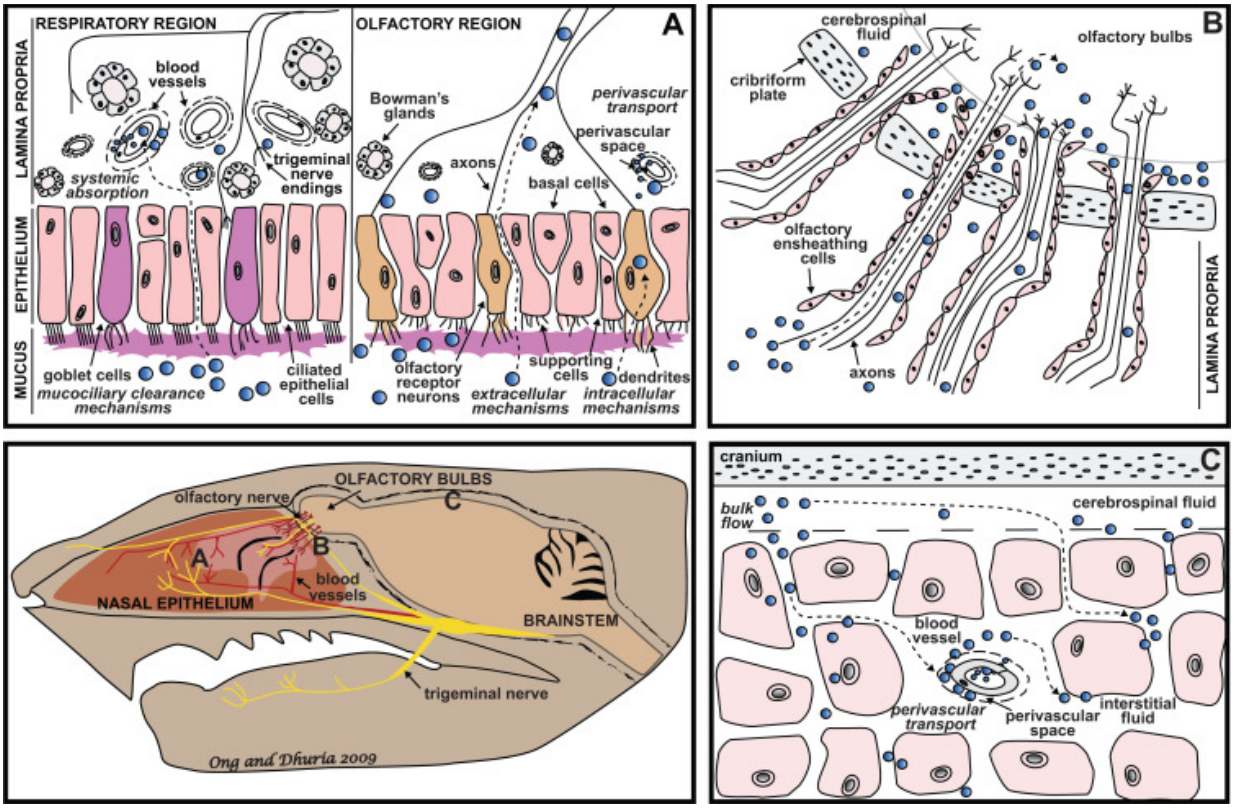

Figure 8-1. Pathways of drug distribution in the nasal cavity and central nervous system. Following intranasal administration, drugs (blue circles) come into contact with the nasal mucosa, which is innervated by olfactory and trigeminal nerves. (A) In the respiratory region, ciliated epithelial cells and mucous secreting goblet cells in the epithelium form the basis of mucociliary clearance mechanisms that remove foreign substances from the mucous layer towards the nasopharynx for elimination. Trigeminal nerve endings residing in the respiratory and olfactory epithelium convey chemosensory information to the CNS. In the olfactory region, olfactory receptor neurons are interspersed among supporting cells and basal cells to form the olfactory epithelium. Drugs can be transported through the nasal mucosa to the CNS by entering perivascular channels (dashed lines surrounding blood vessels) in the lamina propria or via extracellular or intracellular mechanisms involving olfactory and trigeminal nerves (dashed arrows). The blood supply to the respiratory epithelium is relatively greater compared to the olfactory epithelium, making it an ideal site for systemic absorption of nasally applied drugs. (B) After reaching the lamina propria, drugs can enter channels created by olfactory ensheathing cells surrounding the olfactory nerves, where they can access the cerebrospinal fluid (CSF) and olfactory bulbs (dashed arrows). (C) From the CSF, drugs can be distributed via bulk flow mechanisms and mix with brain interstitial fluid throughout the brain (dashed arrows). Drugs can also enter perivascular spaces after reaching the brain to be rapidly distributed throughout the CNS. Drugs that entered perivascular spaces from the nasal mucosa can also exit these spaces in the brain. These same pathways in the reverse direction are involved in the clearance of solutes from the CNS to the periphery. Reprinted from Journal of Pharmaceutical Sciences[277] with permission from Elsevier.

The overarching goal of this work is to reexamine Aβ-binding molecules that have BBB penetrance limitations and repurpose them for *in vivo* applications through use of improved delivery methods. One of such compounds is thioflavin S. It is a benzothiazole dye that exhibits enhanced fluorescence upon binding to amyloid, including those seen in peripheral amyloidosis and AD[434,435]. Also, it has been used in optical imaging studies to visualize Aβ plaques and track their formation longitudinally in transgenic mouse models of AD[421]. However, as demonstrated in chapter seven, thioflavin S has little to no BBB permeability since it is a charged molecule (Fig.7-2B). It is also targeted by ABC transporters and actively efluxed from the CNS[383]. When used in optical imaging, direct application of thioflavin S to the cortical surface is required[436]. Our findings suggest that when aerosolized thioflavin S is administered to 5XFAD transgenic mouse models of AD, thioflavin S can be delivered to the brain and is retained in a plaque-dependent manner. Delivery is likely mediated by the olfactory epithelium and thus bypassing limitations conventionally imposed by the BBB on peripheral administration. Overcoming this barrier enables us to repurpose thioflavin S and other Aβ-binding compounds that previously had limited *in vivo* application due to poor BBB permeability for either diagnostic or therapeutic applications. Also, utilizing thioflavin S' natural fluorescence, we can better understand the mechanism of delivery through the olfactory epithelium by direct visualization of transport and how targeting olfactory uptake may be utilized in treating AD, as well as other neurodegenerative diseases.

Materials and Methods

Materials

Thioflavin S was obtained from Sigma Aldrich (St Louis, MO). All reagents and solvents were of analytical grade and used as received from the commercial source without further purifications.

Animals

5XFAD and control C57BL/6J mice were maintained at Vanderbilt University under standard conditions, in a 12 hr light/dark cycle and with free access to food and water. The 5XFAD mice over express both mutant human APP and PS1, correlating with high burden and accelerated accumulation of the Aβ. A colony of 5XFAD transgenic mice obtained from Jackson Laboratories was maintained by crossing 5XFAD mice with a wild-type (wt) C57BL/6J strain. The mice were genotyped by a standard polymerase chain reaction using DNA isolated from tail tips with the following primers: PSEN1 forward, 5'–TCATGACTATCCTCCTGGTGG-3' and reverse, 5'-CGTTATAGGTTTTAAACACTTCCCC-3'. For APP, forward, 5' -AGGACTGACCACTCGACCAG-3' and reverse, 5'-CGGGGGTCTAGTTCTGCAT-3'. We also genotyped mice for the presence of retinal degeneration Pde6brd1 mutation using forward, 5'-AAGCTAGCTGCAGTAACGCCATTT-3' and reverse, 5'-ACCTGCATGTGAACCCAGTATTCTATC-3'. After polymerase chain reaction amplification, the DNA product of each reaction was analyzed by size fractionation through a 1% agarose gel; with Pde6b mutant=560bp, APP transgene=377bp and PSEN1 transgene=608bp. The 5XFAD mice were maintained as heterozygous. Animal experiments were conducted per the guidelines established by Vanderbilt University's

Institutional Animal Care and Use Committee. At the end of the study, animals were euthanized by cervical dislocation after sedation with isoflurane. Clinical signs were used to verify euthanasia, including heartbeats and reflection to toe-pinching. Further, if animals showed signs of illness (weight loss, food withdrawal, or infection) they were sacrificed before the endpoints. All experimental procedures in this study were approved by the Vanderbilt University IACUC panel.

Thioflavin S formulation and treatment

Mice were treated with 2% thioflavin S solution in ddH_2O (w/v) that was filtered with 45 µm Luer-Lok syringe filters using an atomizer developed within our laboratory and described below. Thioflavin S was injected into the nebulizer at steady rate over 3.5 hrs to aerosolize 6-7 mL solution. The treatment protocol was repeated for two consecutive days and mice were cardiac perfused 2 hr after the final treatment. Brains were fixed in 4% PFA for at least one day, cryoprotected in 10% sucrose for two days at 4°C and stored for sectioning and staining.

Inhalation Exposure and Compound Atomization

The atomizer system is comprised of a polyvinylidene fluoride polymer cross-flow atomizer (Single Pass Atomizer, SPA), an L-shaped conveyer, three inhalation ports, inlets for pressurized gas and liquid and a control unit to regulate aerosol generator air (Fig.8-2). Because of the rapid flow of air across the capillary tip, the airflow shears thioflavin S-containing solution into micron sized droplets that are diluted with a stream of air delivered by an adjacent source. Together, these processes generate the thioflavin S aerosol. Delivery of the generated aerosol to cohorts of experimental animals is facilitated via a delivery

trumpet assembled within each inhalation chamber. Similarly, exhaled aerosol is conveyed to an exhaust outlet via escape channels just below the connector cone. In its current configuration, the stainless-steel inhalation chamber is fitted with multiple ports and protected septum seals that enable the simultaneous respiratory exposure of three animals. The system can be expanded to accommodate up to five animals.

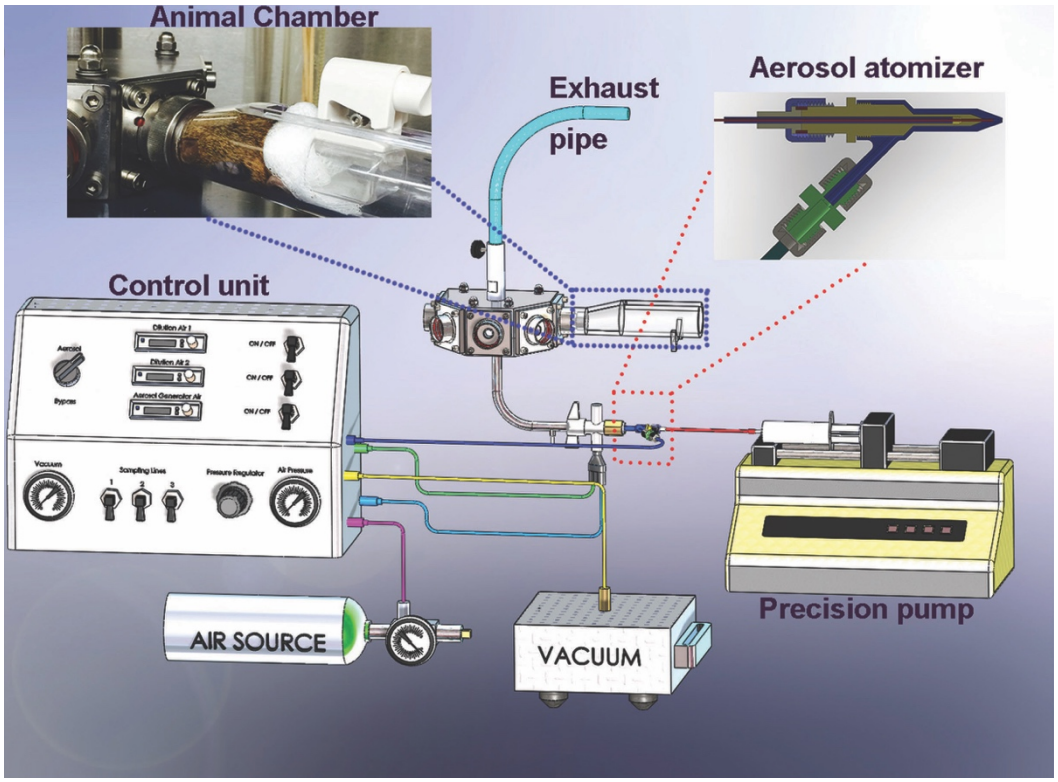

Figure 8-2. Overall design of an innovative, prototype benchtop aerosol generator that produces curcumin aerosols for inhalation therapy. It produces polydisperse aerosols by atomizing a solution. The aerosol particle concentration can be adjusted by changing the flow of the compressed air on the control unit. The air is then expanded through the atomizer nozzle and produces a high-velocity jet. As a result of the decreased static pressure under Bernoulli's law, the liquid solution is drawn from the precision pump. Instantaneously, a high-velocity airflow sheers the solution into a droplet aerosol, which then is conveyed into a chamber. With the current design, the chamber can accommodate five animals, which inhale the aerosols via tapered nose cones attached inside the restraint holder. The chamber has another channel that redirects exhaled air to the system's exhaust, thus rebreathing of exhaled air is prevented. Reprinted from Journal of Alzheimer's Disease with permission from IOS Press[437].

Cardiac perfusion procedure

Following exposure or treatment, mice were anesthetized with isoflurane and laid on a bed of ice after which the thoracic cavity was accessed via a sharp transverse incision into the abdomen. This was followed by a series of longitudinal cuts with surgical scissors to open the thoracic cavity by cutting the sternum to the right of the xyphoid process, which then was stabilized with a thoracic retractor to expose the heart. Perfusion was performed with a 25-gauge syringe containing ice-cold PBS (30 mL, pH 7.4) inserted into the apex of the heart through the left ventricle and injected slowly into the ascending aorta. Upon initiation of perfusion, the right atrium was snipped using micro scissors to facilitate drainage of the systemic venous return. Immediately following PBS perfusion, 30 mL of 4% paraformaldehyde (PFA) (pH 7.4) was perfused. With perfusion completed, the animals were decapitated, and their brains quickly harvested. Brains were removed by making incisions from the cervical spine to the auditory canal. A shallow incision was made at the interparietal and parietal bone junction. Surgical scissors were inserted into the incision in the skull and a cut was made along the sagittal suture, being careful not to damage the brain. The skull was then removed in pieces using forceps. Cranial nerves and the olfactory bulbs were cut to free the brain from the skull. After removal, brains were fixed in 4% PFA overnight at 4°C. Brains to be immuno-stained were cryoprotected for two days in 10% sucrose at 4°C. Cryoprotected brains were then embedded in Tissue-Tek optimum cutting temperature (OCT) compound for cryosectioning and stored at -80°C until sectioned. All other fixed tissue was embedded in paraffin by the histology core for sectioning.

Immunohistochemistry

Brains embedded in OCT were cut into sagittal sections (10 μm) using a Tissue-Tek cryostat and mounted onto Fisher Premium plain, charged glass slides (Fisher Scientific). Prior to staining, slides were washed with PBS for 5min before being subjected to a citrate buffer antigen retrieval protocol. Slide mounted sections were incubated for 30 min in a 100°C bath of sodium citrate buffer (10 mM sodium citrate, 0.05% Tween 20, pH 6.0) and allowed to cool for 20 min before being washed in PBS for another 5min. Sections were blocked in 3% bovine serum albumin (BSA) in PBS with 0.05% Tween-20 (PBST) for 1hr at room temperature. Treated sections were then incubated overnight at 4°C with primary antibodies: beta amyloid 17-24 (4G8) mouse monoclonal antibody (1:200 dilution, Biolegend, San Diego, CA, USA) diluted in blocking solution. Following two 5min washes with PBST, the sections were subsequently incubated with secondary antibodies goat anti-mouse Alexa 647-conjugated IgG (1:200, ThermoFisher Scientific, Pittsburgh, PA, USA) for 1hr at room temperature. The sections were then washed with PBS and coverslipped with a fluorescent-specific antifade mounting medium (Vector Laboratories, Burlingame, CA) and allowed to dry in the dark at room temperature overnight.

Fluorescence microscopy

To localize the distribution of thioflavin S in the brains of treated mice and corroborate its intrinsic fluorescence signal with that of the fluorescently labeled Aβ antibodies, dual channel fluorescence microscopy was employed. For all fluorescence imaging, a GFP-BP filter (excitation filter 450–490 nm; dichroic mirror 495 nm; emission filter 510–560 nm) was used to image thioflavin S fluorescence. A Texas Red filter (excitation filter 540–580 nm; dichroic mirror 595 nm; emission filter 600–660 nm) was utilized to visualize Alexa

647-conjugated secondary antibodies for amyloid plaque detection. All images were acquired using a CCD camera and data were analyzed using Nuance 2.6 software.

Vascular labelling with Lycopersicon esculentum (tomato) lectin

Mice were anesthetized with isoflurane and 100 uL of undiluted Dylight 649 labeled tomato lectin (1mg/mL, Vector Laboratories) was intravenously injected into the caudal tail vein. Mice were removed from anesthesia and allowed to recover for 20 min before being sedated and cardiac perfused using the CLARITY tissue clearing protocol described below.

CLARITY tissue clearing

Tissue clearing was performed using Clear Lipid-exchanged Acrylamide-hybridized Rigid Imaging/Immunostaining/*In situ* hybridization-compatible Tissue-hYdrogel (CLARITY) protocol as previously described[438]. Briefly, hydrogel solution [4% acrylamide (40%), 0.25% VA-044 initiator, 4% PFA, 1x PBS] was prepared on ice and stored at -20°C. Prior to use, hydrogel solution was thawed on ice. Mice were cardiac perfused with 20 mL 1x PBS, followed by 20 mL hydrogel following the previously described profusion procedure. The brain was removed and placed in a 50 mL canonical tube with thawed hydrogel solution and incubated at 4°C for two days to allow for further diffusion of the hydrogel solution into the tissue. Following incubation, the canonical tube lid was placed in a 40°C water bath and the cap was replaced with a vacuum tube adaptor connected to a nitrogen tank and vacuum. The sample was degassed using a fume hood vacuum line and air replaced with nitrogen, then placed on a tube rotator and incubated at 40°C. Incubation was done for 3 hr or until hydrogel solution polymerized. Tissue is then washed with clearing

solution [200mM boric acid, 4% sodium dodecyl sulfate (SDS), dH_2O, NaOH to pH 8.5] in 45°C water bath with shaker for 24 hr to dialyze out PFA, initiator, and hydrogel monomer. Following initial washing, tissue was continuously incubated at 45°C until clearing was achieved, replacing tissue clearing solution every two days for two weeks.

Thioflavin S/immunostaining of CLARITY-processed brain

For thioflavin S staining of cleared 5XFAD mouse brains, 1% thioflavin S (w/v) was prepared in CLARITY clearing solution and filtered using 45 μm Luer-Lok syringe filters. Tissue was immersed in solution and incubated at 40°C overnight while shaking. Then, samples were washed for two days in tissue clearing solution at 40°C, replacing the solution four times.

Immunostaining of cleared mouse brains was done following the System-Wide control of Interaction Time and kinetics of CHemicals (SWITCH) protocol[439]. 5XFAD mouse brains were hemisected for faster and better penetrance of antibodies and equilibrated in antibody-OFF solution (0.5mM SDS, 1x PBS) overnight at 37°C. Samples were then placed in fresh antibody-OFF solution with just enough to cover tissue and primary antibody (beta amyloid 17-24 (4G8) mouse monoclonal antibody) was added to achieve a 1:200 dilution, then incubated at 37°C with gentle shaking for three days. Samples were moved to antibody-ON solution [0.1% Triton-X (v/v), 0.02% sodium azide (w/v), 1x PBS] and incubated at 37°C for two days to initiate antibody binding and wash out unbound antibodies. Samples were then incubated in fresh antibody-ON solution with secondary antibody (goat anti-mouse Alexa 568, 1:200 dilution) at 37°C with gentle shaking for three days. Finally, cleared tissue was incubated in fresh antibody-ON solution at 37°C for two

days with gentle shaking.

Light sheet microscope imaging

Following thioflavin S staining of CLARITY-cleared brains, samples were incubated in refractive index matching solution (RIMS) [88% Sigma D2158 (Histodenz) (w/), 0.1% tween-20, 0.01% sodium azide, in 0.02 M PBS, pH 7.5] overnight at room temperature in the dark to prevent photobleaching. RIMS solution improves imaging of thick tissue be reducing refractive index within a sample to reduce light scattering. Samples were then analyzed using a Zeiss Lightsheet Z.1 microscope, with imaging overseen by Zeiss representatives and Vaibhav Janve as part of a microscope demonstration at Vanderbilt University.

Results

Aerosolized thioflavin S binds Aβ in 5XFAD mouse brain and retention is plaque dependent

To study olfactory-mediated delivery of small molecule Aβ-binding agents via aerosolization, thioflavin S was chosen since it has a high affinity for Aβ and cannot cross the BBB under normal physiological conditions as demonstrated in chapter 7 (Fig.7-2B). Aged 5XFAD mice (>8 months old, n=4) were treated with aerosolized thioflavin S for two consecutive days. Following the second treatment, brains were sectioned and immunostained for Aβ plaques. Fluorescent imaging revealed that thioflavin S is in fact detected in brains of 5XFAD mice, particularly in regions of high plaque burden including the subiculum and hippocampus (Fig.8-3D&G) while areas with low plaque burden exhibited minimal thioflavin S signal (Fig.8-3A). Immunostaining revealed that thioflavin S fluorescence colocalizes with Aβ plaques well (Fig.8-3C,F&G). While many plaques are thioflavin S and anti-Aβ antibody positive, some plaques were only visualized with immunostaining, suggesting that aerosolized thioflavin S binds some but not all plaques. In particular, thioflavin S appears to be associated with smaller plaques rather than larger ones. Together, these findings suggest that when delivered as an aerosol, thioflavin S enters the brain through an alternative uptake mechanism since it is unable to cross the BBB when administered via peripheral intravenous injection as demonstrated in our previous study (Fig.7-2B). When thioflavin S reaches the brain, it can bind and be used to visualize plaques. However, it appears that thioflavin S can bind smaller plaques in regions with higher plaque density more effectively than larger plaques in the same region (Fig.8-3I).

Next, we sought to determine whether Aβ plaques must be present for aerosolized thioflavin S to be retained. For this study, wt mice (n=3) were treated using the same thioflavin S aerosolization protocol as described above. As expected, staining of wt mouse brains with anti-Aβ antibodies confirmed these mice do not have Aβ plaques (Fig.8-4B&E). Interestingly, no thioflavin S fluorescence could be detected in treated wt mice (Fig.8-4A&D). Taken together, this suggests Aβ plaques must be present in order for thioflavin S to be retained in the brain.

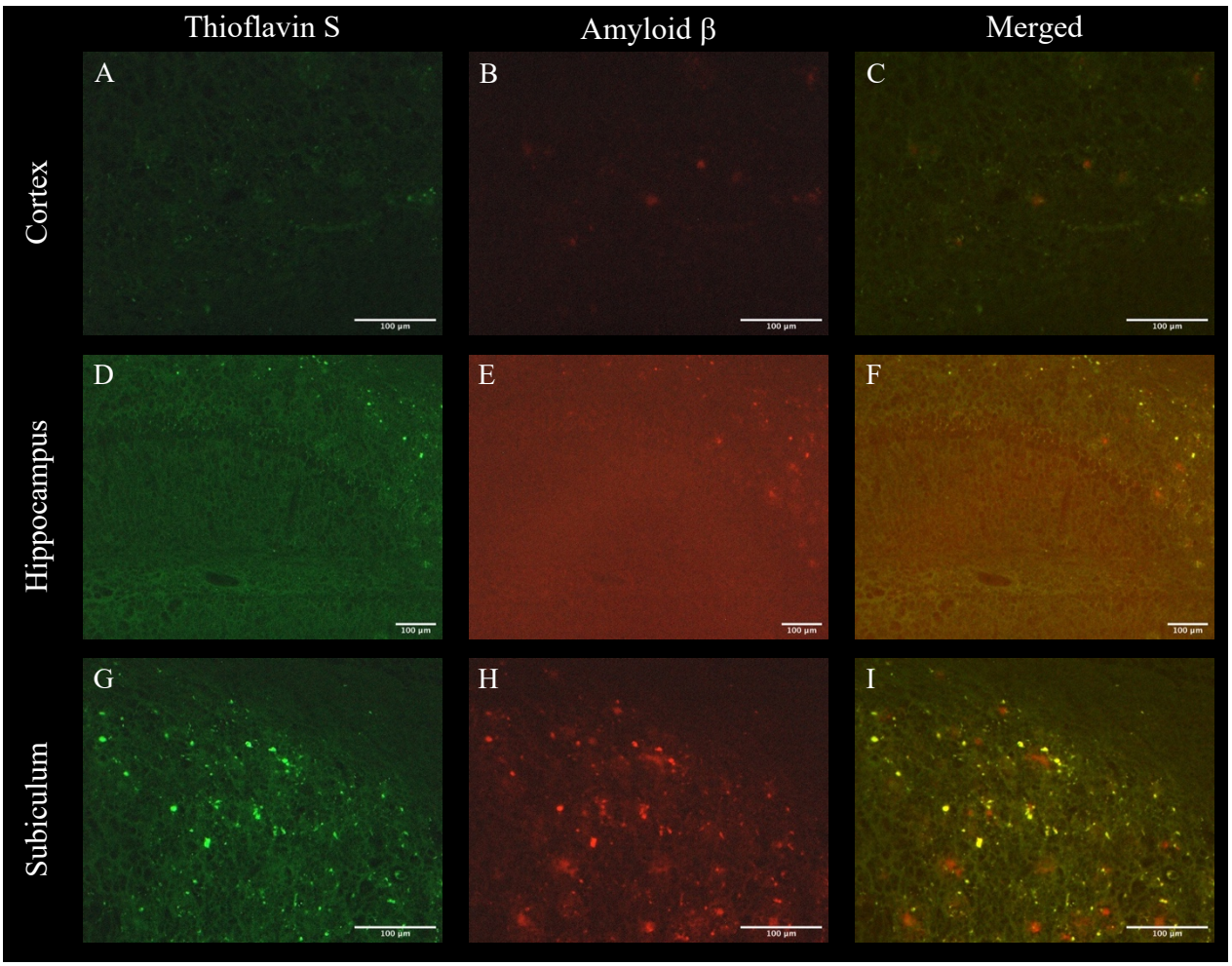

Figure 8-3. Fluorescent imaging on brain sections from aged 5XFAD mouse treated with aerosolized thioflavin S (green) and stained with anti-Aβ antibodies (red) for plaque detection. Merged images show colocalization of thioflavin S and Aβ plaques (yellow). Minimal thioflavin S fluorescence is observed in the cortex (A) and the same region had low plaque burden (B). The plaques that were present were not also bound by thioflavin S (C). Enlarged view of the hippocampus revealed thioflavin S (D) and plaques (E) with excellent colocalization (F). In particular, the subiculum also showed greater thioflavin S retention (G) and high plaque burden (H). Thioflavin S appears to colocalize better with smaller plaques than larger ones seen in the same region (I).

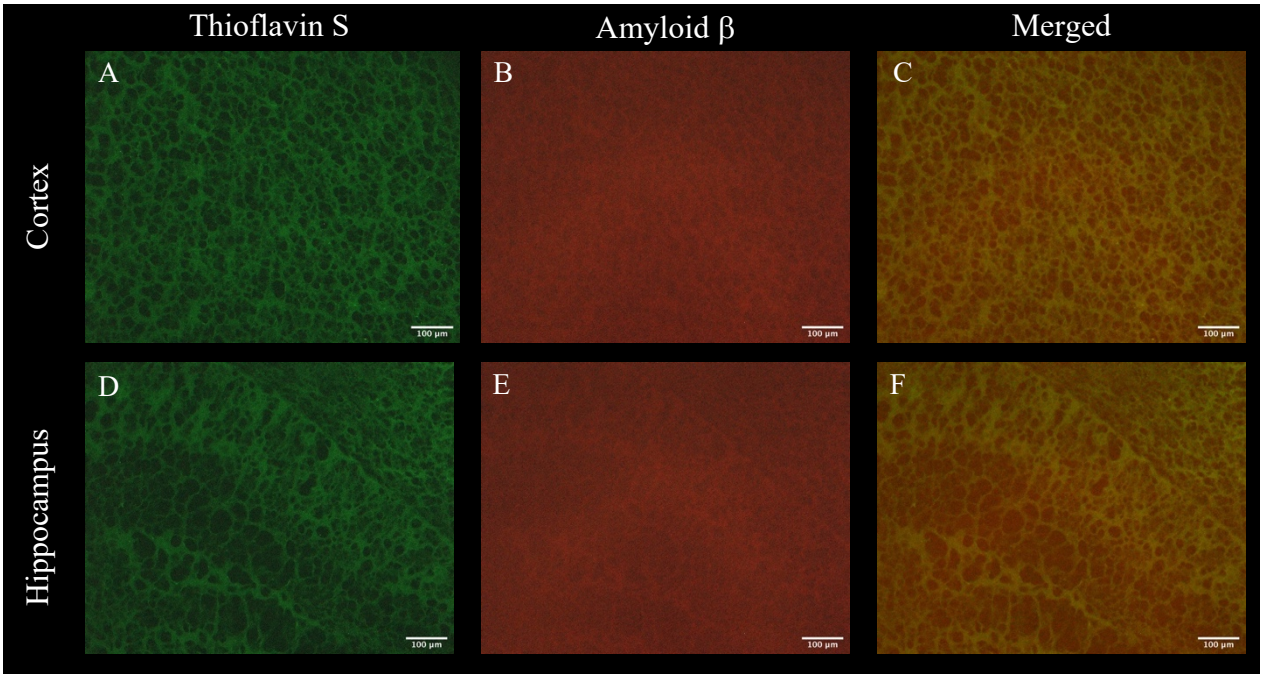

Figure 8-4. Fluorescent imaging on brain sections from wt mouse treated with aerosolized thioflavin S (green) and stained with anti-Aβ antibodies (red) for plaque detection. No thioflavin S fluorescence is observed in the cortex (A) or hippocampus (D). As expected anti-Aβ antibody staining demonstrated an absence of plaque formation in wt mice (B&E). Merged images the cortex and hippocampus are also shown (C&F).

Thioflavin S uptake and distribution analysis using tissue clearing

Next, we sought to directly visualize aerosolized thioflavin S uptake in the brain using the CLARITY tissue clearing protocol. The CLARITY protocol removes lipids from tissue to make it transparent while retaining structure by first perfusing mice with a hydrogel solution that is then polymerized. Cleared tissue allows for staining and imaging of larger brain sections or an entire mouse brain using either confocal or light sheet microscopy. With this approach, our goal is to visualize thioflavin S throughout the entire brain to better elucidate the mechanism of uptake as well as compare distribution with Aβ plaques as visualized through antibody staining of the cleared brains.

To evaluate the tissue clearing protocol and develop imaging parameters, an aged 5XFAD mouse brain (12 months-old) was cleared using the CLARITY protocol (Fig.8-5). Additionally, prior to perfusion with hydrogel solution, the 5XFAD mouse was treated with i.v. tomato-lectin, which labels rodent blood vessel walls. Following tissue clearing, the 5XFAD mouse brain was stained with thioflavin S (Fig.8-5B) and imaged using light-sheet microscopy (Fig.8-6), which allowed for visualization of thioflavin-labeled plaques throughout the brain. Vasculature was also effectively labeled and visualized with i.v. tomato-lectin.

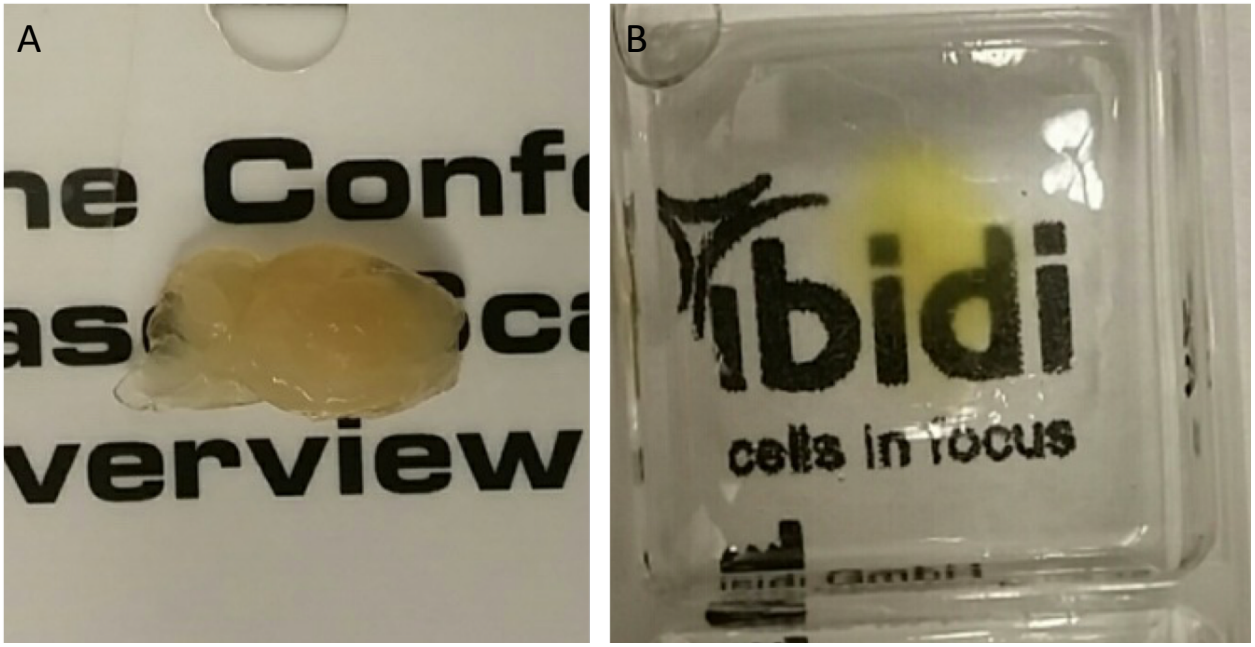

Figure 8-5. 5XFAD mouse brain processed using CLARITY tissue clearing protocol. (A) Brain hemisection after being immersed in tissue clearing solution for five days with observable clearing on the edges. (B) After clearing for two weeks, the same brain hemisection was mostly transparent and stained with thioflavin S, giving it a yellow coloration.

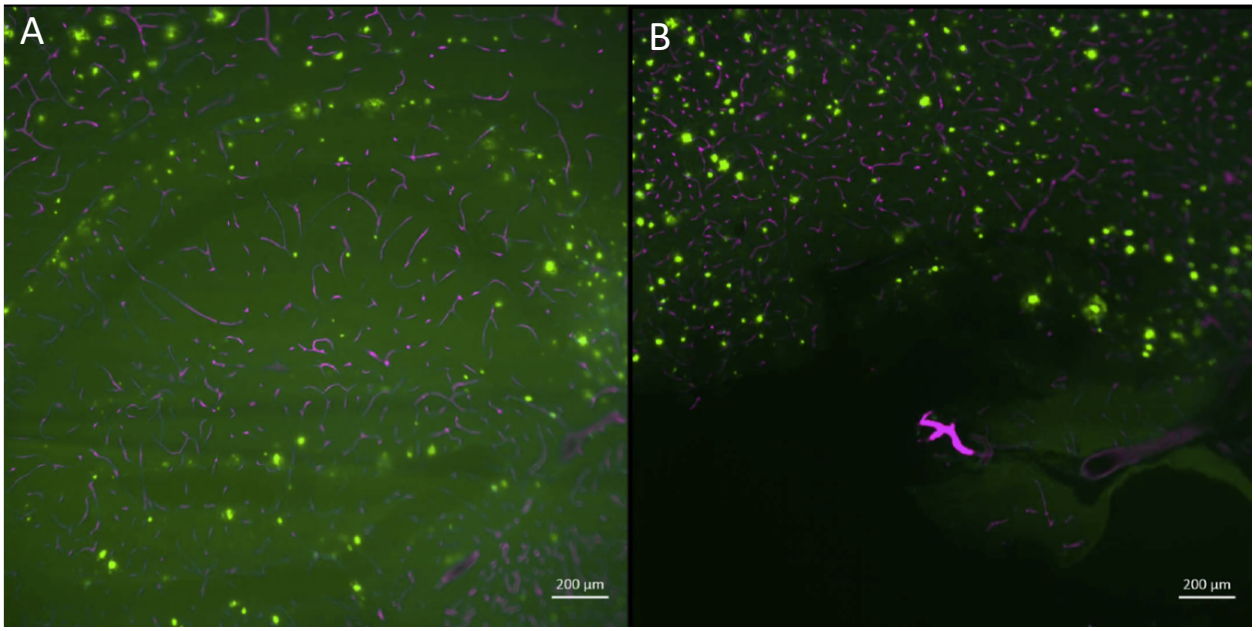

Figure 8-6. Light-sheet microscopy image of CLARITY-cleared brain stained from an aged 5XFAD mouse stained with thioflavin S (green). Mice were also perfused with Dylight 649 labeled tomato lectin (purple) prior to tissue clearing. (A) Medial hippocampus. (B) Lateral cortical region in same mouse brain.

Finally, Aβ was detected by immunostaining of a CLARITY-cleared 5XFAD mouse brain section that had already been stained with thioflavin S. Fluorescent signal from both thioflavin S (blue) and Alexa 568 secondary antibodies (green) used in conjunction with primary anti-Aβ antibodies (Fig.8-7B) were detected using a confocal microscope. Vasculature is also still detectable from tomato lectin perfusion prior to tissue clearing (red). When compared to a wt mouse brain from an animal receiving the same treatment (i.e. tomato lectin perfusion, tissue clearing, thioflavin S & antibody staining), vasculature was still effectively labeled but thioflavin S was not detected, suggesting that thioflavin S binding in cleared tissue is still specific to plaques (Fig.8-7A). However, florescence associated with anti-Aβ immunostaining is also observed in the wt mouse. Based on the morphology, it appears that this signal is associated with white matter tracks, suggesting off-target binding of either the primary or secondary antibody to an epitope present in wt mice. It is unlikely that the antibodies (either primary or secondary) would bind myelin or any other white matter marker since both have been used previously and effectively visualized plaques. However, we have not used either antibody in cleared specimens before and thus, further work is required to elucidate the source of this staining and to develop an effective and specific immunostaining protocol for plaque identification in cleared tissue samples.

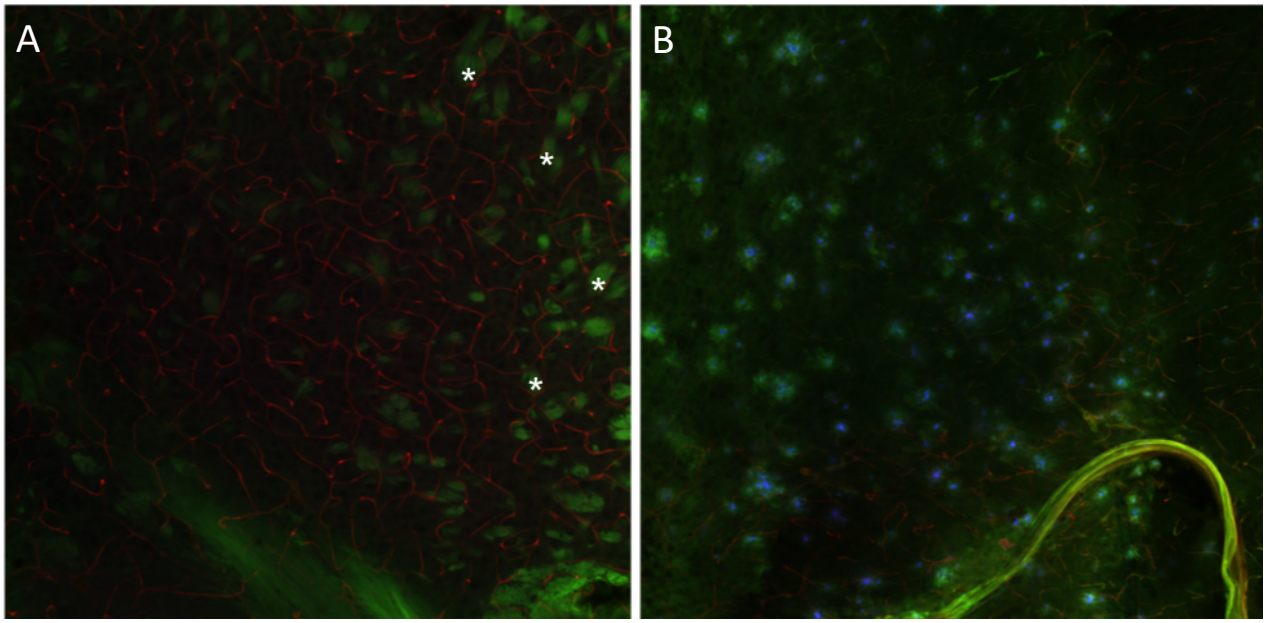

Figure 8-7. CLARITY-cleared brain sections from both wt (A) and 5XFAD mice (B). Both animals were intravenously injected with a vascular marker (red) prior to perfusion. Following tissue clearing, brains were stained with thioflavin S (blue) and anti-Aβ antibodies (red). Antibody associated fluorescence was detected in wt samples that appears to be associated with white matter tracks (examples labeled with *).

Discussion

A major limitation in the development of diagnostic and therapeutic agents for all neurological disorders is the BBB, which prevents delivery of many small molecules and nearly all large molecule compounds[231]. Even when a compound has some BBB permeability, often high doses are required to achieve a concentration in the CNS that would mediate any therapeutic benefit, which can result in adverse effects due to off-target interactions throughout the body[277]. Many studies, including our work using LPS described in chapter seven, has sought to transiently disrupt the BBB as a means to improve drug delivery[231,236,240–248]. However, in many neurodegenerative disorders, including AD, evidence suggests that BBB disruption may itself contribute to or even accelerate disease progression[273] and thus further disruption could have detrimental effects even in the context of administering a therapeutic, though further work must be done to address this concern.

Here we investigate an alternative delivery method of olfactory-mediated transport to the brain as a means of bypassing the BBB. For this work, we utilized aerosol administration that, when compared to standard intranasal administration, allows for exposure of the nasal cavity to a compound over an extended period of time. Also, exposing the nasal for a longer duration reduces risks of reduced transport by saturating olfactory transport mechanisms that may hinder delivery in a single intranasal treatment paradigm[277]. Targeting olfactory uptake offers the potential to be a safe and noninvasive approach that could target drugs more directly to the CNS and thus reduce risk of peripheral toxicity by limiting systemic absorption[273]. Also, since delivery is not dependent on a specific cellular

transport mechanism, a large array of diagnostic and therapeutic agents can be targeted to the brain using this approach, including those with limited BBB permeability.

In this work, we sought to study olfactory uptake in an AD transgenic mouse model using thioflavin S, a fluorescent Aβ-binding compound that cannot cross the BBB when administered under normal physiologic conditions[421] (Fig.7-2B). Thioflavin S was administered as an aerosol over three to four hours for two consecutive days to mice, which are obligate nose breathers, to enhance targeting of olfactory-mediated transport and increase the likelihood that it could be detected within the brain parenchyma with fluorescence microscopy.

5XFAD mice were treated with aerosolized thioflavin S and brains sections were then stained with anti-Aβ antibodies. Thioflavin S fluorescence was detectable within the brain parenchyma and found particularly in regions of high plaque burden, including the hippocampus and subiculum (Fig.8-3D&G). Additionally, thioflavin S fluorescence colocalized with Aβ plaques with the caveat that smaller plaques were better targeted than larger ones (Fig.8-3F&I). It is possible that aerosolized thioflavin S is less able to permeate larger plaques with more dense cores than when used as an *ex vivo* stain. This could potentially be improved by increasing the duration of thioflavin S treatment or by changes in aerosol formulation to improve delivery. Wt mice receiving the same treatment had no detectable thioflavin S fluorescence (Fig.8-4A&D), suggesting that retention is dependent on plaques being present within the brain. It is also important to consider that intranasal delivery in 5XFAD mice may be contingent on a disease-related change in physiology.

However, this seems less likely as intranasal delivery has been studied and implicated in improved delivery to the brain using many other transgenic mouse lines[273,276,440].

To study thioflavin S uptake and distribution, we investigated the CLARITY tissue clearing protocol as a means to directly visualize transport and dispersion through the brain following aerosol administration. First, we demonstrated that CLARITY successfully cleared 5XFAD mouse brains (Fig.8-5). Also, cleared brains stained *ex vivo* with thioflavin S (Fig.8-6B) were imaged using light sheet microscopy and effectively visualized Aβ plaques throughout the brain. Mice were also given i.v. tomato-lectin prior to perfusion and tissue clearing, which effectively stained brain vasculature. Immunostaining of the cleared tissue identified Aβ plaques also stained with thioflavin S (Fig.8-7B). However, when using the same immunostaining protocol on cleared wt mouse brain sections, it appears that white matter tracks were also stained. Thus, further work needs to be done to optimize the specificity of anti-Aβ staining in cleared tissue. In future work, brains of 5XFAD mice treated with aerosolized thioflavin S will be cleared and imaged using the same protocol to visualize thioflavin S distribution throughout the brain. Additional studies using this approach could further support that delivery is in fact mediated by olfactory uptake. For example, if aerosolized thioflavin S is preferentially delivered to brain regions receiving afferent innervation from the olfactory bulb, this would support the hypothesis that delivery and distribution within the brain is in fact mediated by olfactory receptor neurons. Furthermore, it is possible transport of thioflavin S the olfactory epithelium into the olfactory could be observed directly and confirm the mechanism of delivery following aerosol administration. We are also currently investigating alternative methods of tissue

clearing including VISIKOL, which has shorter tissue processing times[441]. Furthermore, rather than removing lipids, VISIKOL acts by treating tissue with reagents that match the refractive index throughout a target tissue to make it transparent. This approach requires less tissue manipulation and is less likely to remove aerosolized thioflavin S during processing.

In conclusion, we have demonstrated that thioflavin S, a compound with poor BBB permeability, can be effectively delivered to the brain of 5XFAD transgenic mice when administered as an aerosol. Delivery is likely mediated via direct uptake through the olfactory epithelium and thus bypasses the BBB. Further work is required to confirm the mechanism of delivery and we are investigating the use of tissue clearing protocols to directly visualize uptake and transport from the nasal cavity to the brain. Since intranasal uptake is not dependent on any specific transport mechanism, this approach has the potential to be applied to a variety of drug classes and thus could significantly increase diagnostic and therapeutic agents available for many neurological disorders including AD.

Chapter IX

Aerosol Delivery of Fluorescent Aβ-Binding Compounds for Noninvasive Detection of Retinal Plaques

Introduction

One reason for failure of AD clinical trials is at the time of treatment, significant and irreversible neurodegenerative changes have already occurred such that a therapeutic benefit cannot be achieved. Therapeutic efficacy could potentially be improved if initiated in early symptomatic or preclinical stages of disease. However, techniques to detect AD pathology are expensive or invasive and thus, cannot be readily implemented as a screening test in an asymptomatic population. Recent studies have shown that Aβ plaques can also be found in the retinas of AD patients and that Aβ plaque burden in the retina correlates with total plaque burden within the brain[351]. Retinal Aβ deposition also occurs in transgenic mouse models of AD[353–355,442] and was shown to closely correlate with total plaque burden in the brain[351]. Importantly, Aβ was detected in the retinas of transgenic mice prior to cognitive decline as measured using behavioral testing and plaques were also observed in postmortem retinal samples from people suspected to be in early stages of AD[351]. Based on these findings, accurate detection and quantification of retinal plaques could serve as a surrogate measure for total plaque burden within the brain and identify those with AD pathology prior to symptom onset.

As such, we are developing a noninvasive method of retinal plaque detection using fluorescent Aβ-binding compounds, curcumin and thioflavin S, delivered via

aerosolization. Curcumin, a natural product found in turmeric, has been extensively studied as a potential therapeutic in a number of disease models including inflammation[443–448], cancer[449–455], and neurodegenerative disorders including AD[370,456–458]. However, curcumin's amphiphilic properties severely limit its BBB permeability. Previously, our lab has shown that when administered as an aerosol to 5XFAD mice, curcumin not only can bind Aβ in the brain but also reduce plaque burden and improve cognitive function[437]. Thioflavin S, as previously described, has poor BBB permeability and thus we suspect it also has limited penetration across the BRB, a similar endothelium in which transport across it is heavily regulated[459]. However, as we have demonstrated in chapter 8, aerosol administration of thioflavin S significantly improves thioflavin S delivery to the brain and effectively binds Aβ in. Thus, we propose this delivery method may similarly be able to overcome BRB limitations. Based on these observations with both curcumin and thioflavin S, our current study is to investigate aerosol administration of both compounds for detection of Aβ plaques in the retina using noninvasive fluorescent retinal imaging.

Wt and 5XFAD mice, a transgenic model of AD, were treated with aerosolized curcumin or thioflavin S. Retinal tissue whole-mounts and transverse sections were prepared and analyzed using confocal microscopy. Curcumin and thioflavin S fluorescence were found to be closely associated with ganglion cell bodies in the same retinal layer where Aβ plaques were detected in non-treated 5XFAD retinas stained with anti-Aβ antibodies, though thioflavin S fluorescence was more readily detected and thus will be used for future studies. Importantly, neither thioflavin S nor curcumin fluorescence was detected in treated wt retinas. These findings demonstrate that retention of both compounds is disease-dependent. In future work, retinas from thioflavin S treated 5XFAD mice will be co-

stained for Aβ to confirm thioflavin S is bound to plaques. Treated mice will also be imaged using a retinal imaging microscope to determine fluorescence associated with retinal plaques can be detected noninvasively. If successful, aerosolization of a fluorescent Aβ-binding compound could be used to evaluate retinal Aβ plaques as a predictive biomarker for future development of AD and facilitate early intervention to improve therapeutic outcomes.

Materials & Methods

Materials

Thioflavin S and curcumin were obtained from Sigma Aldrich (St Louis, MO). All reagents and solvents were of analytical grade and used as received from the commercial source without further purifications.

Thioflavin S and curcumin formulation and treatment

Mice were treated with freshly prepared 2% thioflavin S solution in ddH_2O (w/v) that was filtered using 45µm Luer-Lok syringe filters. 1% curcumin solution was also prepared fresh in ddH2O (w/v) and tween-20 (10%). The mixture was further heated up to 70°C in a water bath and mixed using a stir plate to facilitate the solubility. Both curcumin and thioflavin S were covered with aluminum foil to prevent photobleaching before and during treatment. A syringe was filled with 30 mL of either compound and injected in the nebulizer at a steady rate over three hrs. Flow through was collected and reinjected during that time until at least 6-7 mL of solution was aerosolized. The treatment protocol was repeated for two consecutive days and mice were cardiac perfused 2 hrs after the final treatment using the same protocol described in chapter six. In addition to collecting brains, mouse eyes were enucleated and fixed in 4% PFA overnight, then cryoprotected in 10% sucrose for at least two days at 4°C. One eye was embedded in OCT and stored at -80°C until sectioning and staining while the contralateral eye was prepared as a retinal wholemount and described below.

Retinal tissue preparation (transverse section & wholemount)

Eyes embedded in OCT were cut into transverse sections (10 μm) using a Tissue-Tek cryostat and mounted onto charged glass slides. For retinal wholemounts, eyes were enucleated and the anterior eye cup (cornea, lens) were removed. The posterior eye cup was fixed for 1 hr in 4% PFA at room temperature. Tissue was washed in 1x PBS and the retina was separated from the sclera, with careful removal of excess vitreous humor using a paintbrush. Isolated retinas were sequentially cryoprotected in 10%, 20%, and then 30% sucrose solutions at 4°C. Retinas were transferred to the next solution once tissue sank to the bottom of the tube (typically hours to overnight for each). Both slides and wholemounts were washed with 1x PBS before being subjected to a citrate buffer antigen retrieval protocol. Tissue was incubated for 30 min in a 100°C bath of sodium citrate buffer (10 mM sodium citrate, 0.05% Tween 20, pH 6.0) and allowed to cool for 20 min in the solution before washing with 1x PBS. Both retinal sections and whole mounts were incubated in blocking solution. Retinal sections were blocked in 3% BSA and PBS with 0.05% Tween-20 (PBST) for 1 hr at room temperature. Whole mounts were blocked in 5% BSA in PBS with 0.1% Triton-X 100 and incubated for 2 hrs at room temperature with gentle shaking. Treated sections were then incubated overnight at 4°C with primary antibodies: beta amyloid 17-24 (4G8) mouse monoclonal antibody (1:200 dilution, Biolegend, San Diego, CA, USA). Wholemounts were incubated for 1-3 days also at 4°C while shaking. Following PBS washes after primary antibody incubation, sections were subsequently incubated with secondary antibodies goat anti-mouse Alexa 594-conjugated IgG (1:200, ThermoFisher Scientific, Pittsburgh, PA, USA) for 1 hr at room

temperature while wholemounts were incubated overnight again at 4°C while shaking. Tissues were then washed with PBS and coverslipped with an antifade mounting medium containing DAPI nuclear stain (Vector Laboratories, Burlingame, CA).

MALDI-IMS sample preparation

Eyes were enucleated and rapidly frozen on dry ice. Frozen eyes were embedded in 2.6% carboxymethylcellulose (CMC). Using a cryostat, 12 μm transverse retinal sections were cut and mounted onto a gold plate. Samples were then immersed in the following solutions for fixation and lipid removal: 70% ethanol for 30 seconds, 100% ethanal for 30 seconds, Carnoy's solution (60% ethanol, 30% chloroform, 10% glacial acetic acid) for 2 min, 100% ethanol for 30 seconds, ddH_2O for 30 seconds, and 100% ethanol for 30 seconds. The samples were rehydrated and coated with 2, 6-dihydroxyacetophenone (DHA) as the matrix solution using a TM-sprayer. Once coated, gold plates were placed in a time-of-flight (TOF) mass spectrometer for analysis of the retinal Aβ plaque distribution based on known m/z ratios for APP cleavage products[460].

In vivo retinal imaging

Mice were sedated with intraperitoneally injected ketamine/xylazine (100/10 mg/kg) and pupils dilated with 2.5% phenylephrine hydrochloride and 0.5% tropicamide. Retinas were imaged *in vivo* using a Micron IV Retinal Imaging microscope (Phoenix Research Laboratories, USA). Consisting of a xenon light source and a 3-chip CCD camera, the microscope has a retinal imaging resolution of 3 μm in mice and is capable of *in vivo* brightfield, angiography and fluorescent imaging of commonly used fluorophores.

Anesthetized mice were placed on a positioning stage following pupil dilation and 2.5% hypromellose ophthalmic demulcent solution (AKORN, USA) was used as a wetting and coupling agent. Multiple brightfield and fluorescent images using a FITC filter were taken in rapid succession to ensure in focused image acquisition as mouse respiration made this challenging. Following imaging, mice were returned to their home cage and observed until regaining consciousness (~30 minutes).

Results

Aβ Plaques found in 5XFAD mouse retina

Retinal Aβ plaques have been reported in various transgenic mouse models of AD[166,461,462]. Previous work using enzyme-linked immunosorbent assay (ELISA) and Western analysis showed $A\beta_{40/42}$ peptides are found in 5XFAD mouse retinas by 1.5 months of age[463] but retinal plaque formation had not been previously demonstrated. To facilitate visualization of Aβ plaques, retinal transverse sections were prepared from aged 5XFAD mice (greater than 12-months old) and wt mice. Sections were then stained with anti-Aβ antibodies for retinal plaque identification. After optimization of the staining protocol and retinal imaging, Aβ plaques were seen in 5XFAD mouse retinas (Fig.9-1A), specifically in the inner plexiform layer (IPL) and ganglion cell layer (GCL) layer. Interestingly, Aβ appears to be found within ganglion cell bodies. Wt mice displayed minimal positive stain though significantly less than that seen in 5XFAD mice (Fig.9-1B). Additionally, background levels of Aβ have been previously observed in non-transgenic control and even normal C57Bl/6 retinal samples by our collaborator, Dr. Joanne Matsubara, and thus antibody-positive Aβ may be present at low levels even in control retinal samples.

To further confirm our observations of retinal Aβ, 5XFAD mouse retinas were analyzed using matrix assisted laser desorption-imaging mass spectrometry (MALDI-IMS), which is capable of reporting the location of a specific molecular product within a sample based on measurements of ionization products across a tissue section. Following MALDI-IMS analysis, we detected an ionization product (m/z 4649) in 5XFAD mouse retinal samples that may be an APP cleavage species within the retina, though it does not match previously

described m/z ratios expected from APP cleavage products including Aβ40 or Aβ42 (Fig.9-2)[464]. However, we suspect this signal (m/z 4649) is in fact an APP cleavage product but its weight may be altered due to an alternative cleavage site or the presence of different functional groups than that seen in MALDI measurements done on purified peptide as opposed to ionization directly from a tissue section. Yet, due to the limited spatial resolution of MALDI-IMS and an inability to visualize retinal layers, this technique will not be used for further characterization of retinal plaque development.

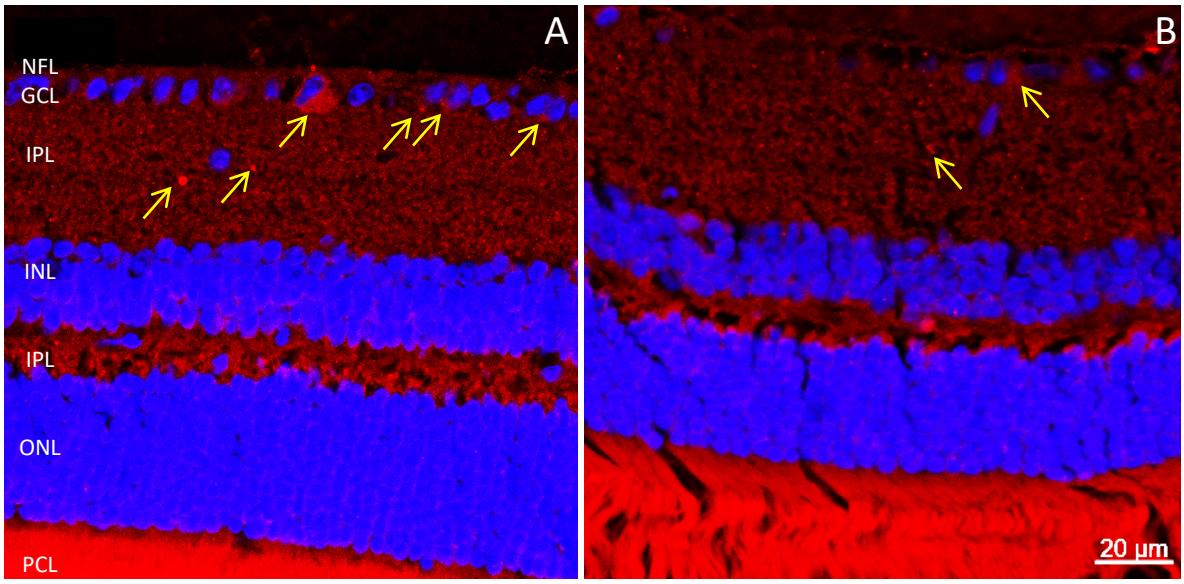

Figure 9-1. Transverse retinal sections from aged 5XFAD (A) and wt mice (B). Sections were stained with anti-Aβ antibodies (red) and DAPI nuclear stain (blue). Significantly more Aβ was detected in 5XFAD mouse retinal samples than in wt tissue (arrows). Fluorescence is seen in the photoreceptor cell layer though this is typical autofluorescence seen in retinal samples. Nerve fiber layer (NFL), ganglion cell layer (GCL), inner plexiform layer (IPL), inner nuclear layer (INL), inner plexiform layer (INL), outer nuclear layer (ONL), photoreceptor cell layer (PCL).

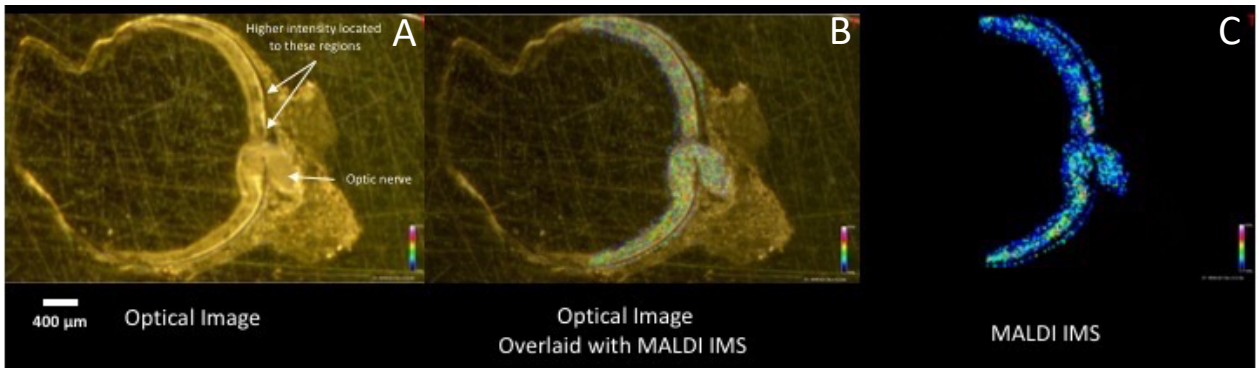

Figure 9-2. MALDI-IMS image of 5XFAD mouse retina. Optical image of section mounted on gold plate (A) with overlay of optical image and MALDI-IMS spectrum for ionization product m/z 4649, suspected to be a cleavage product of APP (B). MALDI-IMS spectrum without optical image overlay (C). Heat map is indicative of the relative concentration of the ionization product as measured at that point on the tissue. Localized signal is indicative of retinal plaque formation.

Aerosolized thioflavin S and curcumin fluorescence detected in retina

Next, in order to determine if aerosolized thioflavin S or curcumin could in fact be used to noninvasively visualize retinal Aβ plaques, we first needed to show if either compound can be successfully delivered to the retina. In our first study, 5XFAD and wt mice were treated with aerosolized thioflavin S for two consecutive days. Retinal wholemounts were prepared and analyzed using confocal microscopy (Fig.9-3A). High magnification of retinal regions within the wholemount tissue preparations demonstrated that localized thioflavin S fluorescence is seen in the 5XFAD mouse retina (Fig.9-3BCD). On closer examination, it appears that thioflavin S is in fact labeling retinal ganglion cells based on the location within the retina as well as cell morphology. Retinal wholemount preparations from wt mice receiving the same thioflavin S treatment had no such labeling, suggesting retention of thioflavin S within the retina is in fact dependent on disease related processes, likely the presence of retinal Aβ plaques (Fig.9-4). Transverse retinal sections were also prepared using the contralateral eye from the same mice and confirmed our findings in the retinal whole mounts that thioflavin S fluorescence is found in retinal ganglion cell cytoplasm (Fig.9-5A&B). No thioflavin S fluorescence was seen in retinal ganglion cells of wt mice receiving the same treatment (Fig.9-5C&D). Enhanced fluorescence seen in the photoreceptor cell layer for both 5XFAD and wt retinal samples is due to background or nonspecific staining characteristic to this retinal region. These results suggest that thioflavin S is retained in 5XFAD mouse retinas, particularly in layers where Aβ plaques were identified with antibody labeling.

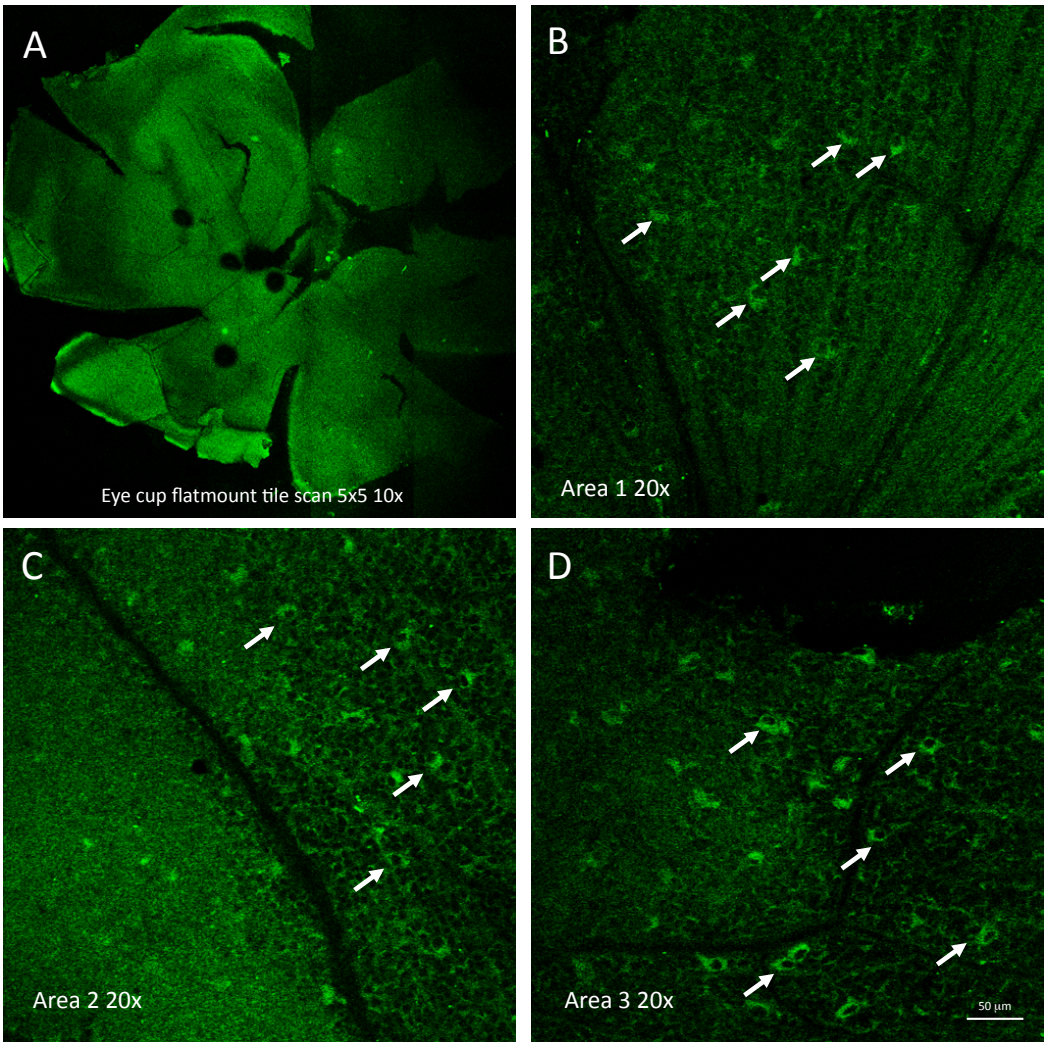

Figure 9-3. (A) Retinal wholemount preparation from aged 5XFAD mouse treated with aerosolized thioflavin S. (C-D) Higher magnification of retina demonstrated localized thioflavin S, which appears to be associated with retinal ganglion cells (arrows).

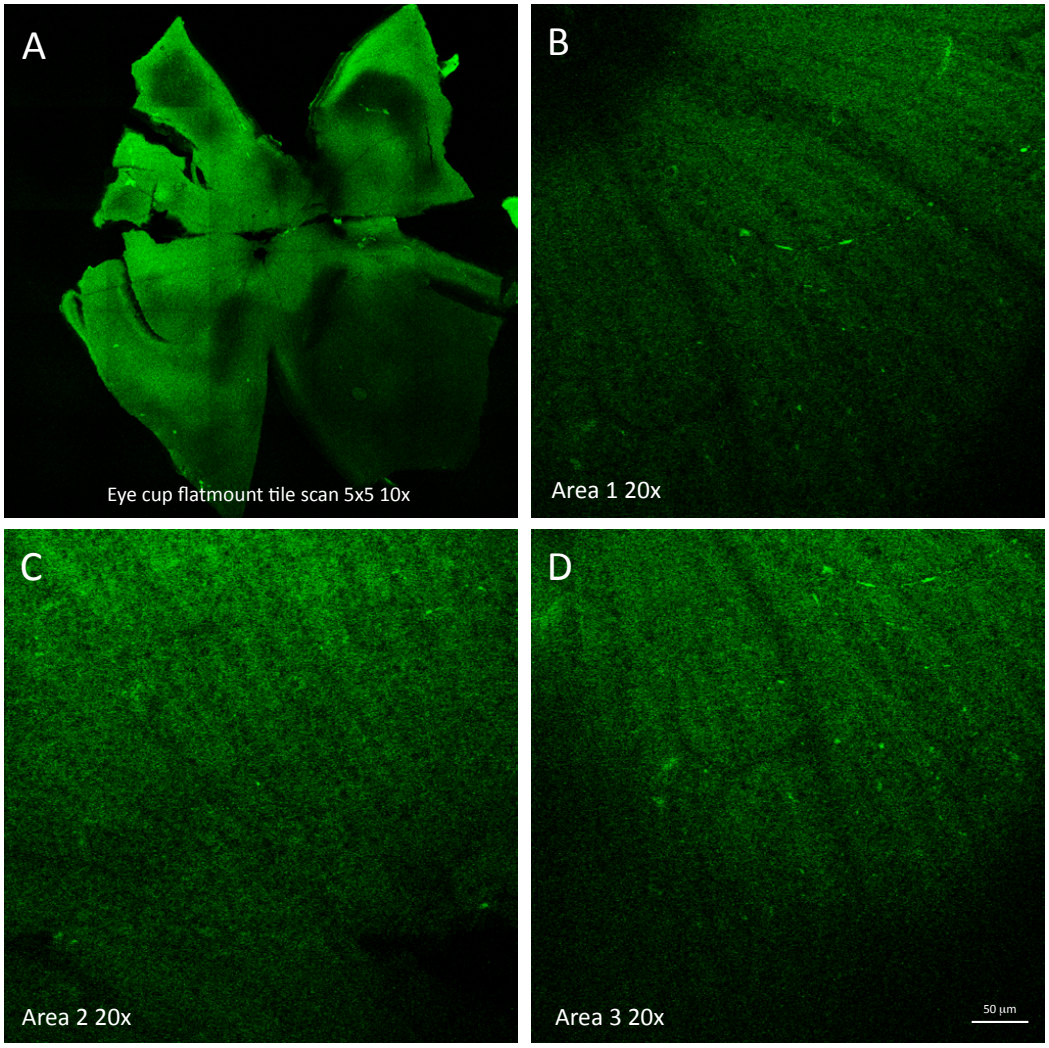

Figure 9-4. (A) Retinal wholemount preparation from wt mouse treated with aerosolized thioflavin S. (C-D) High magnification of select retinal regions demonstrate localized thioflavin S fluorescence that was seen in 5XFAD mouse retina.

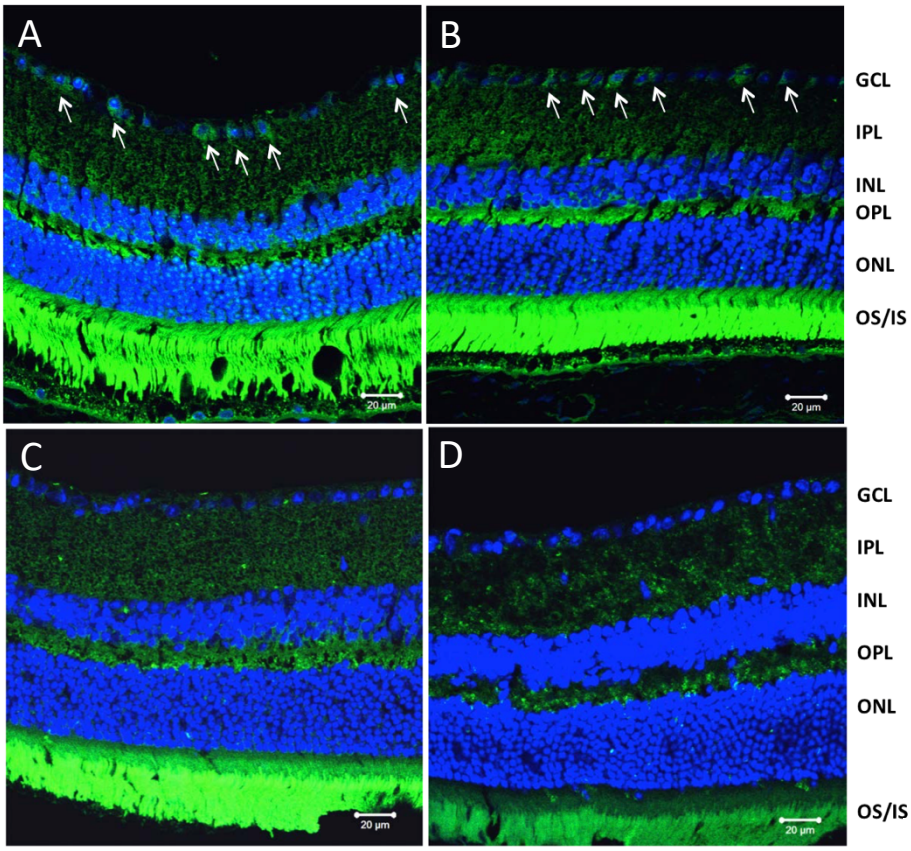

Figure 9-5. Transverse retinal sections from aged 5XFAD (A&B) and wt mice (C&D) treated with aerosolized thioflavin S (green). Sections were stained with DAPI nuclear stain (blue). Thioflavin S fluorescence is localized to retinal ganglion cell cytoplasm in 5XFAD mice (arrow). Wt retinal samples had almost no thioflavin S fluorescence as most signal appears to be due to background signal. High background fluorescence associated with the photoreceptor cell layer is common in retinal sample preparations. Ganglion cell layer (GCL), inner plexiform layer (IPL), inner nuclear layer (INL), outer nuclear layer (ONL), outer segment (OS) and inner segment (IS) of photoreceptor cell layer.

In addition to thioflavin S, we also treated a separate cohort of 5XFAD mice with aerosolized curcumin, which our lab recently demonstrated that plaque burden reduced significantly in young 5XFAD mice treated with aerosolized curcumin for an extended period of time[437]. Similar to thioflavin S, in transverse retinal sections of 5XFAD mice treated with aerosolized curcumin for two consecutive days, curcumin fluorescence was predominantly in the GCL and IPL of the retina (Fig.9-6A). Retinal whole mount preparations from the contralateral eye also demonstrated curcumin fluorescence to be closely associated with retinal ganglion cells (Fig.9-6B). Both preparations localized curcumin to the same regions as where Aβ plaques were detected via immunostaining (Fig.9-6C). In wt mice receiving the same treatment, curcumin was not detected in either transverse sections or retinal wholemounts (Fig.9-6D&E respectively). In comparison to Aβ plaques found in 5XFAD mouse cortices (Fig.9-6F), retinal plaques are smaller and appear to have less variation in size. Overall, these findings confirm that, similar to thioflavin S, aerosolized delivery can effectively target curcumin to the retina and retention is plaque dependent, as curcumin is found preferentially in retinal layers where plaques are also observed, and curcumin is not detected in wt mice receiving the same treatment. However, of the two Aβ-binding fluorescent compounds, thioflavin S appears to be a more robust stain of the two by exhibiting greater fluorescence and therefore is a better candidate for use in noninvasive retinal plaque detection.

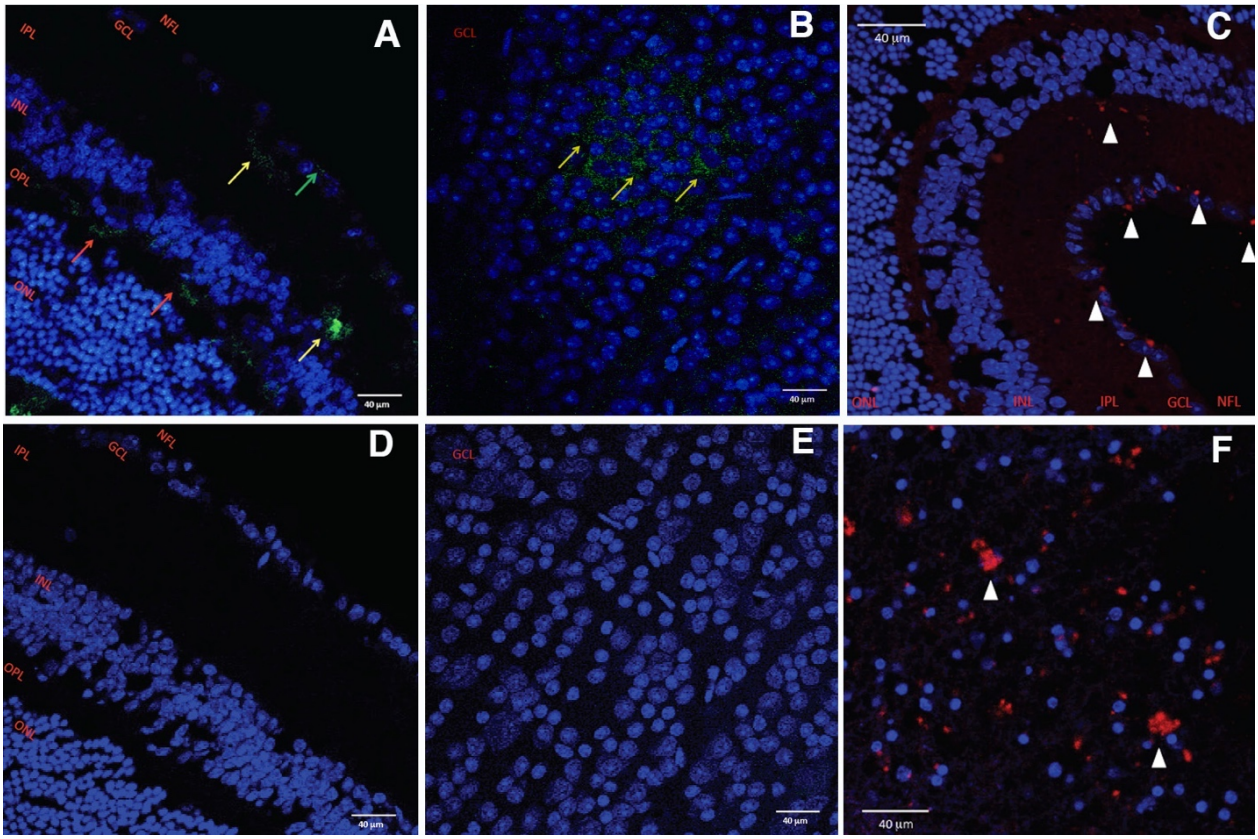

Figure 9-6. Retinal preparations from 5XFAD and wt mice treated with aerosolized curcumin. (A) The distribution of aerosolized curcumin in a transverse retinal section. Curcumin was detected in the inner plexiform layer (IPL) (yellow arrows), outer plexiform layer (OPL) (red arrows), and the nerve fiber layer (NFL) (green arrows). (B) In retinal wholemounts, curcumin is associated with ganglion cells (yellow arrows). (C) Aβ expression in the retinas was confirmed by anti-Aβ antibodies (white arrow heads). Transverse (D) and wholemount (E) preparations from wt mice had no detectable curcumin fluorescence. (F) Aβ expression in the cerebral cortex of 5XFAD mice whose ocular tissue shown in (ABC) demonstrates variation in plaque morphology between the retina and brain. Ganglion cell layer (GCL), outer nuclear layer (ONL), DAPI nuclear stain (blue).

In vivo retinal imaging of curcumin-nebulized 5XFAD mice

Finally, mouse retinas were analyzed *in vivo* using the Phoenix Micron IV rodent retinal imaging microscope. Initial studies were done using aged 5XFAD mice treated with aerosolized curcumin. Mice treated for two days and mice were imaged the same day following the second treatment. During imaging, mice were sedated with ketamine/xylazine and their pupils were dilated by direct application of phenylephrine and tropicamide. Upon imaging, no apparent plaques or gross pathologic changes were seen under standard brightfield imaging. When using a GFP filter to detect curcumin fluorescence, there was no observable signal. Though unsuccessful at detecting retinal plaques noninvasively, this was our first attempt and effective detection may require further optimization of our treatment protocol or of the imaging parameters used on the retinal imaging microscope. Additionally, use of other fluorescent Aβ-binding agents, such as thioflavin S, has the potential to improve noninvasive detection. A similar study will be done on 5XFAD mice following treatment with thioflavin S once retinal plaque formation is further characterized *ex vivo*. This may provide better findings as thioflavin S fluorescence was more readily detected on histological retinal analysis following aerosol administration as previously described above.

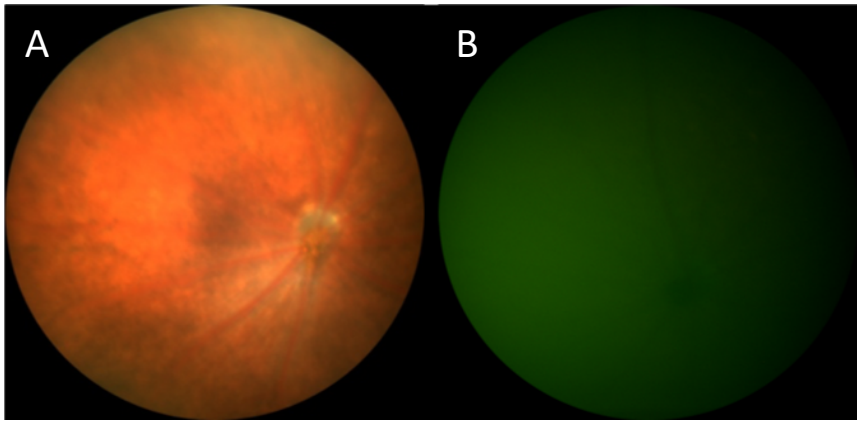

Figure 9-7. *In vivo* retinal images of 5XFAD mouse treated with aerosolized curcumin using the Phoenix Micron IV retinal imaging microscope. No gross pathologic changes were observed on brightfield imaging (A) and curcumin fluorescence was also not observable when using a FITC filter (B).

Discussion

Detection and quantification of retinal Aβ plaques have the potential to serve as a surrogate biomarker for total plaque burden in the brain for patients and transgenic mouse models of AD. This approach has been validated through comparison of retinal plaque burden to that in the CNS in transgenic mouse models of disease[465,466]. Clinical studies also suggest AD disease-related retinal changes, including retinal plaques, may in fact correlate with CNS markers of disease or clinical measures of cognitive impairment[351,467]. However, to evaluate retinal plaques clinically, a method of detection is necessary that can be used to longitudinally track formation and compare progression of development to already validated AD biomarkers as well as clinical measures. Also, if retinal plaques are shown to form in presymptomatic stages of disease, then detection and quantification could be used as a means to screen for future risk of developing AD. Current methods of tracking AD biomarker progression including PET imaging or CSF biomarker detection are limited in their clinical application because they are too invasive and expensive to be applied to a large asymptomatic population. Efforts targeting ocular biomarkers of AD, including lens and retinal pathology, are in early stages of development and have their own caveats such as dependence on instrumentation that was custom built or not readily available, detection of pathologic changes not specific to AD, use of compounds with low retinal bioavailability due to poor BRB penetration, or inconsistent findings between studies[335,345,346,356,358–361,363,367,468]. Moreover, many of these approaches have only been studied in preclinical models of disease and thus further validation is required.

In this work, we sought to develop a test for detecting retinal Aβ plaques that could safely

and readily be implemented clinically to evaluate retinal pathology as a biomarker for AD and potentially be used to screen for the same pathology in an asymptomatic population. To accomplish this, fluorescent Aβ-binding compounds, curcumin and thioflavin S, were administered as an aerosol to 5XFAD mice, serving as a model system for AD. Retinal samples from aged 5XFAD mice were stained with anti-Aβ antibodies to first confirm that retinal plaques form in our transgenic model of AD. Results demonstrated plaques were found in the IPL and GCL of the retina (Fig.9-1A). APP cleavage products were also detectable using MALDI-IMS (Fig.9-2), though spatial resolution was low and thus future work was focused on fluorescence-based methods of detection.

After we had confirmed the presence of retinal plaques, we then tested if aerosolized thioflavin S and curcumin could not only be delivered to the retina but also bind retinal plaques. 5XFAD mice treated over two consecutive days showed that in fact, when delivered as an aerosol, both thioflavin S (Fig.9-3, Fig.9-4A&B) and curcumin (Fig.9-6A&B) can be effectively delivered to the retina. Moreover, both compounds are found particularly in the GCL and may in fact be in ganglion cell cytoplasm. Aβ plaques were also preferentially found in the GCL and thus it appears retention of either compound is dependent on plaques being present. This is further supported by demonstrating thioflavin S and curcumin are not retained in wt mouse retinas following aerosol administration (Fig.9-4, Fig.9-5C&D, Fig.9-6D&E). Preliminary *in vivo* retinal imaging was conducted on 5XFAD mice treated with aerosolized curcumin and resulted in no detectable fluorescence signal. When comparing retinal section preparations from both treatments, thioflavin S retention was more prevalent than curcumin and thus, may provide better results in

noninvasive retinal imaging as well. However, before this, further work will be done to better characterize thioflavin S labeling of retinal ganglion cells in 5XFAD mice.

If thioflavin S fluorescence can be detected noninvasively through retinal imaging, this approach could potentially be used to evaluate retinal Aβ as a biomarker for AD in both preclinical animal models and clinical studies. Aerosol and intranasal administration not only allow for easy administration in clinical settings but has also been shown to increase bioavailability in the brain and exhibits faster delivery kinetics than compared to standard peripheral administration techniques[276]. This was further supported by our work outlined in chapter seven, showing that aerosolized thioflavin S is capable of bypassing the BBB and binding Aβ plaques 5XFAD mice. Based on these findings, we proposed that aerosol administration may improve delivery across the BRB and detect retinal Aβ pathology using fluorescence microscopy. Further, if thioflavin S or curcumin fluorescence effectively targets retinal Aβ, its fluorescence could potentially be detected noninvasively using imaging modalities already available in most research and clinical settings, thus making future clinical validation easier to implement. For clinical testing, longitudinal studies comparing retinal plaque formation to established measures of AD progression including cognitive testing and neuroimaging or CSF biomarkers could demonstrate the efficacy of monitoring retinal pathology. Additionally, retinal plaque detection using thioflavin S or any other fluorescent Aβ-binding agent has the potential to be both noninvasive and inexpensive, such that it could be more readily implemented in an asymptomatic population and identify those with AD pathology in preclinical stages of disease if retinal pathology forms in early stages of AD. This offers the opportunity to not only conduct

more longitudinal and frequent measures in AD patients, but also to initiate experimental therapeutics prior to significant neurodegenerative changes if retinal pathology is detected in presymptomatic stages of disease, which may improve clinical outcomes. Based on our findings, retinal Aβ plaque detection using fluorescent reporter molecules has the potential to be a noninvasive and inexpensive measure that could be readily implemented for studies as a diagnostic test and to monitor AD progression in experimental therapeutic studies both in transgenic models and clinical trials.

Final Thoughts and Future Directions

Based on the described work, we have concluded that inflammatory-mediated opening of the BBB improves delivery of a variety of compounds from small molecule to large theranostic agents as demonstrated using thioflavin S and 30 nm SPIO nanoparticles. Though LPS pretreatment effectively improved delivery of both, this came with the caveats that increased lethality was observed in our 5XFAD transgenic mice when compared to wt mice receiving the same treatment. Additionally, weight loss was observed in all mice 24 hrs following LPS pretreatment with any dosage[420]. Because of these limitations, it is unlikely that this approach for improving drug delivery could be applied clinically, especially in a diseased patient population. However, using a different pro-inflammatory molecule or pairing LPS with a selective anti-inflammatory could potentially achieve a similar effect on increasing BBB permeability while reducing the unwanted side-effects and is thus an area of research we are considering.

Though increasing BBB permeability is an effective approach for improved theranostic delivery, event transient opening comes with inherent risks including leaving the brain

susceptible to peripherally circulating neurotoxins and increased chance of developing CNS infections. As such, we investigated aerosol administration for improved delivery of compounds to the brain parenchyma. We have demonstrated this approach to be effective and, as it is not dependent on altering BBB permeability, may be more applicable in a clinical setting. Future work using this approach will seek to better understand the mechanism of uptake, hypothesized to be from olfactory-mediated transport, and see if a similar approach can be applied for improved delivery and therapeutic efficacy of other experimental treatments including anti-Aβ antibodies.

We have also shown that retinal pathology is found in our 5XFAD transgenic mice and that fluorescent Aβ-binding agents are a potential method of noninvasively evaluating retinal plaques as a predictive biomarker for AD. To further investigate this approach, we must determine whether fluorescence can effectively report retinal Aβ formation in a preclinical mouse model of disease and if it can be used to longitudinally track pathology formation. Also, once successful, we will determine if retinal pathology can be used to effectively predict plaque development in the brain under normal disease progression and in the context of administering a therapeutic targeted at reducing Aβ plaque burden. Finally, we will conduct appropriate toxicity studies such that our approach can be tested in a clinical setting to first evaluate retinal pathology in patients with known cases of effective AD and later to determine if pathology in the retina precedes clinically appreciable cognitive decline. If successful, such a test could thus identify patients at risk for future development of AD and therapeutics could be administered earlier in disease progression. By improving drug delivery across the BBB and initiating treatment earlier, therapeutic efficacy could be

enhanced significantly for both already developed and novel experimental treatments to achieve improved clinical outcomes in AD.

BIBLIOGRAPHY

1. Kochanek, K. D., Murphy, S. L., Xu, J. & Tejada-Vera, B. *National Vital Statisitcs Reports, Volume 65, Number 4, (06/30/2016)*. **65,** (2014).
2. *2018 Alzheimer's Disease Facts and Figures: Includes a Special Report on the Financial and Personal Benefits of Early Diagnosis*.
3. Guerreiro, R. & Bras, J. The age factor in Alzheimer's disease. *Genome Med.* **7,** 106 (2015).
4. Reitz, C. & Mayeux, R. Alzheimer disease: epidemiology, diagnostic criteria, risk factors and biomarkers. *Biochem. Pharmacol.* **88,** 640–51 (2014).
5. Puglielli, L., Tanzi, R. E. & Kovacs, D. M. Alzheimer's disease: the cholesterol connection. *Nat. Neurosci.* **6,** 345–351 (2003).
6. Corder, E. H. *et al.* Gene dose of apolipoprotein E type 4 allele and the risk of Alzheimer's disease in late onset families. *Science* **261,** 921–3 (1993).
7. Farrer, L. A. *et al.* Effects of age, sex, and ethnicity on the association between apolipoprotein E genotype and Alzheimer disease. A meta-analysis. APOE and Alzheimer Disease Meta Analysis Consortium. *JAMA* **278,** 1349–56
8. Lambert, J.-C. *et al.* Genome-wide association study identifies variants at CLU and CR1 associated with Alzheimer's disease. *Nat. Genet.* **41,** 1094–9 (2009).
9. Harold, D. *et al.* Genome-wide association study identifies variants at CLU and PICALM associated with Alzheimer's disease. *Nat. Genet.* **41,** 1088–93 (2009).
10. Seshadri, S. *et al.* Genome-wide analysis of genetic loci associated with Alzheimer disease. *JAMA* **303,** 1832–40 (2010).
11. van Duijn, C. M. *et al.* Familial aggregation of Alzheimer's disease and related disorders: a collaborative re-analysis of case-control studies. *Int. J. Epidemiol.* **20 Suppl 2,** S13-20 (1991).
12. Banerjee, S. Good news on dementia prevalence—we can make a difference. *Lancet* **382,** 1384–1386 (2013).
13. Whitmer, R. A., Sidney, S., Selby, J., Johnston, S. C. & Yaffe, K. Midlife cardiovascular risk factors and risk of dementia in late life. *Neurology* **64,** 277–81 (2005).
14. Freitag, M. H. *et al.* Midlife pulse pressure and incidence of dementia: the Honolulu-Asia Aging Study. *Stroke* **37,** 33–7 (2006).
15. Skoog, I. *et al.* 15-year longitudinal study of blood pressure and dementia. *Lancet (London, England)* **347,** 1141–5 (1996).
16. Kivipelto, M. *et al.* Apolipoprotein E epsilon4 allele, elevated midlife total cholesterol level, and high midlife systolic blood pressure are independent risk factors for late-life Alzheimer disease. *Ann. Intern. Med.* **137,** 149–55 (2002).
17. Solomon, A. *et al.* Serum cholesterol changes after midlife and late-life cognition: twenty-one-year follow-up study. *Neurology* **68,** 751–6 (2007).
18. Ighodaro, E. T. *et al.* Risk factors and global cognitive status related to brain arteriolosclerosis in elderly individuals. *J. Cereb. Blood Flow Metab.* **37,** 201–216 (2017).
19. Chui, H. C. *et al.* Cognitive impact of subcortical vascular and Alzheimer's disease pathology. *Ann. Neurol.* **60,** 677–87 (2006).

20. Troncoso, J. C. *et al.* Effect of infarcts on dementia in the Baltimore longitudinal study of aging. *Ann. Neurol.* **64,** 168–76 (2008).
21. Vemuri, P. *et al.* Vascular and amyloid pathologies are independent predictors of cognitive decline in normal elderly. *Brain* **138,** 761–71 (2015).
22. Profenno, L. A., Porsteinsson, A. P. & Faraone, S. V. Meta-analysis of Alzheimer's disease risk with obesity, diabetes, and related disorders. *Biol. Psychiatry* **67,** 505–12 (2010).
23. Biessels, G. J., Staekenborg, S., Brunner, E., Brayne, C. & Scheltens, P. Risk of dementia in diabetes mellitus: a systematic review. *Lancet. Neurol.* **5,** 64–74 (2006).
24. Hamer, M. & Chida, Y. Physical activity and risk of neurodegenerative disease: a systematic review of prospective evidence. *Psychol. Med.* **39,** 3–11 (2009).
25. Baumgart, M. *et al.* Summary of the evidence on modifiable risk factors for cognitive decline and dementia: A population-based perspective. *Alzheimers. Dement.* **11,** 718–26 (2015).
26. Chen, R. Association of environmental tobacco smoke with dementia and Alzheimer's disease among never smokers. *Alzheimers. Dement.* **8,** 590–5 (2012).
27. Kim, S. H. *et al.* Rapid doubling of Alzheimer's amyloid-β40 and 42 levels in brains of mice exposed to a nickel nanoparticle model of air pollution. *F1000Research* **1,** 70 (2012).
28. Calderón-Garcidueñas, L. *et al.* Brain inflammation and Alzheimer's-like pathology in individuals exposed to severe air pollution. *Toxicol. Pathol.* **32,** 650–8 (2004).
29. Calderón-Garcidueñas, L. *et al.* Long-term air pollution exposure is associated with neuroinflammation, an altered innate immune response, disruption of the blood-brain barrier, ultrafine particulate deposition, and accumulation of amyloid beta-42 and alpha-synuclein in children and young adults. *Toxicol. Pathol.* **36,** 289–310 (2008).
30. Hayden, K. M. *et al.* Occupational exposure to pesticides increases the risk of incident AD: the Cache County study. *Neurology* **74,** 1524–30 (2010).
31. Richardson, J. R. *et al.* Elevated serum pesticide levels and risk for Alzheimer disease. *JAMA Neurol.* **71,** 284–90 (2014).
32. Prince, M. *et al.* The global prevalence of dementia: a systematic review and metaanalysis. *Alzheimers. Dement.* **9,** 63–75.e2 (2013).
33. Larson, E. B. *et al.* Survival after initial diagnosis of Alzheimer disease. *Ann. Intern. Med.* **140,** 501–9 (2004).
34. Wolfson, C. *et al.* A reevaluation of the duration of survival after the onset of dementia. *N. Engl. J. Med.* **344,** 1111–6 (2001).
35. Förstl, H. & Kurz, A. Clinical features of Alzheimer's disease. *Eur. Arch. Psychiatry Clin. Neurosci.* **249,** 288–290 (1999).
36. Mann, D. An atlas of Alzheimer's disease. The encyclopedia of visual medicine series. *J. Neurol. Neurosurg. Psychiatry* **70,** 821l–821 (2001).
37. McKhann, G. *et al.* Clinical diagnosis of Alzheimer's disease: Report of the NINCDS-ADRDA Work Group* under the auspices of Department of Health and Human Services Task Force on Alzheimer's Disease. *Neurology* **34,** 939–944 (1984).
38. McKhann, G. M. *et al.* The diagnosis of dementia due to Alzheimer's disease: recommendations from the National Institute on Aging-Alzheimer's Association workgroups on diagnostic guidelines for Alzheimer's disease. *Alzheimers. Dement.*

7, 263–9 (2011).
39. American Psychiatric Association. *Diagnostic and Statistical Manual of Mental Disorders*. (American Psychiatric Association, 2013). doi:10.1176/appi.books.9780890425596
40. Huang, J. Overview of Delirium and Dementia. *Merck Manuals Prof. Ed.* (2018).
41. Lippmann, S. & Perugula, M. L. Delirium or Dementia? *Innov. Clin. Neurosci.* **13,** 56–57 (2016).
42. Cooper, S. & Greene, J. D. W. The clinical assessment of the patient with early dementia. *J. Neurol. Neurosurg. Psychiatry* **76 Suppl 5,** v15-24 (2005).
43. Seeley, W. W. & Miller, B. L. in *Harrison's Principles of Internal Medicine* 3300–3316 (McGraw-Hill, 2012).
44. Boyle, P. A. *et al.* Person-specific contribution of neuropathologies to cognitive loss in old age. *Ann. Neurol.* **83,** 74–83 (2018).
45. Bang, J., Spina, S. & Miller, B. L. Frontotemporal dementia. *Lancet (London, England)* **386,** 1672–82 (2015).
46. Rosen, H. J. *et al.* Patterns of brain atrophy in frontotemporal dementia and semantic dementia. *Neurology* **58,** 198–208 (2002).
47. Ber, I. L. *et al.* Demographic, neurological and behavioural characteristics and brain perfusion SPECT in frontal variant of frontotemporal dementia. *Brain* **129,** 3051–3065 (2006).
48. Gibb, W. R. & Lees, A. J. The relevance of the Lewy body to the pathogenesis of idiopathic Parkinson's disease. *J. Neurol. Neurosurg. Psychiatry* **51,** 745–52 (1988).
49. DeMaagd, G. & Philip, A. Parkinson's Disease and Its Management: Part 1: Disease Entity, Risk Factors, Pathophysiology, Clinical Presentation, and Diagnosis. *P T* **40,** 504–32 (2015).
50. Kalia, L. V & Lang, A. E. Parkinson's disease. *Lancet (London, England)* **386,** 896–912 (2015).
51. Aarsland, D. *et al.* Risk of dementia in Parkinson's disease: a community-based, prospective study. *Neurology* **56,** 730–6 (2001).
52. Emre, M. Dementia associated with Parkinson's disease. *Lancet. Neurol.* **2,** 229–37 (2003).
53. Sanford, A. M. Lewy Body Dementia. *Clin. Geriatr. Med.* **34,** 603–615 (2018).
54. Mackenzie, G. & Will, R. Creutzfeldt-Jakob disease: recent developments. *F1000Research* **6,** 2053 (2017).
55. Soto, C. & Satani, N. The intricate mechanisms of neurodegeneration in prion diseases. *Trends Mol. Med.* **17,** 14–24 (2011).
56. Morales, R., Abid, K. & Soto, C. The prion strain phenomenon: Molecular basis and unprecedented features. *Biochim. Biophys. Acta - Mol. Basis Dis.* **1772,** 681–691 (2007).
57. Tartaglia, M. C. *et al.* Clinical overlap between Jakob-Creutzfeldt disease and Lewy body disease. *Can. J. Neurol. Sci.* **39,** 304–10 (2012).
58. Tschampa, H. J. *et al. Patients with Alzheimer's disease and dementia with Lewy bodies mistaken for Creutzfeldt-Jakob disease*.
59. Tripathi, M. & Vibha, D. Reversible dementias. *Indian J. Psychiatry* **51 Suppl 1,** S52-5 (2009).
60. *AAN Guideline Summary for CLINICIANS DETECTION, DIAGNOSIS AND MANAGEMENT OF DEMENTIA PRACTICE PARAMETER: DETECTION OF*

DEMENTIA-MILD COGNITIVE IMPAIRMENT.
61. Adelman, A. M. & Daly, M. P. Initial Evaluation of the Patient with Suspected Dementia. *Am. Fam. Physician* **71,** 1745–1750 (2005).
62. Crum, R. M., Anthony, J. C., Bassett, S. S. & Folstein, M. F. Population-Based Norms for the Mini-Mental State Examination by Age and Educational Level. *JAMA J. Am. Med. Assoc.* **269,** 2386 (1993).
63. Knopman, D. S. *et al.* Practice parameter for diagnosis and evaluation of dementia. Report of the Quality Standards Subcommittee of the American Academy of Neurology. *Neurology* **44,** 2203–6 (2001).
64. Harvey, P. D. Clinical applications of neuropsychological assessment. *Dialogues Clin. Neurosci.* **14,** 91–9 (2012).
65. Wolk, D. & Dickerson, B. *Clinical features and diagnosis of Alzheimer disease*. *UptoDate* (2018).
66. Pająk, B., Kania, E. & Orzechowski, A. Killing Me Softly: Connotations to Unfolded Protein Response and Oxidative Stress in Alzheimer's Disease. *Oxid. Med. Cell. Longev.* **2016,** 1805304 (2016).
67. Hardy, J. & Higgins, G. Alzheimer's disease: the amyloid cascade hypothesis. *Science (80-.).* **256,** 184–185 (1992).
68. Evin, G. & Weidemann, A. Biogenesis and metabolism of Alzheimer's disease Aβ amyloid peptides. *Peptides* **23,** 1285–1297 (2002).
69. Eikelenboom, P., Zhan, S.-S., van Gool, W. A. & Allsop, D. Inflammatory mechanisms in Alzheimer's disease. *Trends Pharmacol. Sci.* **15,** 447–450 (1994).
70. McGeer, P. L. & McGeer, E. G. The inflammatory response system of brain: implications for therapy of Alzheimer and other neurodegenerative diseases. *Brain Res. Rev.* **21,** 195–218 (1995).
71. Rogers, J. *et al.* Inflammation and Alzheimer's disease pathogenesis. *Neurobiol. Aging* **17,** 681–686 (1996).
72. De Felice, F. G. *et al.* Alzheimer's disease-type neuronal tau hyperphosphorylation induced by A beta oligomers. *Neurobiol. Aging* **29,** 1334–47 (2008).
73. Kumar, A., Singh, A. & Ekavali. A review on Alzheimer's disease pathophysiology and its management: an update. *Pharmacol. Reports* **67,** 195–203 (2015).
74. Hyman, B. T., Van Hoesen, G. W., Damasio, A. R. & Barnes, C. L. Alzheimer's disease: cell-specific pathology isolates the hippocampal formation. *Science* **225,** 1168–70 (1984).
75. Selkoe, D. J. Alzheimer's Disease: Genes, Proteins, and Therapy. *Physiol. Rev.* **81,** 741–766 (2001).
76. Teller, J. K. *et al.* Presence of soluble amyloid β–peptide precedes amyloid plaque formation in Down's syndrome. *Nat. Med.* **2,** 93–95 (1996).
77. Frederikse, P. H. & Ren, X.-O. Lens defects and age-related fiber cell degeneration in a mouse model of increased AbetaPP gene dosage in Down syndrome. *Am. J. Pathol.* **161,** 1985–90 (2002).
78. McLean, C. A. *et al.* Soluble pool of A? amyloid as a determinant of severity of neurodegeneration in Alzheimer's disease. *Ann. Neurol.* **46,** 860–866 (1999).
79. Josephs, K. A. *et al.* β-amyloid burden is not associated with rates of brain atrophy. *Ann. Neurol.* **63,** 204–212 (2008).
80. Aizenstein, H. J. *et al.* Frequent amyloid deposition without significant cognitive impairment among the elderly. *Arch. Neurol.* **65,** 1509–17 (2008).

81. Lambert, M. P. *et al.* Diffusible, nonfibrillar ligands derived from Abeta1-42 are potent central nervous system neurotoxins. *Proc. Natl. Acad. Sci. U. S. A.* **95,** 6448–53 (1998).
82. Selkoe, D. J. Soluble oligomers of the amyloid beta-protein impair synaptic plasticity and behavior. *Behav. Brain Res.* **192,** 106–13 (2008).
83. Haass, C. & Selkoe, D. J. Soluble protein oligomers in neurodegeneration: lessons from the Alzheimer's amyloid β-peptide. *Nat. Rev. Mol. Cell Biol.* **8,** 101–112 (2007).
84. Barage, S. H. & Sonawane, K. D. Amyloid cascade hypothesis: Pathogenesis and therapeutic strategies in Alzheimer's disease. *Neuropeptides* **52,** 1–18 (2015).
85. Jope, R. S. & Johnson, G. V. . The glamour and gloom of glycogen synthase kinase-3. *Trends Biochem. Sci.* **29,** 95–102 (2004).
86. DaRocha-Souto, B. *et al.* Activation of glycogen synthase kinase-3 beta mediates β-amyloid induced neuritic damage in Alzheimer's disease. *Neurobiol. Dis.* **45,** 425–437 (2012).
87. Sofola, O. *et al.* Inhibition of GSK-3 Ameliorates Aβ Pathology in an Adult-Onset Drosophila Model of Alzheimer's Disease. *PLoS Genet.* **6,** e1001087 (2010).
88. Hurtado, D. E. *et al.* Selectively Silencing GSK-3 Isoforms Reduces Plaques and Tangles in Mouse Models of Alzheimer's Disease. *J. Neurosci.* **32,** 7392–7402 (2012).
89. Martinez, A. & Perez, D. I. GSK-3 inhibitors: a ray of hope for the treatment of Alzheimer's disease? *J. Alzheimers. Dis.* **15,** 181–91 (2008).
90. Kremer, A., Louis, J. V, Jaworski, T. & Van Leuven, F. GSK3 and Alzheimer's Disease: Facts and Fiction…. *Front. Mol. Neurosci.* **4,** 17 (2011).
91. Reddy, P. H. Amyloid beta-induced glycogen synthase kinase 3β phosphorylated VDAC1 in Alzheimer's disease: Implications for synaptic dysfunction and neuronal damage. *Biochim. Biophys. Acta - Mol. Basis Dis.* **1832,** 1913–1921 (2013).
92. Pastorino, J. G., Hoek, J. B. & Shulga, N. Activation of Glycogen Synthase Kinase 3β Disrupts the Binding of Hexokinase II to Mitochondria by Phosphorylating Voltage-Dependent Anion Channel and Potentiates Chemotherapy-Induced Cytotoxicity. *Cancer Res.* **65,** 10545–10554 (2005).
93. Azoulay-Zohar, H., Israelson, A., Abu-Hamad, S. & Shoshan-Barmatz, V. In self-defence: hexokinase promotes voltage-dependent anion channel closure and prevents mitochondria-mediated apoptotic cell death. *Biochem. J.* **377,** 347–55 (2004).
94. Zaid, H., Abu-Hamad, S., Israelson, A., Nathan, I. & Shoshan-Barmatz, V. The voltage-dependent anion channel-1 modulates apoptotic cell death. *Cell Death Differ.* **12,** 751–760 (2005).
95. Abu-Hamad, S., Zaid, H., Israelson, A., Nahon, E. & Shoshan-Barmatz, V. Hexokinase-I Protection against Apoptotic Cell Death Is Mediated via Interaction with the Voltage-dependent Anion Channel-1. *J. Biol. Chem.* **283,** 13482–13490 (2008).
96. Braak, H., Thal, D. R., Ghebremedhin, E. & Del Tredici, K. Stages of the Pathologic Process in Alzheimer Disease: Age Categories From 1 to 100 Years. *J. Neuropathol. Exp. Neurol.* **70,** 960–969 (2011).
97. Snowden, J. S., Neary, D. & Mann, D. M. A. Frontotemporal dementia. *Br. J. Psychiatry* **180,** 140–143 (2002).

98. Attems, J. & Jellinger, K. A. The overlap between vascular disease and Alzheimer's disease--lessons from pathology. *BMC Med.* **12,** 206 (2014).
99. Helzner, E. P. *et al.* Contribution of Vascular Risk Factors to the Progression in Alzheimer Disease. *Arch. Neurol.* **66,** 343–8 (2009).
100. Zipfel, G. J., Han, H., Ford, A. L. & Lee, J.-M. Cerebral Amyloid Angiopathy Progressive Disruption of the Neurovascular Unit. (2009). doi:10.1161/STROKEAHA.108.533174
101. Nelson, P. T. *et al.* APOE-ε2 and APOE-ε4 Correlate With Increased Amyloid Accumulation in Cerebral Vasculature. *J. Neuropathol. Exp. Neurol.* **72,** 708–715 (2013).
102. Thal, D. R., Ghebremedhin, E., Orantes, M. & Wiestler, O. D. Vascular pathology in Alzheimer disease: correlation of cerebral amyloid angiopathy and arteriosclerosis/lipohyalinosis with cognitive decline. *J. Neuropathol. Exp. Neurol.* **62,** 1287–301 (2003).
103. Costanza, A. *et al.* Microvascular burden and Alzheimer-type lesions across the age spectrum. *J. Alzheimers. Dis.* **32,** 643–52 (2012).
104. Yiannopoulou, K. G. & Papageorgiou, S. G. Current and future treatments for Alzheimer's disease. *Ther. Adv. Neurol. Disord.* **6,** 19–33 (2013).
105. *FDA-approved treatments for Alzheimer's*.
106. Cummings, J. L. & Back, C. The Cholinergic Hypothesis of Neuropsychiatric Symptoms in Alzheimer's Disease. *Am. J. Geriatr. Psychiatry* **6,** S64–S78 (1998).
107. Mega, M. S., Cummings, J. L., Fiorello, T. & Gornbein, J. The spectrum of behavioral changes in Alzheimer's disease. *Neurology* **46,** 130–5 (1996).
108. Wragg, R. E. & Jeste, D. V. Overview of depression and psychosis in Alzheimer's disease. *Am. J. Psychiatry* **146,** 577–587 (1989).
109. Sunderland, T. *et al.* Anticholinergic sensitivity in patients with dementia of the Alzheimer type and age-matched controls. A dose-response study. *Arch. Gen. Psychiatry* **44,** 418–26 (1987).
110. Gorman, D. G., Read, S. & Cummings, J. L. Cholinergic therapy of behavioral disturbances in Alzheimer's disease. *Neuropsychiatry, Neuropsychol. Behav. Neurol.* **6,** 229–234 (1993).
111. Bodick, N. C. *et al.* Effects of xanomeline, a selective muscarinic receptor agonist, on cognitive function and behavioral symptoms in Alzheimer disease. *Arch. Neurol.* **54,** 465–73 (1997).
112. Tariot, P. N. & Federoff, H. J. Current Treatment for Alzheimer Disease and Future Prospects. *Alzheimer Dis. Assoc. Disord.* **17,** (2003).
113. Alfirevic, A. *et al.* Tacrine-induced liver damage: an analysis of 19 candidate genes. *Pharmacogenet. Genomics* **17,** 1091–1100 (2007).
114. Farlow, M. A clinical overview of cholinesterase inhibitors in Alzheimer's disease. *Int. psychogeriatrics* **14 Suppl 1,** 93–126 (2002).
115. Cummings, J. *et al.* Effect of Donepezil on Cognition in Severe Alzheimer's Disease: A Pooled Data Analysis. *J. Alzheimer's Dis.* **21,** 843–851 (2010).
116. Hansen, R. A. *et al.* Efficacy and safety of donepezil, galantamine, and rivastigmine for the treatment of Alzheimer's disease: a systematic review and meta-analysis. *Clin. Interv. Aging* **3,** 211–25 (2008).
117. McShane, R., Areosa Sastre, A. & Minakaran, N. Memantine for dementia. *Cochrane Database Syst. Rev.* CD003154 (2006).

doi:10.1002/14651858.CD003154.pub5
118. Maidment, I. D. *et al.* Efficacy of Memantine on Behavioral and Psychological Symptoms Related to Dementia: A Systematic Meta-Analysis. *Ann. Pharmacother.* **42,** 32–38 (2008).
119. Tariot, P. N. *et al.* Memantine Treatment in Patients With Moderate to Severe Alzheimer Disease Already Receiving Donepezil. *JAMA* **291,** 317 (2004).
120. Feldman, H. H., Schmitt, F. A., Olin, J. T. & Memantine MEM-MD-02 Study Group. Activities of Daily Living in Moderate-to-Severe Alzheimer Disease: An Analysis of the Treatment Effects of Memantine in Patients Receiving Stable Donepezil Treatment. *Alzheimer Dis. Assoc. Disord.* **20,** 263–268 (2006).
121. Howard, R. *et al.* Donepezil and Memantine for Moderate-to-Severe Alzheimer's Disease. *N. Engl. J. Med.* **366,** 893–903 (2012).
122. Gervais, F. *et al.* Glycosaminoglycan mimetics: a therapeutic approach to cerebral amyloid angiopathy. *Amyloid* **8 Suppl 1,** 28–35 (2001).
123. Galimberti, D. & Scarpini, E. Disease-modifying treatments for Alzheimer's disease. *Ther. Adv. Neurol. Disord.* **4,** 203–16 (2011).
124. Aisen, P. S. *et al.* A Phase II study targeting amyloid- with 3APS in mild-to-moderate Alzheimer disease. *Neurology* **67,** 1757–1763 (2006).
125. Bilikiewicz, A. & Gaus, W. Colostrinin (a naturally occurring, proline-rich, polypeptide mixture) in the treatment of Alzheimer's disease. *J. Alzheimers. Dis.* **6,** 17–26 (2004).
126. Cummings, J. L. Optimizing phase II of drug development for disease-modifying compounds. *Alzheimer's Dement.* **4,** S15–S20 (2008).
127. Menting, K. W. & Claassen, J. A. H. R. β-secretase inhibitor; a promising novel therapeutic drug in Alzheimer's disease. *Front. Aging Neurosci.* **6,** 165 (2014).
128. Egan, M. F. *et al.* Randomized Trial of Verubecestat for Mild-to-Moderate Alzheimer's Disease. *N. Engl. J. Med.* **378,** 1691–1703 (2018).
129. Siemers, E. *et al.* Safety, tolerability, and changes in amyloid beta concentrations after administration of a gamma-secretase inhibitor in volunteers. *Clin. Neuropharmacol.* **28,** 126–32
130. Imbimbo, B. P. & Giardina, G. A. M. γ-secretase inhibitors and modulators for the treatment of Alzheimer's disease: disappointments and hopes. *Curr. Top. Med. Chem.* **11,** 1555–70 (2011).
131. Siemers, E. R. *et al.* Effects of a -secretase inhibitor in a randomized study of patients with Alzheimer disease. *Neurology* **66,** 602–604 (2006).
132. Fleisher, A. S. *et al.* Phase 2 Safety Trial Targeting Amyloid β Production With a γ-Secretase Inhibitor in Alzheimer Disease. *Arch. Neurol.* **65,** 1031–8 (2008).
133. Lichtenthaler, S. F. Alpha-secretase in Alzheimer's disease: molecular identity, regulation and therapeutic potential. *J. Neurochem.* **116,** 10–21 (2011).
134. MacLeod, R., Hillert, E.-K., Cameron, R. T. & Baillie, G. S. The role and therapeutic targeting of α-, β- and γ-secretase in Alzheimer's disease. *Futur. Sci. OA* **1,** FSO11 (2015).
135. Salah, M., Samy, N. & Fadel, M. Methylene blue mediated photodynamic therapy for resistant plaque psoriasis. *J. Drugs Dermatol.* **8,** 42–9 (2009).
136. Bradberry, S. M. Occupational methaemoglobinaemia. Mechanisms of production, features, diagnosis and management including the use of methylene blue. *Toxicol. Rev.* **22,** 13–27 (2003).

137. Çolakoğlu, M. K., Güven, E., Akgül, G. G., Doğan, L. & Gülçelik, M. A. Biological Subtypes of Breast Cancer and Sentinel Lymph Node Biopsy. *Eur. J. breast Heal.* **14,** 100–104 (2018).
138. Wischik, C. M., Edwards, P. C., Lai, R. Y., Roth, M. & Harrington, C. R. Selective inhibition of Alzheimer disease-like tau aggregation by phenothiazines. *Proc. Natl. Acad. Sci. U. S. A.* **93,** 11213–8 (1996).
139. Balaraman, Y., Limaye, A. R., Levey, A. I. & Srinivasan, S. Glycogen synthase kinase 3β and Alzheimer's disease: pathophysiological and therapeutic significance. *Cell. Mol. Life Sci.* **63,** 1226–1235 (2006).
140. Forlenza, O. V. *et al.* Disease-modifying properties of long-term lithium treatment for amnestic mild cognitive impairment: randomised controlled trial. *Br. J. Psychiatry* **198,** 351–356 (2011).
141. Schenk, D. *et al.* Immunization with amyloid-β attenuates Alzheimer-disease-like pathology in the PDAPP mouse. *Nature* **400,** 173–177 (1999).
142. Gilman, S. *et al.* Clinical effects of A immunization (AN1792) in patients with AD in an interrupted trial. *Neurology* **64,** 1553–1562 (2005).
143. Hock, C. & Nitsch, R. M. Clinical Observations with AN-1792 Using TAPIR Analyses. *Neurodegener. Dis.* **2,** 273–276 (2005).
144. Holmes, C. *et al.* Long-term effects of Aβ42 immunisation in Alzheimer's disease: follow-up of a randomised, placebo-controlled phase I trial. *Lancet* **372,** 216–223 (2008).
145. Brody, D. L. & Holtzman, D. M. Active and Passive Immunotherapy for Neurodegenerative Disorders. *Annu. Rev. Neurosci.* **31,** 175–193 (2008).
146. Wisniewski, T. & Konietzko, U. Amyloid-beta immunisation for Alzheimer's disease. *Lancet. Neurol.* **7,** 805–11 (2008).
147. Vandenberghe, R. *et al.* Bapineuzumab for mild to moderate Alzheimer's disease in two global, randomized, phase 3 trials. *Alzheimers. Res. Ther.* **8,** 18 (2016).
148. Honig, L. S. *et al.* Trial of Solanezumab for Mild Dementia Due to Alzheimer's Disease. *N. Engl. J. Med.* **378,** 321–330 (2018).
149. Bateman, R. J. *et al.* Clinical and Biomarker Changes in Dominantly Inherited Alzheimer's Disease. *N. Engl. J. Med.* **367,** 795–804 (2012).
150. Anoop, A., Singh, P. K., Jacob, R. S. & Maji, S. K. CSF Biomarkers for Alzheimer's Disease Diagnosis. *Int. J. Alzheimers. Dis.* **2010,** (2010).
151. Blennow, K., Hampel, H., Weiner, M. & Zetterberg, H. Cerebrospinal fluid and plasma biomarkers in Alzheimer disease. *Nat. Rev. Neurol.* **6,** 131–144 (2010).
152. Formichi, P., Battisti, C., Radi, E. & Federico, A. Cerebrospinal fluid tau, Aß, and phosphorylated tau protein for the diagnosis of Alzheimer's disease. *J. Cell. Physiol.* **208,** 39–46 (2006).
153. Kitaguchi, N. *et al.* Determination of amyloid beta protein precursors harboring active form of proteinase inhibitor domains in cerebrospinal fluid of Alzheimer's disease patients by trypsin-antibody sandwich ELISA. *Biochem. Biophys. Res. Commun.* **166,** 1453–9 (1990).
154. Ghiso, J., Tagliavini, F., Timmers, W. F. & Frangione, B. Alzheimer's disease amyloid precursor protein is present in senile plaques and cerebrospinal fluid: immunohistochemical and biochemical characterization. *Biochem. Biophys. Res. Commun.* **163,** 430–7 (1989).
155. Henriksson, T. *et al.* Analysis and quantitation of the beta-amyloid precursor protein

in the cerebrospinal fluid of Alzheimer's disease patients with a monoclonal antibody-based immunoassay. *J. Neurochem.* **56,** 1037–42 (1991).
156. Prior, R. *et al.* Quantitative changes in the amyloid beta A4 precursor protein in Alzheimer cerebrospinal fluid. *Neurosci. Lett.* **124,** 69–73 (1991).
157. Chong, J. K., Miller, B. E. & Ghanbari, H. A. Detection of amyloid beta protein precursor immunoreactivity in normal and Alzheimer's disease cerebrospinal fluid. *Life Sci.* **47,** 1163–71 (1990).
158. Craig-Schapiro, R., Fagan, A. M. & Holtzman, D. M. Biomarkers of Alzheimer's disease. *Neurobiol. Dis.* **35,** 128–40 (2009).
159. Andreasen, N. *et al.* Cerebrospinal fluid beta-amyloid(1-42) in Alzheimer disease: differences between early- and late-onset Alzheimer disease and stability during the course of disease. *Arch. Neurol.* **56,** 673–80 (1999).
160. Lewczuk, P. *et al.* Neurochemical diagnosis of Alzheimer's dementia by CSF Aβ42, Aβ42/Aβ40 ratio and total tau. *Neurobiol. Aging* **25,** 273–281 (2004).
161. Galasko, D. *et al.* High cerebrospinal fluid tau and low amyloid beta42 levels in the clinical diagnosis of Alzheimer disease and relation to apolipoprotein E genotype. *Arch. Neurol.* **55,** 937–45 (1998).
162. Motter, R. *et al.* Reduction of beta-amyloid peptide42 in the cerebrospinal fluid of patients with Alzheimer's disease. *Ann. Neurol.* **38,** 643–648 (1995).
163. Csernansky, J. G., Miller, J. P., McKeel, D. & Morris, J. C. Relationships among cerebrospinal fluid biomarkers in dementia of the Alzheimer type. *Alzheimer Dis. Assoc. Disord.* **16,** 144–9
164. Jensen, M. *et al.* Cerebrospinal fluid A beta42 is increased early in sporadic Alzheimer's disease and declines with disease progression. *Ann. Neurol.* **45,** 504–11 (1999).
165. Fagan, A. M. *et al.* Inverse relation between in vivo amyloid imaging load and cerebrospinal fluid Aβ42 in humans. *Ann. Neurol.* **59,** 512–519 (2006).
166. Shah, T., Gupta, S., Chatterjee, P., Campbell, M. & Martins, R. Beta-amyloid sequelae in the eye: a critical review on its diagnostic significance and clinical relevance in Alzheimer's disease. *Mol. Psychiatry* **22,** (2017).
167. Hansson, O. *et al.* Prediction of Alzheimer's Disease Using the CSF Aβ42/Aβ40 Ratio in Patients with Mild Cognitive Impairment. *Dement. Geriatr. Cogn. Disord.* **23,** 316–320 (2007).
168. Lewczuk, P. *et al.* The amyloid-beta (Aβ) peptide pattern in cerebrospinal fluid in Alzheimer's disease: evidence of a novel carboxyterminally elongated Aβ peptide. *Rapid Commun. Mass Spectrom.* **17,** 1291–1296 (2003).
169. Schoonenboom, N. S. *et al.* Amyloid β 38, 40, and 42 species in cerebrospinal fluid: More of the same? *Ann. Neurol.* **58,** 139–142 (2005).
170. Portelius, E. *et al.* An Alzheimer's disease-specific β-amyloid fragment signature in cerebrospinal fluid. *Neurosci. Lett.* **409,** 215–219 (2006).
171. Hesse, C. *et al.* Transient increase in total tau but not phospho-tau in human cerebrospinal fluid after acute stroke. *Neurosci. Lett.* **297,** 187–90 (2001).
172. Ost, M. *et al.* Initial CSF total tau correlates with 1-year outcome in patients with traumatic brain injury. *Neurology* **67,** 1600–1604 (2006).
173. Vandermeeren, M. *et al.* Detection of tau proteins in normal and Alzheimer's disease cerebrospinal fluid with a sensitive sandwich enzyme-linked immunosorbent assay. *J. Neurochem.* **61,** 1828–34 (1993).

174. Morikawa, Y. *et al.* Cerebrospinal fluid tau protein levels in demented and nondemented alcoholics. *Alcohol. Clin. Exp. Res.* **23,** 575–7 (1999).
175. Koopman, K. *et al.* Improved discrimination of autopsy-confirmed Alzheimer's disease (AD) from non-AD dementias using CSF P-tau181P. *Neurochem. Int.* **55,** 214–218 (2009).
176. Kuo, Y.-M. *et al.* Amyloid-β Peptides Interact with Plasma Proteins and Erythrocytes: Implications for Their Quantitation in Plasma. *Biochem. Biophys. Res. Commun.* **268,** 750–756 (2000).
177. Irizarry, M. C. Biomarkers of Alzheimer disease in plasma. *NeuroRX* **1,** 226–234 (2004).
178. Andreasson, U., Blennow, K. & Zetterberg, H. Update on ultrasensitive technologies to facilitate research on blood biomarkers for central nervous system disorders. *Alzheimer's Dement. (Amsterdam, Netherlands)* **3,** 98–102 (2016).
179. Nakamura, A. *et al.* High performance plasma amyloid-β biomarkers for Alzheimer's disease. (2018). doi:10.1038/nature25456
180. Dustin, D., Hall, B. M., Annapragada, A. & Pautler, R. G. Neuroimaging in Alzheimer's disease: preclinical challenges toward clinical efficacy. *Transl. Res.* **175,** 37–53 (2016).
181. Weiner, M. W. *et al.* Impact of the Alzheimer's Disease Neuroimaging Initiative, 2004 to 2014. *Alzheimer's Dement.* **11,** 865–884 (2015).
182. Varghese, T., Sheelakumari, R., James, J. S. & Mathuranath, P. A review of neuroimaging biomarkers of Alzheimer's disease. *Neurol. Asia* **18,** 239–248 (2013).
183. Du, A. T. *et al.* Magnetic resonance imaging of the entorhinal cortex and hippocampus in mild cognitive impairment and Alzheimer's disease. *J. Neurol. Neurosurg. Psychiatry* **71,** 441–7 (2001).
184. Killiany, R. J. *et al.* MRI measures of entorhinal cortex vs hippocampus in preclinical AD. *Neurology* **58,** 1188–96 (2002).
185. Jack, C. R. *et al.* Prediction of AD with MRI-based hippocampal volume in mild cognitive impairment. *Neurology* **52,** 1397–403 (1999).
186. Jack, C. R. *et al.* Rates of hippocampal atrophy correlate with change in clinical status in aging and AD. *Neurology* **55,** 484–89 (2000).
187. Rusinek, H. *et al.* Atrophy rate in medial temporal lobe during progression of Alzheimer disease. *Neurology* **63,** 2354–9 (2004).
188. Colliot, O. *et al.* Discrimination between Alzheimer Disease, Mild Cognitive Impairment, and Normal Aging by Using Automated Segmentation of the Hippocampus. *Radiology* **248,** 194–201 (2008).
189. Duara, R. *et al.* Medial temporal lobe atrophy on MRI scans and the diagnosis of Alzheimer disease. *Neurology* **71,** 1986–92 (2008).
190. Dickerson, B. C. *et al.* Alzheimer-signature MRI biomarker predicts AD dementia in cognitively normal adults. *Neurology* **76,** 1395–1402 (2011).
191. Ferreira, D. *et al.* Brain Changes in Alzheimer's Disease Patients with Implanted Encapsulated Cells Releasing Nerve Growth Factor. *J. Alzheimer's Dis.* **43,** 1059–1072 (2014).
192. Hsu, P. J. *et al.* Amyloid burden in cognitively normal elderly is associated with preferential hippocampal subfield volume loss. *J. Alzheimers. Dis.* **45,** 27–33 (2015).
193. Trzepacz, P. T. *et al.* Relationship of Hippocampal Volume to Amyloid Burden across Diagnostic Stages of Alzheimer's Disease. *Dement. Geriatr. Cogn. Disord.*

41, 68–79 (2016).
194. Yin, J. *et al.* Association of amyloid burden, brain atrophy and memory deficits in aged apolipoprotein ε4 mice. *Curr. Alzheimer Res.* **11,** 283–90 (2014).
195. Bernard, C. *et al.* Time course of brain volume changes in the preclinical phase of Alzheimer's disease. *Alzheimer's Dement.* **10,** 143–151.e1 (2014).
196. Teipel, S. *et al.* Multimodal imaging in Alzheimer's disease: validity and usefulness for early detection. *Lancet Neurol.* **14,** 1037–1053 (2015).
197. Daianu, M. *et al.* An advanced white matter tract analysis in frontotemporal dementia and early-onset Alzheimer's disease. *Brain Imaging Behav.* **10,** 1038–1053 (2016).
198. Hořínek, D. *et al.* Difference in white matter microstructure in differential diagnosis of normal pressure hydrocephalus and Alzheimer's disease. *Clin. Neurol. Neurosurg.* **140,** 52–59 (2016).
199. Delli Pizzi, S. *et al.* Structural Connectivity is Differently Altered in Dementia with Lewy Body and Alzheimer's Disease. *Front. Aging Neurosci.* **7,** 208 (2015).
200. Masutani, Y., Aoki, S., Abe, O., Hayashi, N. & Otomo, K. MR diffusion tensor imaging: recent advance and new techniques for diffusion tensor visualization. *Eur. J. Radiol.* **46,** 53–66 (2003).
201. Firbank, M. J. *et al.* Longitudinal diffusion tensor imaging in dementia with Lewy bodies and Alzheimer's disease. *Parkinsonism Relat. Disord.* **24,** 76–80 (2016).
202. Johnson, K. A., Fox, N. C., Sperling, R. A. & Klunk, W. E. Brain imaging in Alzheimer disease. *Cold Spring Harb. Perspect. Med.* **2,** a006213 (2012).
203. Glover, G. H. Overview of functional magnetic resonance imaging. *Neurosurg. Clin. N. Am.* **22,** 133–9, vii (2011).
204. SPERLING, R. Functional MRI Studies of Associative Encoding in Normal Aging, Mild Cognitive Impairment, and Alzheimer's Disease. *Ann. N. Y. Acad. Sci.* **1097,** 146–155 (2007).
205. Wang, K. *et al.* Altered functional connectivity in early Alzheimer's disease: A resting-state fMRI study. *Hum. Brain Mapp.* **28,** 967–978 (2007).
206. Liu, J. *et al.* Impaired Parahippocampus Connectivity in Mild Cognitive Impairment and Alzheimer's Disease. *J. Alzheimer's Dis.* **49,** 1051–1064 (2015).
207. Zippo, A. G., Castiglioni, I., Borsa, V. M. & Biella, G. E. M. The Compression Flow as a Measure to Estimate the Brain Connectivity Changes in Resting State fMRI and 18FDG-PET Alzheimer's Disease Connectomes. *Front. Comput. Neurosci.* **9,** 148 (2015).
208. Mistur, R. *et al.* Current Challenges for the Early Detection of Alzheimer's Disease: Brain Imaging and CSF Studies. *J. Clin. Neurol.* **5,** 153 (2009).
209. Nobili, F. & Morbelli, S. [18F]FDG-PET as a Biomarker for Early Alzheimer`s Disease. *Open Nucl. Med. J.* **2,** 46–52 (2010).
210. Klunk, W. E. *et al.* Imaging brain amyloid in Alzheimer's disease with Pittsburgh Compound-B. *Ann. Neurol.* **55,** 306–319 (2004).
211. Clark, C. M. *et al.* Cerebral PET with florbetapir compared with neuropathology at autopsy for detection of neuritic amyloid-β plaques: a prospective cohort study. *Lancet Neurol.* **11,** 669–678 (2012).
212. Yeo, J. M., Waddell, B., Khan, Z. & Pal, S. A systematic review and meta-analysis of (18)F-labeled amyloid imaging in Alzheimer's disease. *Alzheimer's Dement. (Amsterdam, Netherlands)* **1,** 5–13 (2015).

213. Jack, C. R. *et al.* Hypothetical model of dynamic biomarkers of the Alzheimer's pathological cascade. *Lancet. Neurol.* **9,** 119–28 (2010).
214. Chien, D. T. *et al.* Early Clinical PET Imaging Results with the Novel PHF-Tau Radioligand [F-18]-T807. *J. Alzheimer's Dis.* **34,** 457–468 (2013).
215. Chien, D. T. *et al.* Early Clinical PET Imaging Results with the Novel PHF-Tau Radioligand [F18]-T808. *J. Alzheimer's Dis.* **38,** 171–184 (2013).
216. Saint-Aubert, L. *et al.* Tau PET imaging: present and future directions. *Mol. Neurodegener.* **12,** 19 (2017).
217. Klunk, W. E. *et al.* Imaging the pathology of Alzheimer's disease: amyloid-imaging with positron emission tomography. *Neuroimaging Clin. N. Am.* **13,** 781–9, ix (2003).
218. Daneman, R. & Prat, A. The blood-brain barrier. *Cold Spring Harb. Perspect. Biol.* **7,** a020412 (2015).
219. Zlokovic, B. V. The Blood-Brain Barrier in Health and Chronic Neurodegenerative Disorders. *Neuron* **57,** 178–201 (2008).
220. Ballabh, P., Braun, A. & Nedergaard, M. The blood–brain barrier: an overview: Structure, regulation, and clinical implications. *Neurobiol. Dis.* **16,** 1–13 (2004).
221. Hawkins, B. T. & Davis, T. P. The Blood-Brain Barrier/Neurovascular Unit in Health and Disease. *Pharmacol. Rev.* **57,** 173–185 (2005).
222. Pardridge, W. M. doi:10.1016/j.drudis.2006.10.013. *Drug Discov. Today* **12,** (2007).
223. Löscher, W. & Potschka, H. Drug resistance in brain diseases and the role of drug efflux transporters. *Nat. Rev. Neurosci.* **6,** 591–602 (2005).
224. Hermann, D. M. & Bassetti, C. L. Implications of ATP-binding cassette transporters for brain pharmacotherapies. doi:10.1016/j.tips.2007.01.007
225. Attwell, D. *et al.* Glial and neuronal control of brain blood flow. *Nature* **468,** 232–243 (2010).
226. Gordon, G. R. J., Howarth, C. & MacVicar, B. A. Bidirectional control of arteriole diameter by astrocytes. *Exp. Physiol.* **96,** 393–9 (2011).
227. Brightman, M. W. & Reese, T. S. Junctions between intimately apposed cell membranes in the vertebrate brain. *J. Cell Biol.* **40,** 648–77 (1969).
228. Janzer, R. C. & Raff, M. C. Astrocytes induce blood–brain barrier properties in endothelial cells. *Nature* **325,** 253–257 (1987).
229. Von Tell, D., Armulik, A. & Betsholtz, C. Pericytes and vascular stability. (2005). doi:10.1016/j.yexcr.2005.10.019
230. Armulik, A., Abramsson, A. & Betsholtz, C. Endothelial/pericyte interactions. *Circ. Res.* **97,** 512–23 (2005).
231. Pardridge, W. M. The blood-brain barrier: bottleneck in brain drug development. *NeuroRx* **2,** 3–14 (2005).
232. Pardridge, W. M. BLOOD-BRAIN BARRIER DRUG TARGETING: THE FUTURE OF BRAIN DRUG DEVELOPMENT. *Mol. Interv.* **3,** 90–105 (2003).
233. Begley, D. J. ABC transporters and the blood-brain barrier. *Curr. Pharm. Des.* **10,** 1295–312 (2004).
234. Dong, X. Current Strategies for Brain Drug Delivery. *Theranostics* **8,** 1481–1493 (2018).
235. Fung, L. K., Shin, M., Tyler, B., Brem, H. & Saltzman, W. M. Chemotherapeutic Drugs Released from Polymers: Distribution of 1,3-bis(2-chloroethyl)-l-nitrosourea in the Rat Brain. *Pharm. Res.* **13,** 671–682 (1996).

236. Zünkeler, B. *et al.* Quantification and pharmacokinetics of blood-brain barrier disruption in humans. *J. Neurosurg.* **85,** 1056–1065 (1996).
237. Salahuddin, T. S., Johansson, B. B., Kalimo, H. & Olsson, Y. Structural changes in the rat brain after carotid infusions of hyperosmolar solutions. An electron microscopic study. *Acta Neuropathol.* **77,** 5–13 (1988).
238. Neuwelt, E. A. & Rapoport, S. I. Modification of the blood-brain barrier in the chemotherapy of malignant brain tumors. *Fed. Proc.* **43,** 214–9 (1984).
239. Doolittle, N. D., Petrillo, A., Bell, S., Cummings, P. & Eriksen, S. Blood-brain barrier disruption for the treatment of malignant brain tumors: The National Program. *J. Neurosci. Nurs.* **30,** 81–90 (1998).
240. Hanig, J. P., Morrison, J. M. & Krop, S. Ethanol enhancement of blood-brain barrier permeability to catecholamines in chicks. *Eur. J. Pharmacol.* **18,** 79–82 (1972).
241. Broadwell, R. D., Salcman, M. & Kaplan, R. S. Morphologic effect of dimethyl sulfoxide on the blood-brain barrier. *Science* **217,** 164–6 (1982).
242. Saija, A., Princi, P., Trombetta, D., Lanza, M. & De Pasquale, A. Changes in the permeability of the blood-brain barrier following sodium dodecyl sulphate administration in the rat. *Exp. brain Res.* **115,** 546–51 (1997).
243. Rabchevsky, A. G., Degos, J. D. & Dreyfus, P. A. Peripheral injections of Freund's adjuvant in mice provoke leakage of serum proteins through the blood-brain barrier without inducing reactive gliosis. *Brain Res.* **832,** 84–96 (1999).
244. Duffy, K. R. & Pardridge, W. M. Blood-brain barrier transcytosis of insulin in developing rabbits. *Brain Res.* **420,** 32–8 (1987).
245. Boje, K. M. K. Inhibition of nitric oxide synthase attenuates blood-brain barrier disruption during experimental meningitis. *Brain Res.* **720,** 75–83 (1996).
246. Minami, T., Okazaki, J., Kawabata, A., Kuroda, R. & Okazaki, Y. Penetration of cisplatin into mouse brain by lipopolysaccharide. *Toxicology* **130,** 107–13 (1998).
247. Mayhan, W. G. Effect of lipopolysaccharide on the permeability and reactivity of the cerebral microcirculation: role of inducible nitric oxide synthase. *Brain Res.* **792,** 353–7 (1998).
248. Xaio, H., Banks, W. A., Niehoff, M. L. & Morley, J. E. Effect of LPS on the permeability of the blood–brain barrier to insulin. *Brain Res.* **896,** 36–42 (2001).
249. Hynynen, K. *et al.* Focal disruption of the blood–brain barrier due to 260-kHz ultrasound bursts: a method for molecular imaging and targeted drug delivery. *J. Neurosurg.* **105,** 445–454 (2006).
250. Etame, A. B. *et al.* Focused ultrasound disruption of the blood-brain barrier: a new frontier for therapeutic delivery in molecular neurooncology. *Neurosurg. Focus* **32,** E3 (2012).
251. Hynynen, K., McDannold, N., Vykhodtseva, N. & Jolesz, F. A. Noninvasive MR Imaging–guided Focal Opening of the Blood-Brain Barrier in Rabbits. *Radiology* **220,** 640–646 (2001).
252. Treat, L. H. *et al.* Targeted delivery of doxorubicin to the rat brain at therapeutic levels using MRI-guided focused ultrasound. *Int. J. Cancer* **121,** 901–907 (2007).
253. Treat, L. H., Zhang, Y., McDannold, N., Hynynen, K. & Ebbini, E. S. Impact of Focused Ultrasound-enhanced Drug Delivery on Survival in Rats with Glioma. in *AIP Conference Proceedings* **1113,** 443–447 (American Institute of Physics, 2009).
254. Thakker, D. R. *et al.* Intracerebroventricular amyloid- antibodies reduce cerebral amyloid angiopathy and associated micro-hemorrhages in aged Tg2576 mice. *Proc.*

Natl. Acad. Sci. **106,** 4501–4506 (2009).
255. Jordão, J. F. *et al.* Antibodies targeted to the brain with image-guided focused ultrasound reduces amyloid-beta plaque load in the TgCRND8 mouse model of Alzheimer's disease. *PLoS One* **5,** e10549 (2010).
256. Jordão, J. F. *et al.* Amyloid-β plaque reduction, endogenous antibody delivery and glial activation by brain-targeted, transcranial focused ultrasound. *Exp. Neurol.* **248,** 16–29 (2013).
257. Lajoie, J. M. & Shusta, E. V. Targeting receptor-mediated transport for delivery of biologics across the blood-brain barrier. *Annu. Rev. Pharmacol. Toxicol.* **55,** 613–31 (2015).
258. Ohtsuki, S. & Terasaki, T. Contribution of Carrier-Mediated Transport Systems to the Blood–Brain Barrier as a Supporting and Protecting Interface for the Brain; Importance for CNS Drug Discovery and Development. *Pharm. Res.* **24,** 1745–1758 (2007).
259. Gynther, M. *et al.* Large neutral amino acid transporter enables brain drug delivery via prodrugs. *J. Med. Chem.* **51,** 932–6 (2008).
260. Strazielle, N. & Ghersi-Egea, J. F. Physiology of blood-brain interfaces in relation to brain disposition of small compounds and macromolecules. *Mol. Pharm.* **10,** 1473–91 (2013).
261. Descamps, L., Dehouck, M. P., Torpier, G. & Cecchelli, R. Receptor-mediated transcytosis of transferrin through blood-brain barrier endothelial cells. *Am. J. Physiol. Circ. Physiol.* **270,** H1149–H1158 (1996).
262. Dehouck, B. *et al.* A new function for the LDL receptor: transcytosis of LDL across the blood-brain barrier. *J. Cell Biol.* **138,** 877–89 (1997).
263. Candela, P. *et al.* Physiological pathway for low-density lipoproteins across the blood-brain barrier: transcytosis through brain capillary endothelial cells in vitro. *Endothelium* **15,** 254–64 (2008).
264. Chung, N. S. & Wasan, K. M. Potential role of the low-density lipoprotein receptor family as mediators of cellular drug uptake. *Adv. Drug Deliv. Rev.* **56,** 1315–1334 (2004).
265. Friden, P. M. *et al.* Anti-transferrin receptor antibody and antibody-drug conjugates cross the blood-brain barrier. *Proc. Natl. Acad. Sci. U. S. A.* **88,** 4771–5 (1991).
266. Pardridge, W. M., Kang, Y. S., Buciak, J. L. & Yang, J. Human insulin receptor monoclonal antibody undergoes high affinity binding to human brain capillaries in vitro and rapid transcytosis through the blood-brain barrier in vivo in the primate. *Pharm. Res.* **12,** 807–16 (1995).
267. Boado, R. J., Zhang, Y., Zhang, Y. & Pardridge, W. M. Humanization of anti-human insulin receptor antibody for drug targeting across the human blood-brain barrier. *Biotechnol. Bioeng.* **96,** 381–91 (2007).
268. Wang, D. *et al.* Engineering a lysosomal enzyme with a derivative of receptor-binding domain of apoE enables delivery across the blood-brain barrier. *Proc. Natl. Acad. Sci. U. S. A.* **110,** 2999–3004 (2013).
269. Spencer, B. *et al.* Peripheral delivery of a CNS targeted, metalo-protease reduces aβ toxicity in a mouse model of Alzheimer's disease. *PLoS One* **6,** e16575 (2011).
270. Sorrentino, N. C. *et al.* A highly secreted sulphamidase engineered to cross the blood-brain barrier corrects brain lesions of mice with mucopolysaccharidoses type IIIA. *EMBO Mol. Med.* **5,** 675–90 (2013).

271. Moos, T. & Morgan, E. H. Transferrin and transferrin receptor function in brain barrier systems. *Cell. Mol. Neurobiol.* **20,** 77–95 (2000).
272. Yu, Y. J. *et al.* Therapeutic bispecific antibodies cross the blood-brain barrier in nonhuman primates.
273. Malerba, F., Paoletti, F., Capsoni, S. & Cattaneo, A. Intranasal delivery of therapeutic proteins for neurological diseases. *Expert Opin. Drug Deliv.* **8,** 1277–1296 (2011).
274. Torika, N., Asraf, K., Cohen, H. & Fleisher-Berkovich, S. Intranasal telmisartan ameliorates brain pathology in five familial Alzheimer's disease mice. *Brain. Behav. Immun.* (2017). doi:10.1016/j.bbi.2017.04.001
275. Reger, M. A. *et al.* Intranasal Insulin Administration Dose-Dependently Modulates Verbal Memory and Plasma β-Amyloid in Memory-Impaired Older Adults. *J Alzheimers Dis* **13,** 323–331 (2008).
276. Chauhan, M. B. & Chauhan, N. B. Brain Uptake of Neurotherapeutics after Intranasal versus Intraperitoneal Delivery in Mice. *J. Neurol. Neurosurg.* **2,** (2015).
277. Dhuria, S. V, Hanson, L. R. & Frey Ii, W. H. Intranasal Delivery to the Central Nervous System: Mechanisms and Experimental Considerations. (2010). doi:10.1002/jps.21924
278. Frenkel, D., Maron, R., Burt, D. S. & Weiner, H. L. Nasal vaccination with a proteosome-based adjuvant and glatiramer acetate clears beta-amyloid in a mouse model of Alzheimer disease. *J. Clin. Invest.* **115,** 2423–33 (2005).
279. Thorne, R. G., Pronk, G. J., Padmanabhan, V. & Frey, W. H. Delivery of insulin-like growth factor-I to the rat brain and spinal cord along olfactory and trigeminal pathways following intranasal administration. *Neuroscience* **127,** 481–496 (2004).
280. Baker, H. & Spencer, R. F. Transneuronal transport of peroxidase-conjugated wheat germ agglutinin (WGA-HRP) from the olfactory epithelium to the brain of the adult rat. *Exp. brain Res.* **63,** 461–73 (1986).
281. Mackay-Sim, A., John, J. S. & Schwob, J. E. in *Handbook of Olfaction and Gustation* 133–156 (John Wiley & Sons, Inc, 2015). doi:10.1002/9781118971758.ch7
282. Balin, B. J., Broadwell, R. D., Salcman, M. & El-Kalliny, M. Avenues for entry of peripherally administered protein to the central nervous system in mouse, rat, and squirrel monkey. *J. Comp. Neurol.* **251,** 260–280 (1986).
283. Williams, S. K., Franklin, R. J. M. & Barnett, S. C. Response of olfactory ensheathing cells to the degeneration and regeneration of the peripheral olfactory system and the involvement of the neuregulins. *J. Comp. Neurol.* **470,** 50–62 (2004).
284. Rey, E., Tréluyer, J. M. & Pons, G. Pharmacokinetic optimization of benzodiazepine therapy for acute seizures. Focus on delivery routes. *Clin. Pharmacokinet.* **36,** 409–24 (1999).
285. Veldhorst-Janssen, N. M. L., Fiddelers, A. A. A., van der Kuy, P.-H. M., Neef, C. & Marcus, M. A. E. A review of the clinical pharmacokinetics of opioids, benzodiazepines, and antimigraine drugs delivered intranasally. *Clin. Ther.* **31,** 2954–87 (2009).
286. Zurbriggen, R., Metcalfe, I. C., Glück, R., Viret, J.-F. & Moser, C. Nonclinical safety evaluation of Escherichia coli heat-labile toxin mucosal adjuvant as a component of a nasal influenza vaccine. *Expert Rev. Vaccines* **2,** 295–304 (2003).
287. Maier, M. *et al.* Short amyloid-beta (Abeta) immunogens reduce cerebral Abeta load

and learning deficits in an Alzheimer's disease mouse model in the absence of an Abeta-specific cellular immune response. *J. Neurosci.* **26,** 4717–28 (2006).
288. Kim, H.-D. *et al.* Nasal inoculation of an adenovirus vector encoding 11 tandem repeats of Abeta1-6 upregulates IL-10 expression and reduces amyloid load in a Mo/Hu APPswe PS1dE9 mouse model of Alzheimer's disease. *J. Gene Med.* **9,** 88–98 (2007).
289. Lemere, C. A., Maier, M., Peng, Y., Jiang, L. & Seabrook, T. J. Novel Abeta immunogens: is shorter better? *Curr. Alzheimer Res.* **4,** 427–36 (2007).
290. Lemere, C. A. in 83–93 (2009). doi:10.1016/S0079-6123(09)17506-4
291. Chen, Y. *et al.* Intranasal insulin prevents anesthesia-induced hyperphosphorylation of tau in 3xTg-AD mice. *Front. Aging Neurosci.* **6,** 100 (2014).
292. Alagiakrishnan, K., Sankaralingam, S., Ghosh, M., Mereu, L. & Senior, P. Antidiabetic drugs and their potential role in treating mild cognitive impairment and Alzheimer's disease. *Discov. Med.* **16,** 277–86 (2013).
293. de la Monte, S. M. Intranasal insulin therapy for cognitive impairment and neurodegeneration: current state of the art. *Expert Opin. Drug Deliv.* **10,** 1699–709 (2013).
294. Zemva, J. & Schubert, M. The role of neuronal insulin/insulin-like growth factor-1 signaling for the pathogenesis of Alzheimer's disease: possible therapeutic implications. *CNS Neurol. Disord. Drug Targets* **13,** 322–37 (2014).
295. Brünner, Y. F., Benedict, C. & Freiherr, J. Targeting the brain through the nose. Effects of intranasally administered insulin. *Nervenarzt* **84,** 949–954 (2013).
296. Freiherr, J. *et al.* Intranasal insulin as a treatment for Alzheimer's disease: a review of basic research and clinical evidence. *CNS Drugs* **27,** 505–14 (2013).
297. Claxton, A. *et al.* Sex and ApoE Genotype Differences in Treatment Response to Two Doses of Intranasal Insulin in Adults with Mild Cognitive Impairment or Alzheimer's Disease. *J. Alzheimer's Dis.* **35,** 789–797 (2013).
298. Dhamoon, M. S., Noble, J. M. & Craft, S. Intranasal insulin improves cognition and modulates beta-amyloid in early AD. *Neurology* **72,** 292–294 (2009).
299. Jogani, V. V, Shah, P. J., Mishra, P., Mishra, A. K. & Misra, A. R. Intranasal mucoadhesive microemulsion of tacrine to improve brain targeting. *Alzheimer Dis. Assoc. Disord.* **22,** 116–24 (2008).
300. Leonard, A. K. *et al.* In vitro formulation optimization of intranasal galantamine leading to enhanced bioavailability and reduced emetic response in vivo. *Int. J. Pharm.* **335,** 138–46 (2007).
301. Costantino, H. R., Leonard, A. K., Brandt, G., Johnson, P. H. & Quay, S. C. Intranasal administration of acetylcholinesterase inhibitors. *BMC Neurosci.* **9 Suppl 3,** S6 (2008).
302. Arumugam, K. *et al.* A study of rivastigmine liposomes for delivery into the brain through intranasal route. *Acta Pharm.* **58,** 287–97 (2008).
303. Bhavna *et al.* Donepezil nanosuspension intended for nose to brain targeting: In vitro and in vivo safety evaluation. *Int. J. Biol. Macromol.* **67,** 418–25 (2014).
304. Yang, Z.-Z. *et al.* Enhanced brain distribution and pharmacodynamics of rivastigmine by liposomes following intranasal administration. *Int. J. Pharm.* **452,** 344–54 (2013).
305. Li, W. *et al.* Pharmacokinetic behavior and efficiency of acetylcholinesterase inhibition in rat brain after intranasal administration of galanthamine hydrobromide

loaded flexible liposomes. *Environ. Toxicol. Pharmacol.* **34,** 272–279 (2012).
306. Fazil, M. *et al.* Development and evaluation of rivastigmine loaded chitosan nanoparticles for brain targeting. *Eur. J. Pharm. Sci.* **47,** 6–15 (2012).
307. Yang, Z., Zhang, Y., Wu, K., Wang, Z. & Qi, X. Tissue distribution and pharmacodynamics of rivastigmine after intranasal and intravenous administration in rats. *Curr. Alzheimer Res.* **9,** 315–25 (2012).
308. Agrawal, M. *et al.* Nose-to-brain drug delivery: An update on clinical challenges and progress towards approval of anti-Alzheimer drugs. *J. Control. Release* **281,** 139–177 (2018).
309. Reynolds, D. S. & Morton, A. J. Changes in blood-brain barrier permeability following neurotoxic lesions of rat brain can be visualised with trypan blue. *J. Neurosci. Methods* **79,** 115–21 (1998).
310. Kago, T. *et al.* Cerebral ischemia enhances tyrosine phosphorylation of occludin in brain capillaries. *Biochem. Biophys. Res. Commun.* **339,** 1197–203 (2006).
311. van der Flier, M. *et al.* Vascular endothelial growth factor and blood-brain barrier disruption in tuberculous meningitis. *Pediatr. Infect. Dis. J.* **23,** 608–13 (2004).
312. Toborek, M. *et al.* Mechanisms of the blood-brain barrier disruption in HIV-1 infection. *Cell. Mol. Neurobiol.* **25,** 181–99 (2005).
313. Desai, B. S., Monahan, A. J., Carvey, P. M. & Hendey, B. Blood–Brain Barrier Pathology in Alzheimer's and Parkinson's Disease: Implications for Drug Therapy. *Cell Transplant.* **16,** 285–299 (2007).
314. Weiss, N., Miller, F., Cazaubon, S. & Couraud, P.-O. The blood-brain barrier in brain homeostasis and neurological diseases. *BBA - Biomembr.* **1788,** 842–857 (2008).
315. Juhler, M., Blasberg, R. G., Fenstermacher, J. D., Patlak, C. S. & Paulson, O. B. A Spatial Analysis of the Blood—Brain Barrier Damage in Experimental Allergic Encephalomyelitis. *J. Cereb. Blood Flow Metab.* **5,** 545–553 (1985).
316. Claudio, L. Ultrastructural features of the blood-brain barrier in biopsy tissue from Alzheimer's disease patients. *Acta Neuropathol.* **91,** 6–14 (1996).
317. Farrall, A. J. & Wardlaw, J. M. Blood–brain barrier: Ageing and microvascular disease – systematic review and meta-analysis. *Neurobiol. Aging* **30,** 337–352 (2009).
318. Alafuzoff, I., Adolfsson, R., Grundke-Iqbal, I. & Winblad, B. Blood-brain barrier in Alzheimer dementia and in non-demented elderly. An immunocytochemical study. *Acta Neuropathol.* **73,** 160–6 (1987).
319. Nakayama, M. *et al.* Cyclooxygenase-2 inhibition prevents delayed death of CA1 hippocampal neurons following global ischemia. *Proc. Natl. Acad. Sci. U. S. A.* **95,** 10954–9 (1998).
320. Baik, E. J., Kim, E. J., Lee, S. H. & Moon, C. Cyclooxygenase-2 selective inhibitors aggravate kainic acid induced seizure and neuronal cell death in the hippocampus. *Brain Res.* **843,** 118–29 (1999).
321. Dickstein, D. L. *et al.* Aβ peptide immunization restores blood-brain barrier integrity in Alzheimer disease. *FASEB J.* **20,** 426–433 (2006).
322. Poduslo, J. F. & Curran, G. L. Amyloid beta peptide as a vaccine for Alzheimer's disease involves receptor-mediated transport at the blood-brain barrier. *Neuroreport* **12,** 3197–200 (2001).
323. Armstrong, R. A. Alzheimer's Disease and the Eye. *J. Optom.* **2,** 103–111 (2009).

324. Mendez, M. F., Mendez, M. A., Martin, R., Smyth, K. A. & Whitehouse, P. J. Complex visual disturbances in Alzheimer's disease. *Neurology* **40,** 439–43 (1990).
325. Chang, L. Y. L. *et al.* Alzheimer's disease in the human eye. Clinical tests that identify ocular and visual information processing deficit as biomarkers. *Alzheimer's Dement.* **10,** 251–261 (2014).
326. Francis, P. T., Palmer, A. M., Snape, M. & Wilcock, G. K. The cholinergic hypothesis of Alzheimer's disease: a review of progress. *J. Neurol. Neurosurg. Psychiatry* **66,** 137–47 (1999).
327. Scinto, L. F. *et al.* A potential noninvasive neurobiological test for Alzheimer's disease. *Science* **266,** 1051–4 (1994).
328. Scinto, L. F. M. *et al.* Focal pathology in the Edinger-Westphal nucleus explains pupillary hypersensitivity in Alzheimer's disease. *Acta Neuropathol.* **97,** 557–564 (1999).
329. Scinto, L. F. M. *et al.* Selective cell loss in Edinger-Westphal in asymptomatic elders and Alzheimer's patients. *Neurobiol. Aging* **22,** 729–736 (2001).
330. Caputo, L. *et al.* The 'eye test' in recognition of late-onset Alzheimer's disease. *Arch. Gerontol. Geriatr.* **27,** 171–177 (1998).
331. Granholm, E. *et al.* Tropicamide effects on pupil size and pupillary light reflexes in Alzheimer's and Parkinson's disease. *Int. J. Psychophysiol.* **47,** 95–115 (2003).
332. Goldstein, L. E. *et al.* Cytosolic β-amyloid deposition and supranuclear cataracts in lenses from people with Alzheimer's disease. *Lancet* **361,** 1258–1265 (2003).
333. Chylack, L. T., White, O. & Tung, W. H. Classification of human senile cataractous change by the American Cooperative Cataract Research Group (CCRG) method: II. Staged simplification of cataract classification. *Invest. Ophthalmol. Vis. Sci.* **25,** 166–73 (1984).
334. Tian, T., Zhang, B., Jia, Y. & Li, Z. Promise and challenge: the lens model as a biomarker for early diagnosis of Alzheimer's disease. *Dis. Markers* **2014,** 826503 (2014).
335. Moncaster, J. A. *et al.* Alzheimer's disease amyloid-beta links lens and brain pathology in Down syndrome. *PLoS One* **5,** e10659 (2010).
336. Beyreuther, K. *et al.* Regulation and expression of the Alzheimer's beta/A4 amyloid protein precursor in health, disease, and Down's syndrome. *Ann. N. Y. Acad. Sci.* **695,** 91–102 (1993).
337. Lott, I. T. & Head, E. Alzheimer disease and Down syndrome: factors in pathogenesis. *Neurobiol. Aging* **26,** 383–389 (2005).
338. Robb, R. M. & Marchevsky, A. Pathology of the Lens in Down's Syndrome. *Arch. Ophthalmol.* **96,** 1039–1042 (1978).
339. Melov, S., Wolf, N., Strozyk, D., Doctrow, S. R. & Bush, A. I. Mice transgenic for Alzheimer disease β-amyloid develop lens cataracts that are rescued by antioxidant treatment. *Free Radic. Biol. Med.* **38,** 258–261 (2005).
340. Frederikse, P. H. & Ren, X.-O. Lens Defects and Age-Related Fiber Cell Degeneration in a Mouse Model of Increased AβPP Gene Dosage in Down Syndrome. *Am. J. Pathol.* **161,** 1985–1990 (2002).
341. Goldstein, L. E. *et al.* Cytosolic beta-amyloid deposition and supranuclear cataracts in lenses from people with Alzheimer's disease. *Lancet (London, England)* **361,** 1258–65 (2003).
342. Michael, R. *et al.* Absence of beta-amyloid in cortical cataracts of donors with and

without Alzheimer's disease. *Exp. Eye Res.* **106,** 5–13 (2013).
343. Michael, R. *et al.* Absence of amyloid-beta in lenses of Alzheimer patients: A confocal Raman microspectroscopic study. (2014). doi:10.1016/j.exer.2013.11.016
344. Ho, C.-Y., Troncoso, J. C., Knox, D., Stark, W. & Eberhart, C. G. Beta-amyloid, phospho-tau and alpha-synuclein deposits similar to those in the brain are not identified in the eyes of Alzheimer's and Parkinson's disease patients. *Brain Pathol.* **24,** 25–32 (2014).
345. Minaeva, O. V. *et al.* Noninvasive Detection of Alzheimer's Disease Lens Pathology in Down Syndrome by Quasi-Elastic Light Scattering. in *Optics in the Life Sciences* JT3A.26 (OSA, 2015). doi:10.1364/BODA.2015.JT3A.26
346. Kerbage, C., Sadowsky, C. H., Jennings, D., Cagle, G. D. & Hartung, P. D. Alzheimer's disease diagnosis by detecting exogenous fluorescent signal of ligand bound to Beta amyloid in the lens of human eye: an exploratory study. *Front. Neurol.* **4,** 62 (2013).
347. Sutharsan, J. *et al.* Rational design of amyloid binding agents based on the molecular rotor motif. *ChemMedChem* **5,** 56–60 (2010).
348. Blanks, J. C., Torigoe, Y., Hinton, D. R. & Blanks, R. H. I. Retinal pathology in Alzheimer's disease. I. Ganglion cell loss in foveal/parafoveal retina. *Neurobiol. Aging* **17,** 377–384 (1996).
349. Hinton, D. R., Sadun, A. A., Blanks, J. C. & Miller, C. A. Optic-Nerve Degeneration in Alzheimer's Disease. *N. Engl. J. Med.* **315,** 485–487 (1986).
350. Cordeiro, M. F. *et al.* Imaging multiple phases of neurodegeneration: a novel approach to assessing cell death in vivo. *Cell Death Dis.* **1,** e3 (2010).
351. Koronyo-Hamaoui, M. *et al.* Identification of amyloid plaques in retinas from Alzheimer's patients and noninvasive in vivo optical imaging of retinal plaques in a mouse model. *Neuroimage* **54 Suppl 1,** S204-17 (2011).
352. Ning, A., Cui, J., To, E., Ashe, K. H. & Matsubara, J. Amyloid-beta deposits lead to retinal degeneration in a mouse model of Alzheimer disease. *Invest. Ophthalmol. Vis. Sci.* **49,** 5136–43 (2008).
353. Dutescu, R. M. *et al.* Amyloid precursor protein processing and retinal pathology in mouse models of Alzheimer's disease. *Graefes Arch Clin Exp Ophthalmol* **247,** 1213–1221 (2009).
354. Liu, B. *et al.* Amyloid-peptide vaccinations reduce {beta}-amyloid plaques but exacerbate vascular deposition and inflammation in the retina of Alzheimer's transgenic mice. *Am. J. Pathol.* **175,** 2099–110 (2009).
355. Ohno-Matsui, K. Parallel findings in age-related macular degeneration and Alzheimer's disease. *Prog. Retin. Eye Res.* **30,** 217–238 (2011).
356. Danesh-Meyer, H. V, Birch, H., Ku, J. Y.-F., Carroll, S. & Gamble, G. Reduction of optic nerve fibers in patients with Alzheimer disease identified by laser imaging. *Neurology* **67,** 1852–4 (2006).
357. Koronyo, Y., Salumbides, B. C., Black, K. L. & Koronyo-Hamaoui, M. Alzheimer's disease in the retina: imaging retinal aβ plaques for early diagnosis and therapy assessment. *Neurodegener. Dis.* **10,** 285–93 (2012).
358. Valenti, D. A. Neuroimaging of retinal nerve fiber layer in AD using optical coherence tomography. *Neurology* **69,** 1060 (2007).
359. Paquet, C. *et al.* Abnormal retinal thickness in patients with mild cognitive impairment and Alzheimer's disease. *Neurosci. Lett.* **420,** 97–99 (2007).

360. Iseri, P. K., Altinas, zgül, Tokay, T. & xen Yüksel, N. *Relationship between Cognitive Impairment and Retinal Morphological and Visual Functional Abnormalities in Alzheimer Disease*.
361. Parisi, V. Correlation between morphological and functional retinal impairment in patients affected by ocular hypertension, glaucoma, demyelinating optic neuritis and Alzheimer's disease. *Semin. Ophthalmol.* **18,** 50–7 (2003).
362. Parisi, V. *et al.* Morphological and functional retinal impairment in Alzheimer's disease patients. *Clin. Neurophysiol.* **112,** 1860–1867 (2001).
363. Jindahra, P., Hedges, T. R., Mendoza-Santiesteban, C. E. & Plant, G. T. Optical coherence tomography of the retina: applications in neurology. *Curr. Opin. Neurol.* **23,** 16–23 (2010).
364. Guo, L. *et al.* Assessment of neuroprotective effects of glutamate modulation on glaucoma-related retinal ganglion cell apoptosis in vivo. *Invest. Ophthalmol. Vis. Sci.* **47,** 626–33 (2006).
365. Guo, L. *et al.* Retinal ganglion cell apoptosis in glaucoma is related to intraocular pressure and IOP-induced effects on extracellular matrix. *Invest. Ophthalmol. Vis. Sci.* **46,** 175–82 (2005).
366. Jentsch, S. *et al.* Retinal fluorescence lifetime imaging ophthalmoscopy measures depend on the severity of Alzheimer's disease. *Acta Ophthalmol.* **93,** e241–e247 (2015).
367. Frost, S. *et al.* Retinal vascular biomarkers for early detection and monitoring of Alzheimer's disease. *Transl. Psychiatry* **3,** e233 (2013).
368. Yang, F. *et al.* Curcumin inhibits formation of amyloid beta oligomers and fibrils, binds plaques, and reduces amyloid in vivo. *J. Biol. Chem.* **280,** 5892–901 (2005).
369. Dhillon, N. *et al.* Phase II Trial of Curcumin in Patients with Advanced Pancreatic Cancer. *Clin. Cancer Res.* **14,** 4491–4499 (2008).
370. McClure, R. *et al.* Inhalable curcumin: offering the potential for translation to imaging and treatment of Alzheimer's disease. *J. Alzheimers. Dis.* **44,** 283–95 (2015).
371. Frost, S. *et al.* Retinal Amyloid Fluorescent Imaging Predicts Cerebral Amyloid Burden and Alzheimer's Disease. *Alzheimer's Dement.* **10,** P234–P235 (2014).
372. Ringman, J. M. *et al.* Oral curcumin for Alzheimer's disease: tolerability and efficacy in a 24-week randomized, double blind, placebo-controlled study. *Alzheimers. Res. Ther.* **4,** 43 (2012).
373. Anand, P., Kunnumakkara, A. B., Newman, R. A. & Aggarwal, B. B. Bioavailability of Curcumin: Problems and Promises. *Mol. Pharm.* **4,** 807–818 (2007).
374. Selkoe, D. J. Alzheimer's Disease. *Cold Spring Harb. Perspect. Biol.* **3,** a004457–a004457 (2011).
375. Saunders, J. C. *et al.* An in vivo platform for identifying inhibitors of protein aggregation. *Nat. Chem. Biol.* **12,** 94–101 (2016).
376. Young, L. M. *et al.* Screening and classifying small-molecule inhibitors of amyloid formation using ion mobility spectrometry-mass spectrometry. *Nat. Chem.* **7,** 73–81 (2015).
377. van Dyck, C. H. Anti-Amyloid-β Monoclonal Antibodies for Alzheimer's Disease: Pitfalls and Promise. *Biol. Psychiatry* **83,** 311–319 (2018).
378. Klunk, W. E. *et al.* Uncharged thioflavin-T derivatives bind to amyloid-beta protein

with high affinity and readily enter the brain. *Life Sci.* **69,** 1471–84 (2001).
379. Maiti, P., Paladugu, L. & Dunbar, G. L. Solid lipid curcumin particles provide greater anti-amyloid, anti-inflammatory and neuroprotective effects than curcumin in the 5xFAD mouse model of Alzheimer's disease. *BMC Neurosci.* **19,** (2018).
380. Okuda, M. *et al. Design and synthesis of curcumin derivatives as tau and amyloid β dual aggregation inhibitors*. *Bioorganic & Medicinal Chemistry Letters* (2016). doi:10.1016/j.bmcl.2016.08.092
381. Pardridge, W. M. Drug and gene delivery to the brain: the vascular route. *Neuron* **36,** 555–8 (2002).
382. Brightman, M. W. Morphology of blood-brain interfaces. *Exp. Eye Res.* **25 Suppl,** 1–25 (1977).
383. Darghal, N., Garnier-Suillerot, A. & Salerno, M. Mechanism of thioflavin T accumulation inside cells overexpressing P-glycoprotein or multidrug resistance-associated protein: Role of lipophilicity and positive charge. *Biochem. Biophys. Res. Commun.* **343,** 623–629 (2006).
384. Schinkel. P-Glycoprotein, a gatekeeper in the blood-brain barrier. *Adv. Drug Deliv. Rev.* **36,** 179–194 (1999).
385. Ishimoto, T., Chiba, S. & Omori, N. Convulsive seizures induced by alpha-amino-3-hydroxy-5-methyl-4-isoxazolepropionic acid microinjection into the mesencephalic reticular formation in rats. *Brain Res.* **1021,** 69–75 (2004).
386. Chakrabarti, R., Wylie, D. E. & Schuster, S. M. Transfer of monoclonal antibodies into mammalian cells by electroporation. *J. Biol. Chem.* **264,** 15494–500 (1989).
387. Connor, J. & Huang, L. Efficient cytoplasmic delivery of a fluorescent dye by pH-sensitive immunoliposomes. *J. Cell Biol.* **101,** 582–9 (1985).
388. Chen, H.-T., Neerman, M. F., Parrish, A. R. & Simanek, E. E. Cytotoxicity, hemolysis, and acute in vivo toxicity of dendrimers based on melamine, candidate vehicles for drug delivery. *J. Am. Chem. Soc.* **126,** 10044–8 (2004).
389. Prior, T. I., FitzGerald, D. J. & Pastan, I. Barnase toxin: a new chimeric toxin composed of pseudomonas exotoxin A and barnase. *Cell* **64,** 1017–23 (1991).
390. Stenmark, H., Moskaug, J. O., Madshus, I. H., Sandvig, K. & Olsnes, S. Peptides fused to the amino-terminal end of diphtheria toxin are translocated to the cytosol. *J. Cell Biol.* **113,** 1025–32 (1991).
391. Hynynen, K., McDannold, N., Sheikov, N. A., Jolesz, F. A. & Vykhodtseva, N. Local and reversible blood-brain barrier disruption by noninvasive focused ultrasound at frequencies suitable for trans-skull sonications. *Neuroimage* **24,** 12–20 (2005).
392. Lopez-Quintero, S. V *et al.* DBS-relevant electric fields increase hydraulic conductivity of in vitro endothelial monolayers. *J. Neural Eng.* **7,** 16005 (2010).
393. Liu, C. H. *et al.* Imaging Cerebral Gene Transcripts in Live Animals. *J. Neurosci.* **27,** 713–722 (2007).
394. Liu, C. H. *et al.* Noninvasive detection of neural progenitor cells in living brains by MRI. *FASEB J.* **26,** 1652–62 (2012).
395. Rapoport, S. *Blood-Brain Barrier in Physiology and Medicine*. (Raven Press, 1976).
396. Abbott, N. J., Patabendige, A. A. K., Dolman, D. E. M., Yusof, S. R. & Begley, D. J. Structure and function of the blood–brain barrier. *Neurobiol. Dis.* **37,** 13–25 (2009).
397. De Vries, H. E., Kuiper, J., De Boer, A. G., Van Berkel, T. J. C. & Breimer, D. D.

The Blood-Brain Barrier in Neuroinflammatory Diseases.
398. Üllen, A. *et al.* Myeloperoxidase-Derived Oxidants Induce Blood-Brain Barrier Dysfunction In Vitro and In Vivo. *PLoS One* **8,** e64034 (2013).
399. Choi, J. J. *et al.* Lipopolysaccharide potentiates polychlorinated biphenyl-induced disruption of the blood-brain barrier via TLR4/IRF-3 signaling. *Toxicology* **302,** 212–20 (2012).
400. Wang, H., Sun, J. & Goldstein, H. Human immunodeficiency virus type 1 infection increases the in vivo capacity of peripheral monocytes to cross the blood-brain barrier into the brain and the in vivo sensitivity of the blood-brain barrier to disruption by lipopolysaccharide. *J. Virol.* **82,** 7591–600 (2008).
401. Awasthi, S. Toll-Like Receptor-4 Modulation for Cancer Immunotherapy. *Front. Immunol.* **5,** 328 (2014).
402. Banks, W. A. *et al.* Lipopolysaccharide-induced blood-brain barrier disruption: roles of cyclooxygenase, oxidative stress, neuroinflammation, and elements of the neurovascular unit. *Endocrinology* **156,** 3066–3068 (2015).
403. de Vries, H. E. *et al.* Lymphocyte adhesion to brain capillary endothelial cells in vitro. *J. Neuroimmunol.* **52,** 1–8 (1994).
404. Verma, S., Nakaoke, R., Dohgu, S. & Banks, W. A. Release of cytokines by brain endothelial cells: A polarized response to lipopolysaccharide. (2005). doi:10.1016/j.bbi.2005.10.005
405. Carlyle Clawson, C., Francis Hartmann, J. & Vernier, R. L. Electron microscopy of the effect of gram-negative endotoxin on the blood-brain barrier. *J. Comp. Neurol.* **127,** 183–197 (1966).
406. Eckman, P. L., King, W. M. & Brunson, J. G. Studies on the blood brain barrier. I. Effects produced by a single injection of gramnegative endotoxin on the permeability of the cerebral vessels. *Am. J. Pathol.* **34,** 631–43
407. Banks, W. A. Physiology and pathology of the blood-brain barrier: implications for microbial pathogenesis, drug delivery and neurodegenerative disorders. *J. Neurovirol.* **5,** 538–55 (1999).
408. Persidsky, Y. *et al.* A model for monocyte migration through the blood-brain barrier during HIV-1 encephalitis. *J. Immunol.* **158,** 3499–510 (1997).
409. Jaeger, L. B. *et al.* Lipopolysaccharide alters the blood-brain barrier transport of amyloid beta protein: a mechanism for inflammation in the progression of Alzheimer's disease. *Brain. Behav. Immun.* **23,** 507–17 (2009).
410. Fang, H. *et al.* Lipopolysaccharide-induced macrophage inflammatory response is regulated by SHIP. *J. Immunol.* **173,** 360–6 (2004).
411. Fujihara, M. *et al.* Molecular mechanisms of macrophage activation and deactivation by lipopolysaccharide: roles of the receptor complex. *Pharmacol. Ther.* **100,** 171–94 (2003).
412. Meng, F. & Lowell, C. A. Lipopolysaccharide (LPS)-induced macrophage activation and signal transduction in the absence of Src-family kinases Hck, Fgr, and Lyn. *J. Exp. Med.* **185,** 1661–70 (1997).
413. Tsai, C.-K. *et al.* Imaging granularity of leukocytes with third harmonic generation microscopy. *Biomed. Opt. Express* **3,** 2234–43 (2012).
414. Tu, Y. *et al.* EFhd2/swiprosin-1 regulates LPS-induced macrophage recruitment via enhancing actin polymerization and cell migration. *Int. Immunopharmacol.* **55,** 263–271 (2018).

415. Wu, T.-T., Chen, T.-L. & Chen, R.-M. Lipopolysaccharide triggers macrophage activation of inflammatory cytokine expression, chemotaxis, phagocytosis, and oxidative ability via a toll-like receptor 4-dependent pathway: validated by RNA interference. *Toxicol. Lett.* **191,** 195–202 (2009).
416. Al Faraj, A., Sultana Shaik, A., Pureza, M. A., Alnafea, M. & Halwani, R. Preferential macrophage recruitment and polarization in LPS-induced animal model for COPD: noninvasive tracking using MRI. *PLoS One* **9,** e90829 (2014).
417. Munford, R. S. Severe Sepsis and septic shock: the role of gram-negative bacteremia. *Annu. Rev. Pathol. Mech. Dis.* **1,** 467–496 (2006).
418. Kobukai, S. *et al.* Magnetic nanoparticles for imaging dendritic cells. *Magn. Reson. Med.* **63,** 1383–1390 (2010).
419. Erickson, M. A. & Banks, W. A. Cytokine and chemokine responses in serum and brain after single and repeated injections of lipopolysaccharide: multiplex quantification with path analysis. *Brain. Behav. Immun.* **25,** 1637–48 (2011).
420. Barton, S. *et al.* Lipopolysaccharide-induced opening of the blood-brain barrier on aging 5XFAD mouse model. *J. Alzheimer's Dis.* **In Press,** (2018).
421. Bacskai, B. J. *et al.* Four-dimensional multiphoton imaging of brain entry, amyloid binding, and clearance of an amyloid-beta ligand in transgenic mice. *Proc. Natl. Acad. Sci. U. S. A.* **100,** 12462–7 (2003).
422. Toki, S. *et al.* A comprehensive analysis of transfection-assisted delivery of iron oxide nanoparticles to dendritic cells. *Nanomedicine* **9,** 1235–44 (2013).
423. Hirase, T. *et al.* Occludin as a possible determinant of tight junction permeability in endothelial cells. *J. Cell Sci.* **110 (Pt 14),** 1603–13 (1997).
424. Kaplan, S. L. *et al.* Decrease of invasive pneumococcal infections in children among 8 children's hospitals in the United States after the introduction of the 7-valent pneumococcal conjugate vaccine. *Pediatrics* **113,** 443–9 (2004).
425. Pignol, B., Henane, S., Chaumeron, S., Mencia-Huerta, J. M. & Braquet, P. Modulation of the priming effects of platelet-activating factor on the release of interleukin-1 from lipopolysaccharide-stimulated rat spleen macrophages. *J. Lipid Mediat.* **2 Suppl,** S93-9 (1990).
426. Ramilo, O. *et al.* Tumor necrosis factor alpha/cachectin and interleukin 1 beta initiate meningeal inflammation. *J. Exp. Med.* **172,** 497–507 (1990).
427. Leib, S. L. & Täuber, M. G. Pathogenesis of bacterial meningitis. *Infect. Dis. Clin. North Am.* **13,** 527–48, v–vi (1999).
428. Garabedian, B. V, Lemaigre-Dubreuil, Y. & Mariani, J. Central origin of IL-1beta produced during peripheral inflammation: role of meninges. *Brain Res. Mol. Brain Res.* **75,** 259–63 (2000).
429. Jaworowicz, D. J., Korytko, P. J., Singh Lakhman, S. & Boje, K. M. Nitric oxide and prostaglandin E2 formation parallels blood-brain barrier disruption in an experimental rat model of bacterial meningitis. *Brain Res. Bull.* **46,** 541–6 (1998).
430. Shamsipour, F. *et al.* Conjugation of Monoclonal Antibodies to Super Paramagnetic Iron Oxide Nanoparticles for Detection of her2/neu Antigen on Breast Cancer Cell Lines. *Avicenna J. Med. Biotechnol.* **1,** 27–31 (2009).
431. Hilger, I. *et al.* MR imaging of Her-2/neu protein using magnetic nanoparticles. *Nanotechnology* **18,** 135103 (2007).
432. White, H., Pieper, C., Schmader, K. & Fillenbaum, G. Weight change in Alzheimer's disease. *J. Am. Geriatr. Soc.* **44,** 265–72 (1996).

433. Lemere, C. A. in *Progress in brain research* **175,** 83–93 (2009).
434. Sun, A., Nguyen, X. V. & Bing, G. Comparative Analysis of an Improved Thioflavin-S Stain, Gallyas Silver Stain, and Immunohistochemistry for Neurofibrillary Tangle Demonstration on the Same Sections. *J. Histochem. Cytochem.* **50,** 463–472 (2002).
435. Kelényi, G. Thioflavin S fluorescent and congo red anisotropic stainings in the histologic demonstration of amyloid. *Acta Neuropathol.* **7,** 336–348 (1967).
436. Bacskai, B. J. *et al.* Imaging of amyloid-[beta] deposits in brains of living mice permits direct observation of clearance of plaques with immunotherapy. *Nat Med* **7,** 369–372 (2001).
437. McClure, R. *et al.* Aerosol Delivery of Curcumin Reduced Amyloid-β Deposition and Improved Cognitive Performance in a Transgenic Model of Alzheimer's Disease. *J. Alzheimers. Dis.* **55,** 797–811 (2017).
438. Chung, K. *et al.* Structural and molecular interrogation of intact biological systems. *Nature* **497,** 332–7 (2013).
439. Murray, E. *et al.* Simple, Scalable Proteomic Imaging for High-Dimensional Profiling of Intact Systems. *Cell* **163,** 1500–14 (2015).
440. De Rosa, R. *et al.* Intranasal administration of nerve growth factor (NGF) rescues recognition memory deficits in AD11 anti-NGF transgenic mice. *Proc. Natl. Acad. Sci.* **102,** 3811–3816 (2005).
441. Villani, T. S., Koroch, A. R. & Simon, J. E. An improved clearing and mounting solution to replace chloral hydrate in microscopic applications. *Appl. Plant Sci.* **1,** (2013).
442. Ning, A., Cui, J., To, E., Ashe, K. H. & Matsubara, J. Amyloid-beta deposits lead to retinal degeneration in a mouse model of Alzheimer disease. *Invest. Ophthalmol. Vis. Sci.* **49,** 5136–43 (2008).
443. Ghosh, S., Banerjee, S. & Sil, P. C. The beneficial role of curcumin on inflammation, diabetes and neurodegenerative disease: A recent update. *Food Chem. Toxicol.* **83,** 111–24 (2015).
444. Parada, E. *et al.* Microglial HO-1 induction by curcumin provides antioxidant, antineuroinflammatory, and glioprotective effects. *Mol. Nutr. Food Res.* **59,** 1690–700 (2015).
445. Sandersen, C. *et al.* Effect of inhaled hydrosoluble curcumin on inflammatory markers in broncho-alveolar lavage fluid of horses with LPS-induced lung neutrophilia. *Multidiscip. Respir. Med.* **10,** 16 (2015).
446. Santos, A. M. *et al.* Curcumin inhibits gastric inflammation induced by Helicobacter pylori infection in a mouse model. *Nutrients* **7,** 306–20 (2015).
447. Galaly, S. R., Ahmed, O. M. & Mahmoud, A. M. Thymoquinone and curcumin prevent gentamicin-induced liver injury by attenuating oxidative stress, inflammation and apoptosis. *J. Physiol. Pharmacol.* **65,** 823–32 (2014).
448. Rashid, K. & Sil, P. C. Curcumin enhances recovery of pancreatic islets from cellular stress induced inflammation and apoptosis in diabetic rats. *Toxicol. Appl. Pharmacol.* **282,** 297–310 (2015).
449. Das, L. & Vinayak, M. Long term effect of curcumin in restoration of tumour suppressor p53 and phase-II antioxidant enzymes via activation of Nrf2 signalling and modulation of inflammation in prevention of cancer. *PLoS One* **10,** e0124000 (2015).

450. Das, L. & Vinayak, M. Curcumin attenuates carcinogenesis by down regulating proinflammatory cytokine interleukin-1 (IL-1α and IL-1β) via modulation of AP-1 and NF-IL6 in lymphoma bearing mice. *Int. Immunopharmacol.* **20,** 141–7 (2014).
451. Das, L. & Vinayak, M. Anti-carcinogenic action of curcumin by activation of antioxidant defence system and inhibition of NF-κB signalling in lymphoma-bearing mice. *Biosci. Rep.* **32,** 161–70 (2012).
452. Loch-Neckel, G. *et al.* Orally Administered Chitosan-Coated Polycaprolactone Nanoparticles Containing Curcumin Attenuate Metastatic Melanoma in the Lungs. *J. Pharm. Sci.* **104,** 3524–34 (2015).
453. Mancarella, S. *et al.* Polymer-Coated Magnetic Nanoparticles for Curcumin Delivery to Cancer Cells. *Macromol. Biosci.* **15,** 1365–1374 (2015).
454. Parashar, G. & Capalash, N. Promoter methylation-independent reactivation of PAX1 by curcumin and resveratrol is mediated by UHRF1. *Clin. Exp. Med.* **16,** 471–8 (2016).
455. Ahmad, M. Z. *et al.* Progress in nanotechnology-based drug carrier in designing of curcumin nanomedicines for cancer therapy: current state-of-the-art. *J. Drug Target.* **24,** 273–93 (2016).
456. Endo, H., Nikaido, Y., Nakadate, M., Ise, S. & Konno, H. Structure activity relationship study of curcumin analogues toward the amyloid-beta aggregation inhibitor. *Bioorg. Med. Chem. Lett.* **24,** 5621–5626 (2014).
457. Maiti, P., Manna, J., Veleri, S. & Frautschy, S. Molecular Chaperone Dysfunction in Neurodegenerative Diseases and Effects of Curcumin. *Biomed Res. Int.* **2014,** 1–14 (2014).
458. Malar, D. S. & Devi, K. P. Dietary polyphenols for treatment of Alzheimer's disease--future research and development. *Curr. Pharm. Biotechnol.* **15,** 330–42 (2014).
459. Campbell, M. & Humphries, P. The blood-retina barrier: tight junctions and barrier modulation. *Adv. Exp. Med. Biol.* **763,** 70–84 (2012).
460. Kaneko, N., Yamamoto, R., Sato, T.-A. & Tanaka, K. Identification and quantification of amyloid beta-related peptides in human plasma using matrix-assisted laser desorption/ionization time-of-flight mass spectrometry. *Proc. Jpn. Acad. Ser. B. Phys. Biol. Sci.* **90,** 104–17 (2014).
461. Park, S. W. *et al.* Dry age-related macular degeneration like pathology in aged 5XFAD mice: Ultrastructure and microarray analysis. *Oncotarget* **8,** 40006–40018 (2017).
462. Mahajan, D. & Votruba, M. Can the retina be used to diagnose and plot the progression of Alzheimer's disease? *Acta Ophthalmol.* **95,** 768–777 (2017).
463. Pogue, A., Dua, P., Hill, J. & Lukiw, W. Progressive inflammatory pathology in the retina of aluminum-fed 5xFAD transgenic mice. *J. Inorg. Biochem.* **152,** 206–209 (2015).
464. Stoeckli, M., Staab, D., Staufenbiel, M., Wiederhold, K.-H. & Signor, L. Molecular imaging of amyloid beta peptides in mouse brain sections using mass spectrometry. *Anal. Biochem.* **311,** 33–9 (2002).
465. Koronyo, Y., Salumbides, B. C., Black, K. L. & Koronyo-Hamaoui, M. Alzheimer's Disease in the Retina: Imaging Retinal Aß Plaques for Early Diagnosis and Therapy Assessment. *Neurodegener. Dis.* **10,** 285–293 (2012).
466. Lim, J. K. H. *et al.* The Eye As a Biomarker for Alzheimer's Disease. *Front.*

Neurosci. **10,** 536 (2016).
467. Snyder, P. J. *et al.* Nonvascular retinal imaging markers of preclinical Alzheimer's disease. *Alzheimer's Dement. (Amsterdam, Netherlands)* **4,** 169–178 (2016).
468. Koronyo-Hamaoui, M. *et al.* Identification of amyloid plaques in retinas from Alzheimer's patients and noninvasive in vivo optical imaging of retinal plaques in a mouse model. *Neuroimage* **54 Suppl 1,** S204-17 (2011).